

Linling Kuang
Chunxiao Jiang
Yi Qian
Jianhua Lu

Terrestrial-Satellite Communication Networks

Transceivers Design and Resource
Allocation

Wireless Networks

Series editor

Xuemin (Sherman) Shen

University of Waterloo, Waterloo, Ontario, Canada

More information about this series at <http://www.springer.com/series/14180>

Linling Kuang • Chunxiao Jiang • Yi Qian
Jianhua Lu

Terrestrial-Satellite Communication Networks

Transceivers Design and Resource Allocation



Springer

Linling Kuang
Tsinghua Space Center
Tsinghua University
Beijing, China

Yi Qian
Department of Electrical
and Computer Engineering
University of Nebraska-Lincoln
Lincoln, NE, USA

Chunxiao Jiang
Tsinghua Space Center
Tsinghua University
Beijing, China

Jianhua Lu
Tsinghua Space Center
Tsinghua University
Beijing, China

ISSN 2366-1186
Wireless Networks
ISBN 978-3-319-61767-1
DOI 10.1007/978-3-319-61768-8

ISSN 2366-1445 (electronic)
ISBN 978-3-319-61768-8 (eBook)

Library of Congress Control Number: 2017944138

© Springer International Publishing AG 2018

This work is subject to copyright. All rights are reserved by the Publisher, whether the whole or part of the material is concerned, specifically the rights of translation, reprinting, reuse of illustrations, recitation, broadcasting, reproduction on microfilms or in any other physical way, and transmission or information storage and retrieval, electronic adaptation, computer software, or by similar or dissimilar methodology now known or hereafter developed.

The use of general descriptive names, registered names, trademarks, service marks, etc. in this publication does not imply, even in the absence of a specific statement, that such names are exempt from the relevant protective laws and regulations and therefore free for general use.

The publisher, the authors and the editors are safe to assume that the advice and information in this book are believed to be true and accurate at the date of publication. Neither the publisher nor the authors or the editors give a warranty, express or implied, with respect to the material contained herein or for any errors or omissions that may have been made. The publisher remains neutral with regard to jurisdictional claims in published maps and institutional affiliations.

Printed on acid-free paper

This Springer imprint is published by Springer Nature
The registered company is Springer International Publishing AG
The registered company address is: Gewerbestrasse 11, 6330 Cham, Switzerland

Preface

Nowadays, mobile service coverage is crucial for economic development. Up to now, there are still a large number of population without mobile service coverage, especially in less developed areas. Moreover, future wireless networks should also guarantee service continuity for emerging applications and heterogeneous networks. On the other hand, the cost of providing ubiquitous coverage has to be taken into account for mobile network operators. Current urban areas are mainly covered by terrestrial cellular networks, while the usage of wireless network in less developed areas, such as remote rural areas, is far less than urban areas. The cost of pure terrestrial coverage quickly becomes unbearable with increasing network requirements for those remote rural areas.

While the terrestrial networks can provide high-speed data service at low cost, satellite-based access is one way to complement the terrestrial-based networks for achieving ubiquitous, 100% geographic coverage. A satellite network is an ideal solution to address such a dilemma. One satellite is able to cover areas of thousands of kilometers in radius instead of several kilometers with a terrestrial base station. The coexistence and cooperation between terrestrial and satellite networks are of great potential in future communication networks. Therefore, investigations of innovative technologies in terrestrial-satellite networks are in great need to reveal their true potentials.

In a typical communication system, transmission and reception are the fundamental problems. We consider the technique of beamforming to achieve multiple access transmission in the terrestrial-satellite network and the interference cancellation reception to mitigate the inter-beam interference as well as intersystem interference. Meanwhile, due to the limited spectrum resources, spectrum sharing will become one critical issue in terrestrial-satellite communication networks, and efficient spectrum sensing techniques are also worthy of being investigated. Finally, taking the interference and limited spectrum resources into account, it is important to design efficient resource allocation schemes to achieve optimal system performance.

Recently, array multi-beam antennas have drawn more attention for the possible application of digital beamforming techniques, which is an efficient transmitting

method for multiple access. By adjusting the weighting factors on antennas, it can steer nulls to mitigate co-channel interferences and form independent beams toward different directions, which contribute to improve the performance of mobile communication systems. We investigated the technique of beamforming in the integrated terrestrial and satellite communication systems we also concluded the main challenges and prospective applications in the integrated terrestrial and satellite systems. Based on beamforming, we proposed a multimedia multicast integrated terrestrial-satellite network, in which base stations (BSs) and the satellite work cooperatively to provide ubiquitous service for ground users. By serving users that require the same contents as a group using multicasting, higher efficiency can be achieved. As a practical application of beamforming in satellite networks, we launched the Smart Communication Satellite (SCS) on 4 Sept. 2014, which is the first low Earth orbit (LEO) mobile communication experimental satellite of China, and the smart beamforming technology was experimented on this satellite. Part of these works is introduced in Chap. 2.

In the terrestrial-satellite networks, inter-network interference may become severe when reusing the frequency in the system. When satellite terminals and base stations transmit signals at the same time with the same frequency, it will cause considerable co-channel interference (CCI) which will significantly deteriorate the system performance. Based on channel estimation and centralized processing, we proposed several interference coordination schemes for different scenarios in the integrated satellite and terrestrial network, which is introduced in Chap. 3.

In fifth-generation (5G) networks, millimeter-wave (mmWave) bands have drawn great attention for the large amount of possible bandwidth. Meanwhile, satellite communications have also shown great interest in the mmWave bands, especially the Ka band. Under such a circumstance, due to the limitation of spectrum resources, spectrum sharing will become one critical issue in terrestrial-satellite communication networks. We investigated the problems of spectrum coexistence between the geostationary (GEO) satellite system and terrestrial systems and between the GEO satellite system and the non-geostationary (NGEO) satellite system, respectively. We first analyzed the interference caused by terrestrial systems and the NGEO satellite system to the GEO satellite system in two transmission modes and then introduced the concept of protection radius to protect the GEO system. Then, in the scenario of spectrum coexistence between the GEO and the NGEO satellite systems, we investigated the issue of blind spot where spectrum awareness techniques may fail to identify the spectrum holes. Part of this work is introduced in Chap. 4.

The technique of cognitive radio (CR), which enables dynamic access of spectrum, can improve the utilization rate of the spectrum. To meet the communication need in terrestrial-satellite networks with limited spectrum resources, we investigated the technique of spectrum sensing in this network. The satellite systems having the licensed spectrum are considered as primary users, while the terrestrial systems are regarded as secondary users. We first advanced a strategy for SU to search available spectrums with asynchronous MAC-layer sensing. With this method, SUs need not know the communication mechanisms in PU's network when dynamically accessing. Then, we discussed the asynchronous cooperative spectrum

sensing and derive the optimal sensing parameters under such asynchronous scenario. Also, we proposed a density control mechanism for managing the number of secondary transmitters around one primary receiver in order to guarantee that primary communications are not interfered. Some important ideas are included in Chap. 5.

In terrestrial-satellite networks, the resource allocation problem, such as spectrum resource, time resource, antenna resource, power resource, space resource, orbit resource, etc., will be more complex due to the coupling between resources and the interference. Against this issue, we proposed several resource allocation schemes in different scenarios of terrestrial-satellite communication networks, which can optimize the capacity performance of the entire system. In order to protect the terrestrial users, we introduced the interference temperature limit for the satellite to control the interference caused to BS users. Furthermore, we proposed the concept of the cloud-based integrated terrestrial-satellite network (CTSN), in which both the terrestrial network and the satellite network are connected to the cloud for centralized resource management. Some interesting results are briefly presented in Chap. 6.

Overall, this book aims at giving a comprehensive discussion on the motivation, problem formulation, and research methodology on the transceivers' design and resource allocation in future terrestrial-satellite communication networks.

Beijing, China

Beijing, China

Omaha, NE, USA

Beijing, China

Linling Kuang

Chunxiao Jiang

Yi Qian

Jianhua Lu

Acknowledgments

Thanks to all the collaborators who have also contributed to this book. They are Xiangming Zhu, Boyu Deng, and Yuanzhi Zhong. Meanwhile, we would like to thank the continued support from the National Natural Science Foundation of China under grants 91438206, 91638205, 91538203, 61621091, and 61371079.

Contents

1	Introduction	1
1.1	Background	1
1.2	Integrated Terrestrial-Satellite Network Architecture	2
1.3	Related Research and Development	3
1.4	Organizations of this Book	4
1.5	Summary	6
2	Beamforming Transmission	7
2.1	Beamforming in Satellite Communication Systems	7
2.1.1	Multi-Beam Joint Processing	9
2.1.2	Multigroup Precoding	10
2.1.3	Cooperative Beamforming in Terrestrial-Satellite Networks	12
2.2	Multicast Beamforming	13
2.2.1	System Model	15
2.2.2	Problem Formulation	16
2.2.3	Optimal Power Allocation Algorithm	18
2.2.4	Performance Evaluation	22
2.3	Smart Communication Satellite	26
2.3.1	System Design	27
2.3.2	Smart Beamforming	28
2.4	Summary	29
	References	29
3	Interference Cancelation Reception	31
3.1	Position-Assisted Interference Coordination	32
3.1.1	System Model	32
3.1.2	Scheme of Interference Coordination	34
3.1.3	Precision Analysis	37
3.1.4	Performance Evaluation	40
3.2	Channel State Information Based Interference Coordination	41
3.2.1	Model and Formulation	41

3.2.2	Lagrangian Multiplier Method and Algorithm	44
3.2.3	Performance Evaluation	45
3.3	Summary	46
	References	47
4	Spectrum Sharing	49
4.1	Spectrum Coexistence Between GEO and Terrestrial Systems	49
4.1.1	Interference Analysis and Network Mode	49
4.1.2	Channel and Signal Model	51
4.1.3	Outage Constraint of the GEO System	52
4.1.4	Downlink Link of the Normal Mode	53
4.1.5	Uplink Link of the Reverse Mode	56
4.2	Spectrum Coexistence Between GEO and NGEO Systems	59
4.2.1	Interference Analysis and Network Mode	59
4.2.2	Channel and Signal Model	61
4.2.3	Downlink Normal Mode	61
4.2.4	Uplink Normal Mode	64
4.3	Blind Spot of Spectrum Awareness Techniques	67
4.3.1	System Model	68
4.3.2	Blind Spot Analysis of Uplink Scenario	69
4.3.3	Blind Spot Analysis of Downlink Scenario	71
4.3.4	Simulations and Analysis	73
4.4	Summary	79
	References	79
5	Spectrum Sensing	83
5.1	Asynchronous MAC-Layer Spectrum Sensing	83
5.1.1	System Model	86
5.1.2	Searching Available Channels	88
5.1.3	Vacating Strategy	93
5.1.4	Estimation of Channel IPP Parameters	96
5.1.5	Impact on PU's Achievable Rate	98
5.1.6	Numerical Results	99
5.2	Asynchronous Cooperative Spectrum Sensing	105
5.2.1	System Model	105
5.2.2	Detection and False Alarm Probability	107
5.2.3	Optimal Sensing Parameters	112
5.2.4	Simulation and Numerical Results	113
5.3	Effective Management of Terrestrial User's Density	115
5.3.1	System Model	115
5.3.2	Density Control Mechanism	117
5.3.3	Achievable Rate of Secondary Users	120
5.3.4	Simulation	121
5.4	Summary	123
	References	124

6	Multiple Access Resource Allocation	127
6.1	Power Allocation in Terrestrial-Satellite Networks	127
6.1.1	Background	127
6.1.2	System Model	128
6.1.3	Optimal Power Allocation Scheme	130
6.1.4	Performance Evaluation	133
6.2	Resource Allocation in Cloud Based	
	Terrestrial-Satellite Networks	135
6.2.1	Background	135
6.2.2	System Model	136
6.2.3	Problem Formulation	139
6.2.4	Subchannel and Power Allocation Algorithm	140
6.2.5	Performance Evaluation	144
6.3	Summary	147
	References	147
7	Conclusions and Future Challenges	149
7.1	Conclusions	149
7.2	Future Challenges	150

Chapter 1

Introduction

1.1 Background

The rapid growing data traffic brings more and more pressure to the wireless networks, which is predicted to increase by over 10,000 times in the next 20 years. In order to improve the system capacity and satisfy the increasing demands, ultra-dense networks (HetUDNs), massive MIMO, and new spectrum of millimeter wave band are considered as promising methods in future terrestrial networks, especially for the fifth generation (5G). Meanwhile, mobile service coverage is also crucial for the development and economics. However, currently, there are still large number of population without coverage of mobile service. By 2015, there are about 71% rural population that are not yet covered. Furthermore, for the less developed countries, the population that have access to mobile broadband service is only 12%. In addition to the issue of coverage, future wireless networks also need to guarantee the service continuity for emerging services such as Machine-to-Machine and Internet of Things. Many emerging scenarios, such as Unmanned Aerial Vehicle (UAV) control, pipeline monitoring, or global container tracking, require the aid of wireless networks. However, existing networks are severely hindering these services from achieving their true potentials. Considering the deficiency in existing wireless networks nowadays, ubiquitous on-demand coverage is the key to ensure service continuity in future communication paradigm.

On the other hand, the cost of providing ubiquitous converge has also to be taken into account for mobile networks operators. The concept of a “Long tail” distribution is embodied in many innovative Internet business models. It indicates that the revenues may be made from infrequent usage if one can effectively cater to various individual demands. It is applicable to wireless networks operation as well, where the usages far from urban centers can also lead to considerable revenue, as illustrated in Fig. 1.1. However, the cost of pure terrestrial coverage quickly becomes unbearable with the increasing network requirements for those rural, remote and other areas.

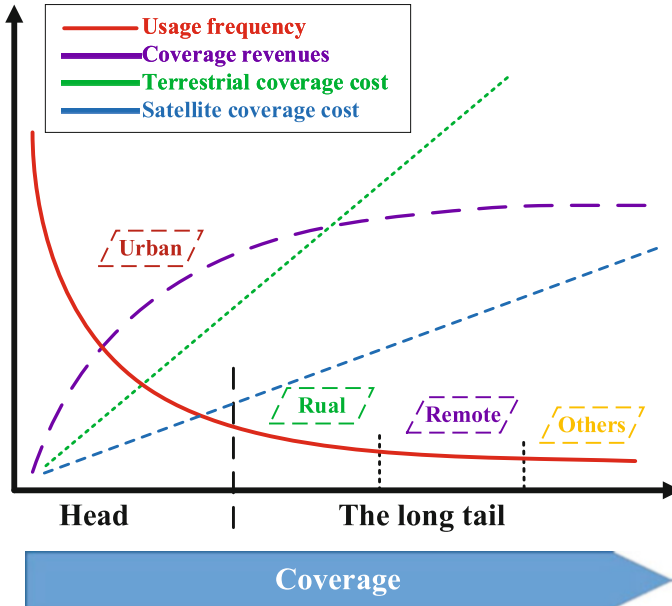


Fig. 1.1 Background: cost

Satellite network is a ideal solution to address such a dilemma. While the terrestrial networks can achieve high-speed data services at low cost, satellite based access is one way to complement terrestrial based networks to ensure ubiquitous, 100% geographic coverage. As depicted in Fig. 1.2, one satellite may cover an area of thousands of kilometers in radius instead of the several kilometers possible with a terrestrial base station. In addition, satellites provide coverage to otherwise inaccessible locations, efficiently satisfying the demands from the “long tail” with lower cost, as depicted in Fig. 1.1. Therefore, the satellite and terrestrial networks should be deeply integrated to realize the full benefits of each of them.

1.2 Integrated Terrestrial-Satellite Network Architecture

Considering a conventional “2D” network with only terrestrial components, satellites can be added to the picture to provide coverage and service continuity over a wide area. Since it is confronted with multiple levels of coverage, we call this extension from 2D to 3D, as shown in Fig. 1.3. On top of the 3D network, we can further tailor the services accordingly with techniques such as adaptive beamforming. By adding another degree of freedom with service driven coverage, we can extend the network from “3D” to “3D+”. The coexistence and cooperation between terrestrial and satellite networks are of great potential in future communication networks. As a

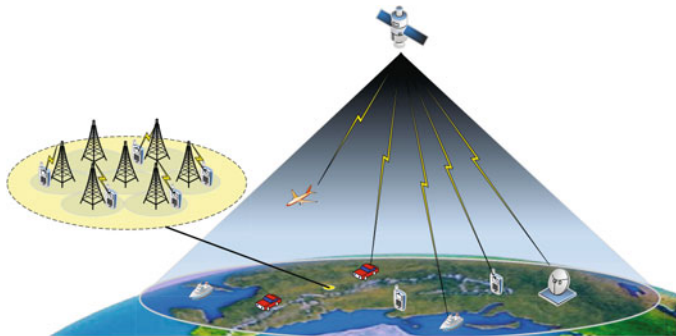


Fig. 1.2 Satellite comes to rescue

matter of fact, the satellite radio access network has already been considered in the fifth-generation (5G) networks to be supported for Phase 2. A new vision of next-generation networks (NGN) has been proposed by International telecommunication union (ITU), in which the integrated and/or hybrid satellite and terrestrial network is supposed to play important roles.

1.3 Related Research and Development

Notable research groups are focusing on satellite applications in 5G, such as the 5G CHAMPION program (8 European and 13 Korean partners), mainly investigating integrated 5G radio-access, core-network and satellites. Meanwhile, FCC, ITU will discuss the Ka-band spectrum sharing between satellites and 5G in WRC 2019. Furthermore, China launched the Space Integrated Ground Network Program in 2016, as a national major project. Previously, the 3GPP standard has proposed satellite radio access network to be supported for 5G Phase 2. On the other hand, in the satellite mobile communication field, integration, miniaturization and multifunction are the developing trends. In the past, the satellite stations are usually large scale with very low mobility, and the satellite can only realize the point to point communication. Recently, the Sat-Fi was developed by Globalstar, in which the mobile antenna and modem are integrated into a hotspot box that can establish a bridge between the satellite and smart phones. Meanwhile, the users' terminals are also becoming increasingly miniaturized, compared with the past heavy and big satellite terminals with less functionality. As technology continues to develop, the Thuraya XT-Pro was produced by Thuraya, on which the satellite modem was designed as a phone companion, providing quite convenient experience to users.

When it comes to the space network, there are two trends: the evolution towards broader bandwidth, and the extension of the IP protocol to the space networks. Orbcomm is building a high-speed IoT infrastructure based on satellite

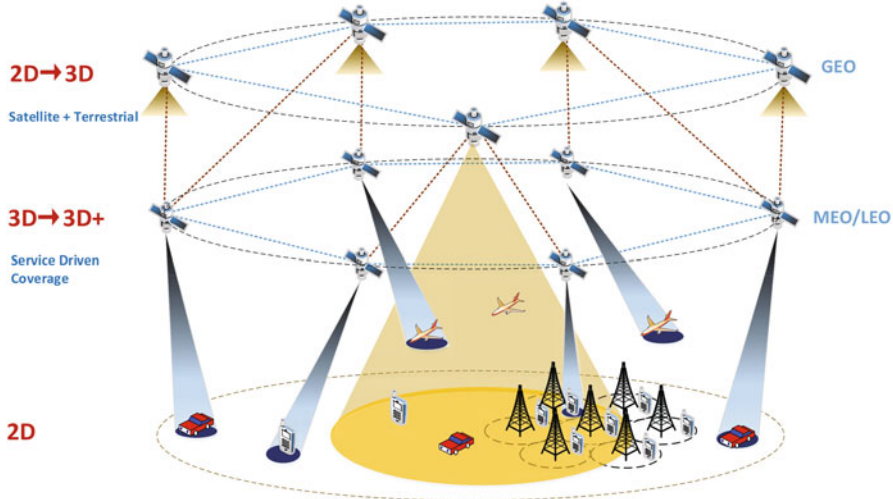


Fig. 1.3 3D+ network

constellations, including LEO (Low Earth Orbit), MEO (Medium Earth Orbit) and GEO (Geostationary Earth Orbit) satellites. At the same time, the Iridium system is evolving to the next generation with higher bandwidth. Moreover, the O3b project was also proposed by Google, where the name “O3b” stands for “[The] Other 3 Billion”, referring to the population of the world where broadband Internet is not available. By building a MEO satellite constellation, the network with the speed of fiber can provide Internet services and mobile backhaul services to the emerging markets. It was reported that Google just invested 1 Billion to spaceX to create a satellite based internet.

1.4 Organizations of this Book

This book is organized as depicted in Fig. 1.4. We first introduce the technique of beamforming in satellite communication systems, which is an efficient transmitting method for multiple access, and discuss the main challenges as well as prospective applications. Beamforming is one of the array processing methods of antenna arrays. By adjusting the weighting factors on antennas, it can steer nulls to mitigate co-channel interferences and forming independent beams toward different directions, which contributes to improve the performance of mobile communication systems. In mobile communication systems, transmit beamforming is a powerful mean of interference mitigation and capacity improvement by providing isolation among users in different directions. Based on the technique of beamforming, a

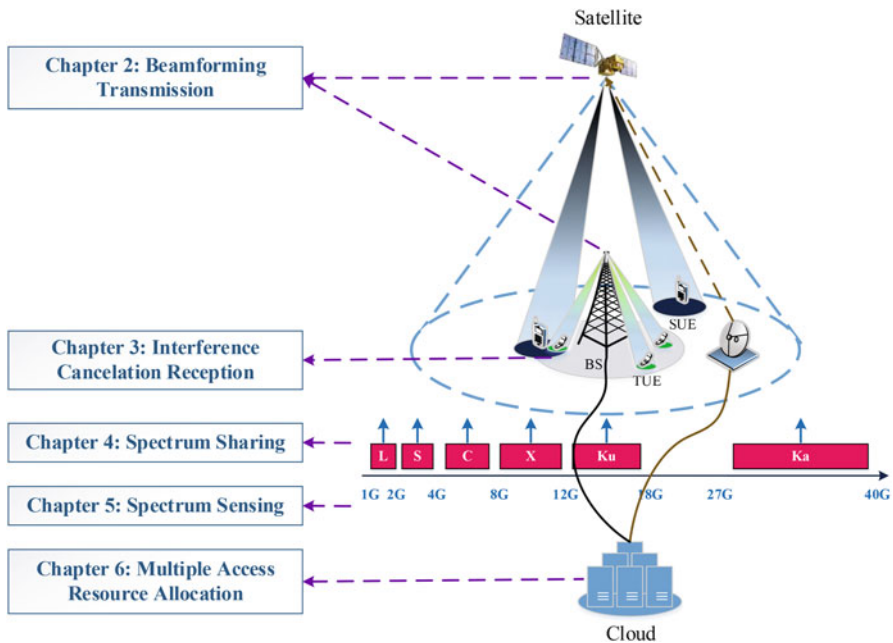


Fig. 1.4 Organizations of this book

multimedia multicast integrated terrestrial-satellite network is proposed, in which base stations (BSs) and the satellite work cooperatively to provide ubiquitous service for ground users. Due to the content diversity of multimedia services, users that require the same contents will be served as a group using multicasting. As a practical application of beamforming in satellite networks, the work of Smart Communication Satellite (SCS), the Chinese first low-earth-orbit communication satellite, is presented briefly.

Then, we discuss the possible methods for interference cancellation reception in terrestrial-satellite communication networks when reusing the frequency band between the two networks. The rapid development of wireless communication has led to increasing demand of frequency resources, and the problem of spectrum scarcity is becoming more and more serious. Due to the lack of frequency spectrum, frequency reuse is considered in the satellite network and the terrestrial network for enhancing spectral efficiency. However, this will cause considerable Co-Channel Interference (CCI) when satellite terminals and base stations transmit signals at the same time with the same frequency. Thus interference coordination is imperative to mitigate the interference at the satellite. Based on channel estimation and centralized processing, we propose several interference coordination schemes for different scenarios in the integrated satellite and terrestrial network.

Due to the limitation of spectrum resources, spectrum sharing will become one important issues in terrestrial-satellite communication networks. We first analyze the interference caused by terrestrial cellular systems to the geostationary (GEO) system, and discuss the problems of spectrum coexistence between GEO and Terrestrial Systems, and between GEO and NEGO systems. Then, the technique of cognitive radio (CR), which enables dynamic access of spectrum, is investigated to improve the utilization rate of the spectrum and meet the communication needs. The satellite systems having the licensed spectrum are considered as primary users, while the terrestrial systems are regarded as secondary users. We first advances a strategy for SU to search available spectrums with asynchronous MAC-layer sensing. With this method, SUs need not know the communication mechanisms in PU's network when dynamically accessing. Then, we discuss the asynchronous cooperative spectrum sensing, and derive the optimal sensing parameters under such asynchronous scenario. Furthermore, we propose a density control mechanism for managing number of secondary transmitters around one primary receiver in order to guarantee that primary communications are not interfered.

Finally, taking both the two systems into consideration, the resource allocation problem will be more complex due to the coupling between resources and the interference, such as spectrum resource, power resource, time resource, space resource, antenna resource, and orbit resource. In this case, it is of great importance to allocate the system resources reasonably to optimize the system performance. Upon this, we propose two resource allocation schemes for two multiple access integrated system. First, we investigate the problem of interference controlling and power allocation in a terrestrial-satellite spectrum sharing network. In order to protect the terrestrial users, interference temperature limit is introduced for the satellite to control the interference caused to BS users, and the optimal power allocation scheme is proposed to maximize the total capacity of the satellite system. Second, we propose the concept of the Cloud Based Integrated Terrestrial-Satellite Network (CTSN), where both base stations of the cellular networks and the satellite are connected to a cloud central unit and the signal processing procedures are executed centrally at the cloud. By utilizing the channel state information (CSI), we propose a resource allocation scheme in respect to subchannel and power to maximize the total capacity of the terrestrial system.

1.5 Summary

In this chapter, we mainly introduce the background. We first introduce the motivation of this book. Based on the motivation, we propose the coordinated network architecture, and discuss the key technologies and challenges in the architecture. Then, the related research and development is provided. Finally, we give the organizations of this book.

Chapter 2

Beamforming Transmission

Multi-beam Satellites have been widely adopted in current satellite communication systems due to its energy efficiency and potential for frequency reuse. Recently, array multi-beam antennas have drawn more attention for the possible applications of digital beamforming techniques. In this chapter, we discuss the main challenges when applying beamforming to satellite communication systems and introduce several prospective applications of satellite beamforming technology. Then, a multi-media multicast beamforming method for the integrated terrestrial-satellite network is proposed, in which base stations (BSs) and the satellite work cooperatively to provide ubiquitous service for ground users. Due to the content diversity of multimedia services, users that require the same contents will be served as a group using multicasting. With multiple transmit antennas, multicast beamforming is executed among groups while reusing the entire bandwidth. Finally, a practical work of Smart Communication Satellite (SCS), the Chinese first low-earth-orbit communication satellite, is presented briefly.

2.1 Beamforming in Satellite Communication Systems

The deployment of multi-beam satellites has increased during the last few years to cover designated areas with the minimum effective isotropic radiated power (EIRP). By projecting higher power density, narrow spot beams can provide higher data capacity for small user terminals. In recent developed multi-beam satellite systems, a large number of beams were employed, such as 228 beams in Inmarsat-4 and 500 beams in SkyTerra-1 [1]. Meanwhile, frequency reuse is possible in multi-beam satellite systems as long as the inter-beam interference can be carefully managed, which can significantly increase the spectrum efficiency [2]. Three types of multi-beam antennas have been utilized in today's multi-beam satellite systems: reflector multi-beam antenna, lens multi-beam antenna, and array multi-

beam antenna, among which the reflector multi-beam antenna and lens multi-beam antenna have been widely deployed due to the mature solutions and effortless realization. Recently, array multi-beam antennas are drawing more and more attention for their superior performance of aperture efficiency and leakage loss. What is more attracting for array multi-beam antennas is the possible application of digital beamforming techniques, which can flexibly construct beams of different shapes/sizes in different cases. Beamforming is one of the array processing methods of antenna arrays. By adjusting the weighting factors on antennas, it can steer nulls to mitigate co-channel interferences and forming independent beams toward different directions, which contributes to improve the performance of mobile communication systems [3]. Generally, it is not practical to equip user terminals with antennas arrays, while satellites and base stations are more applicable to do so. In mobile communication systems, transmit beamforming is a powerful mean of interference mitigation and capacity improvement by providing isolation among users in different directions [4].

The application of beamforming in satellite communication systems is confronted with multiple challenges caused by the special characteristics of satellites [5, 6], which can be summarized as follows.

- The Long and Variable Delay of Channel State Information (CSI)

Adopting beamforming techniques generally requires CSI of desired users and sometimes also the interference users, such as the typical zero-forcing (ZF) or regularized ZF (RZF) beamforming [7]. However, different from terrestrial networks, there is a long time delay between the satellite and terrestrial users due to the long communication distance. Under such a circumstance, it is difficult to obtain the real-time CSI, especially in frequency division duplexing (FDD) scenarios, which is widely utilized nowadays. Some special beamforming algorithms are required in satellite communication systems to adapt to the long time delay of CSI. For instance, the blind beamforming technique can be executed when no information of the source direction or signals is available [8]. Also, since the earth is not a perfect sphere, the delay of CSI would be variable as the satellite is moving. Thus, in time division multiple access (TDMA) systems, accurate time controlling methods are required to ensure system performance.

- The Small Channel Fluctuations

There is generally a strong main path between the satellite and terrestrial users. In such a case, the channel model is regarded as either an additive white Gaussian noise (AWGN) channel or a Rician channel with a dominant line-of-sight path in most of the cases. Apparently, both of the two channel models experience small channel fluctuations. When the terrestrial users distribute close to each other, their channel matrices would have low spatial orthogonality, making it difficult to separate the terrestrial users by means of beamforming. Opportunistic beamforming techniques can be considered in this case, which can induce large and fast channel fluctuations so that spatial orthogonality can be utilized for beamforming [9]. Moreover, when terrestrial users distribute relatively far from each other, the spatial orthogonality can also be exploited since the channels would have low relevance due to the sparse distribution.

- Heterogeneous Users with Individual Features

For the terrestrial cellular networks, although there are various types of mobile phones and various standards, the communication architectures are all identical. In such a case, the beamforming models in cellular networks are also universal for different users and situations. However, the user types of satellite networks are heterogeneous with various features, which can be hand-held terminals, aircrafts, ships, and earth stations. Moreover, in some specific application scenarios, different types of users may be served simultaneously. While hand-held terminals may only be equipped with a single antenna, earth stations are able to afford large-scale antenna arrays. Instead of a universal beamforming technique for a single type of users, the beamforming models should be different according to the types of serviced users, or a universal solution is expected to address all these different cases. Besides, in satellite systems, constant envelope modulation are employed for the sake of maximizing the efficiency of EIRP. It would also be a challenge to generate constant envelope signals for heterogeneous users with individual features.

- High Mobility of Satellites

Except geostationary earth orbit (GEO) satellites, the satellites generally move at a high speed relative to the earth, especially in terms of LEOs. For example, the period of the Iridium system at the orbit of 780 km is about 100 min, which means an angular velocity of $3.6^\circ/\text{min}$. The beams of the satellite need to change in a fast manner according to the relative location between the satellite and terrestrial users. Moreover, when the user is out of the coverage range of beamforming, the link would be terminated, and thus a high-efficient handover is also required. In cases of LEO and MEO, the fast moving of the satellite would also cause large doppler shift, which may significantly deteriorate the system performance, particularly for narrowband signals. Doppler shift compensation techniques need to be adopted to ensure reliable communication.

2.1.1 *Multi-Beam Joint Processing*

As stated in the introduction, frequency reuse is possible in multi-beam satellite systems as long as the inter-beam interferences can be carefully controlled. In current multi-beam satellite systems, the typical frequency reuse factor of four is generally adopted for the sake of inter-beam interference limitation, as illustrated in Fig. 2.1a. Full frequency reuse, as illustrated in Fig. 2.1b, can exploit higher spectrum efficiency with the reuse factor of one. However, the inter-beam interference may significantly deteriorate the system performance, especially in the overlap area of adjacent beams.

Multi-beam joint processing, which is based on the technique of digital beam-forming, provides a possible way of full frequency reuse without significant performance loss [2]. Instead of each beam serving its users separately, signals of all users of all beams are joint precoded by means of beamforming, and then

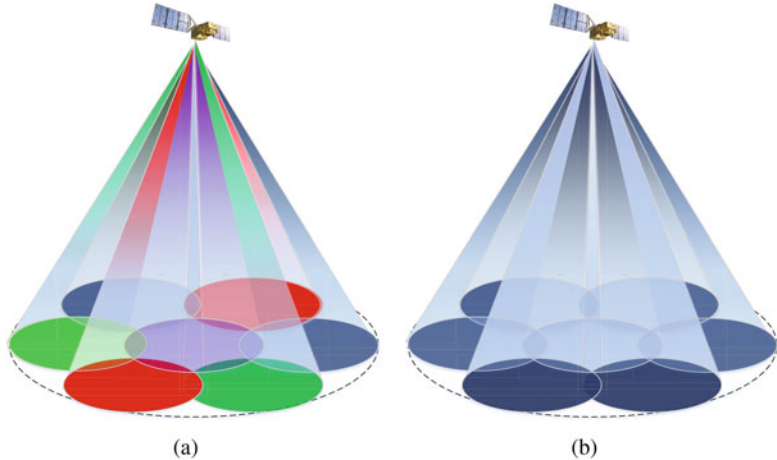


Fig. 2.1 The beams with the same color use the same frequency. Thus in (a), four different frequencies are used among beams, while in (b) only one frequency is used among all beams

transmitted by all beams with full frequency reuse. The inter-beam interference can be mitigated by adjusting the beamforming weighting factors on antennas at the transmitting with the help of CSI. By utilizing the spatial orthogonality of users, higher spectrum efficiency can be exploited when digital beamforming techniques are adopted. Generally, the multi-beam joint processing is more potential to be adopted in the uplink case than the downlink case. For the downlink transmission of satellites, due to the power constraints, it may not be practical to serve all users with full frequency reuse simultaneously, in which user scheduling techniques need to be considered combined with frequency reuse techniques to optimize the system performance.

2.1.2 *Multigroup Precoding*

The channel between the satellite and terrestrial users is usually modeled as an AWGN channel or a Rician channel, which experiences small channel fluctuations. When terrestrial users distribute close to each other, it is difficult to separate different users by means of beamforming with full frequency reuse. In this case, instead of employing beamforming for each user separately, we can divide the users into groups according to the location distribution and employ multigroup precoding. As illustrated in Fig. 2.2, terrestrial users are divided into groups according to their locations and serviced by the satellite. For users in different groups, spatial orthogonality can be utilized, and beamforming is employed between groups when full frequency reuse is adopted. For users within the same group, since beamforming is difficult to be exploited due to small channel fluctuations, other multi-access techniques may be considered, such as time division multiple access (TDMA) or frequency division multiple access (FDMA).

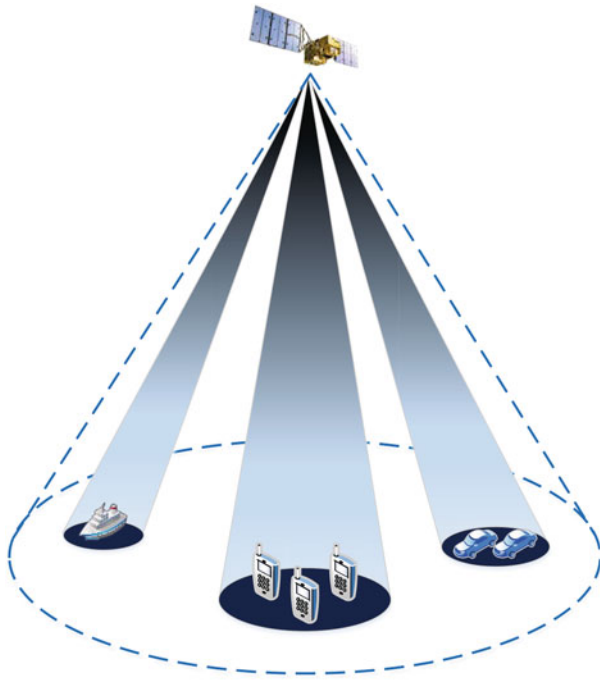


Fig. 2.2 Multigroup precoding satellite system

Although beamforming techniques is difficult to be employed within each group to achieve frequency reuse, this problem can be avoided when it comes to multicasting. Multicast multigroup precoding is studied for satellite communication systems [10], in which users are divided in to groups and the same symbol is broadcasted to multiple users in the same group. Also, for users in different groups, digital beamforming techniques are employed to achieve full frequency reuse. Moreover, user scheduling methods can be exploited in this system to achieve higher multiuser diversity gaining.

Digital beamforming techniques are based on antenna arrays and CSI is needed when calculating the weighting factors on antennas. In next generation wireless systems, massive MIMO is attractive for its potential high data rates and energy efficiency based on large antenna arrays. However, when it comes to large antenna arrays, there exist several challenges especially in frequency division duplexing (FDD) cases. When the scale of antenna arrays increases, the number of CSIs required for beamforming also increases, leading to a large number of training symbols for channel estimation. Furthermore, in FDD systems, the CSI feedback will become a prominent problem if large scale of antenna arrays are equipped. To overcome these problems, the method of two-stage beamforming is proposed to reduce the CSI needed for beamforming in large antenna arrays systems [11]. Terrestrial users are divided into groups with approximately the same channel

Table 2.1 ITU-R table of allocations in Ka band

Frequency bands	ITU-R region 1	ITU-R region 2	ITU-R region 3
17.3–17.7 GHz	FSS (space-Earth)	FSS	FSS
	BSS (feeder links)	BSS	BSS
	Radiolocation	Radiolocation	Radiolocation
17.7–19.7 GHz	FSS (space-Earth)	FSS	FSS
	BSS (feeder links)	FS	BSS
	FS		FS
27.5–29.5 GHz	FSS (Earth to space)	FSS	FSS
	FS	FS	FS
	MS (mobile services)	MS	MS

covariance matrix, and the beamforming process is then decomposed into two stages: the outer beamforming and the inner beamforming. In the two-stage beamforming, only the inner beamforming requires actual CSI, which has much smaller dimensions compared with the initial problem.

2.1.3 Cooperative Beamforming in Terrestrial-Satellite Networks

The rapid growing data traffic brings more and more pressure to the wireless network, which is predicted to increase by over 10,000 times in the next 20 years. Spectrum sharing has shown great potential for improving the capacity performance. For example, in the S-band, 1885–1980, 2010–2025 and 2110–2170 MHz are allocated to the terrestrial communication systems IMT-2000 (International Mobile Telecom System-2000), while 1980–2010 and 2170–2200 MHz are allocated to satellite communication. Since the service in satellite systems is usually scheduled instead of burst, it is possible for terrestrial systems to share the satellite frequency band when the satellite frequency band is not occupied. Moreover, in the next generation wireless networks, the millimeter-wave (mm-wave) band of 30–90 GHz has drawn great attention for the large amount of possible bandwidth. Meanwhile, satellite communications have also shown interest in the mm-wave band for the sake of the increasing traffic demands, especially the Ka band of 26.5–40 GHz [12]. Table 2.1 gives the ITU-R table of allocation in 27.5–29.5 GHz, part of the Ka band. We can observe that parts of the Ka band has already be allocated to the satellite service. It can be envisioned that the developing of mm-wave in both terrestrial and satellite communications may result in spectrum conflict in the future, and thus the spectrum-sharing techniques would be rather important.

Cognitive ratio (CR) technique is considered as one of the spectrum-sharing techniques in terrestrial-satellite networks, in which the second user dynamically utilizes the spectrum when managing the interference caused to the main user. In CR

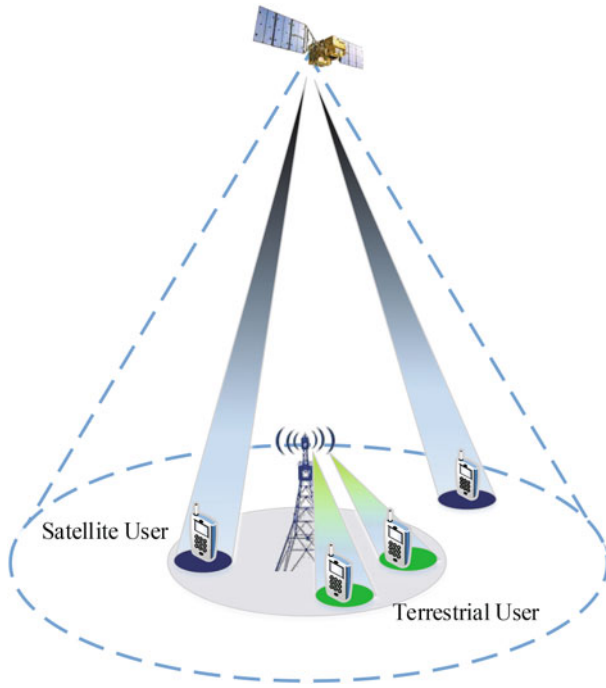


Fig. 2.3 Cooperative beamforming in terrestrial-satellite networks

networks, co-channel interference (CCI) management is the key problem, and thus interference mitigation techniques play an important role in the system performance. The digital beamforming technique, which is based on antenna arrays, can be exploited for interference mitigation in terrestrial-satellite networks by utilizing the spatial orthogonality [12]. Cooperative beamforming is employed at the satellite when both the satellite users and terrestrial users are taken into consideration as constraints for beamforming. By carefully adjusting the weighting factors on antennas at the satellite, the satellite can share the spectrum with terrestrial networks while limiting the interference caused to terrestrial users, as illustrated in Fig. 2.3. Since the satellite generally has limited computation capability, for the sake of reducing complexity, one semi-adaptive beamforming technique is proposed for OFDM based terrestrial-satellite mobile system [13].

2.2 Multicast Beamforming

Due to the rapid development and popularity of mobile devices, such as smartphones and tablets, as well as the development of mobile communication, wireless data service is extended from conventional text messaging or web browsing to multimedia

services such as video streaming, music streaming, and mobile TV [14]. Compared with conventional services, multimedia services generally require larger data traffic, which adds more pressure to the wireless networks. On the other hand, the same multimedia services may be required by multiple users simultaneously, especially for popular videos or TV programs, which is called as content diversity in [15]. Considering both the large data traffic and content diversity, one efficient technique for multimedia services is multicasting. Instead of providing service via point-to-point transmission, multicast transmission delivers the same content to multiple users simultaneously, which can significantly improve the system performance.

A typical max-min fair problem for multicast transmission was discussed in [16], in which multiple groups were served by one base station (BS), and the optimal beamforming vectors were calculated when maximizing the minimum rate of all users under the total power constraint. In [17], coordinated multicast beamforming was investigated for multicell networks, when only one group of users were served by each BS. The problem of minimum power multicast beamforming was investigated in [18], in which the non-orthogonal multiple access technique was adopted within groups. In [19], a content-centric multicast beamforming model for cache-enabled cloud RAN was proposed. In the cloud RAN, all BSs were connected to a central processor, and worked cooperatively to provide multicast transmission for multiple groups. Then, the multicast transmission for satellite communications was also studied in [20], in which the system capacity was maximized under per-antenna power constraints.

While the terrestrial networks can achieve high-speed data service at low cost [21, 22], in the next generation of wireless communication, satellite based access is one way to complement terrestrial based networks to ensure ubiquitous, 100% geographic coverage [23]. The coexistence and cooperation of terrestrial and satellite networks have been investigated in recent works. In [24], the author applied the technique of Cognitive Radio (CR) into terrestrial-satellite networks, enabling dynamic spectrum access for the satellite. Then, in [25], the scenario of the hybrid satellite terrestrial relay network (HSTRN) is investigated, in which a relay with single antenna is utilized to assist the transmission of the satellite in the presence of co-channel interference (CCI).

In this part, we consider a multimedia multicast integrated terrestrial-satellite network, in which the BSs and satellite cooperatively provide ubiquitous coverage for ground users. Due to the content diversity of multimedia services, multicast transmission can be utilized to serve multiple users that require the same contents simultaneously. For both BSs and the satellite, users will be divided into groups according to the required contents, while beamforming is executed among groups reusing the entire bandwidth. Taking both the system performance and user fairness into consideration, we maximize the total capacity of the system while introducing a minimum capacity constraint for the satellite. Then, by means of the successive convex approximation (SCA) approach and the Lagrangian dual method, we obtain the optimal power allocation scheme for the system.

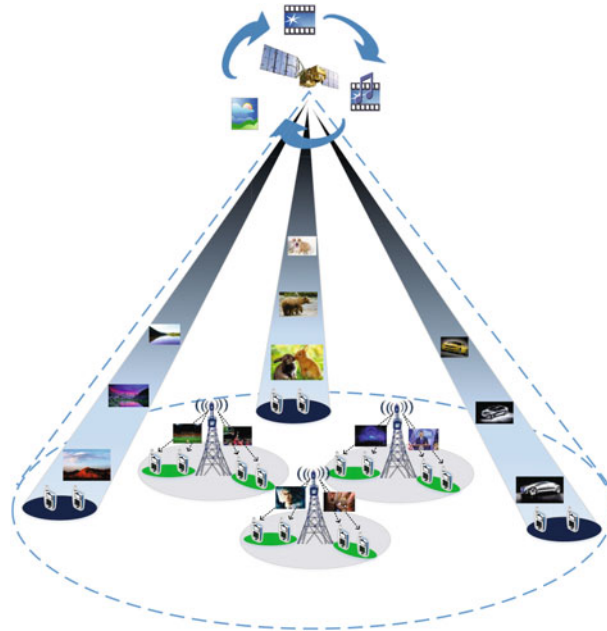


Fig. 2.4 System model of the multimedia multicast integrated terrestrial-satellite network

2.2.1 System Model

Consider a multimedia multicast network as shown in Fig. 2.4, in which L BSs and a satellite cooperatively provide service for ground users. The BSs are equipped with N antennas, and can provide high speed data transmission for high density populations in urban areas. On the other hand, the satellite, equipped with M antennas, can provide extra data service for those users without coverage of BSs, such as users in suburban areas or mountain areas.

All users are assumed to be equipped with a single antenna, and will be grouped according to the required contents. Considering the content diversity of multimedia services, multicasting can be utilized to improve the system performance. The users that require the same contents, such as video streaming or mobile TV, will be divided into the same group for multicast transmission. With multi-antennas, each BS will serve N groups with N different requiring contents within its coverage, when beamforming is executed for reusing the entire bandwidth. The user set of group J in the coverage of BS I is represented by $U_{B,I,J} = \{u_{B,I,J,1}, \dots, u_{B,I,J,|U_{B,I,J}|}\}$, in which $|U_{B,I,J}|$ is the total user number of user set $U_{B,I,J}$. Also, the satellite will provide multicast transmission for M groups, and the user set of group J of the satellite is $U_{S,J} = \{u_{S,J,1}, \dots, u_{S,J,|U_{S,J}|}\}$, in which $|U_{S,J}|$ is the total user number of satellite group J . Note that the entire bandwidth is reused in the whole system, and thus there will exist CCI among groups and also between two systems.

2.2.2 Problem Formulation

In the multimedia multicast integrated terrestrial-satellite network, each BS provide multicast transmission for N groups when beamforming is executed. The transmit signal of BS I is

$$\mathbf{x}_I = \sum_{j=1}^N \boldsymbol{\omega}_{I,j} \sqrt{P_{B,I,j}} s_{B,I,j}, \quad (2.1)$$

in which $\boldsymbol{\omega}_{I,j}$, $\|\boldsymbol{\omega}_{I,j}\| = 1$, is the beamforming vector, $P_{B,I,j}$ is the transmit power, and $s_{B,I,j}$, $E[|s_{B,I,j}|^2] = 1$, is the multicast signal for all the users in group j . As stated in the system model, all users in the same group require the same contents, and thus for each group only one multicast signal is transmitted.

Since there are multiple users that experience distinct channels within each group, we cannot completely cancel the interference among groups. In conventional point-to-point transmission, the beamforming vectors of maximum ratio transmission (MRT) is designed as

$$\boldsymbol{\omega}_i = \frac{\mathbf{h}_i}{\|\mathbf{h}_i\|}, \quad (2.2)$$

where \mathbf{h}_i is the channel from the transmitter equipped with multi-antennas to the corresponding user with single antenna. We extend this to point-to-multipoint transmission, and then the multicast beamforming vectors based on MRT is:

$$\boldsymbol{\omega}_{I,j} = \frac{\sum_{k=1}^{|U_{B,I,j}|} \mathbf{h}_{I,j,k}}{\left\| \sum_{k=1}^{|U_{B,I,j}|} \mathbf{h}_{I,j,k} \right\|}, \quad (2.3)$$

where $\mathbf{h}_{I,j,k}$ is the channel from the BS I to user k in group j .

Similarly, the transmit signal of the satellite is

$$\mathbf{x}_S = \sum_{j=1}^M \boldsymbol{\nu}_j \sqrt{P_{S,j}} s_{S,j}, \quad (2.4)$$

where $\boldsymbol{\nu}_j$, $\|\boldsymbol{\nu}_j\| = 1$, is the beamforming vector, $P_{S,j}$ is the transmit power and $s_{S,j}$, $E[|s_{S,j}|^2] = 1$, is the multicast signal for group j .

For simplification, in the grouping scheme of the satellite, the satellite users will be grouped according to both the required contents and the geographic locations. The users that require the same contents in the same small area will be divided into one group. Due to the small channel fluctuations of the satellite channel, the

channels of the users in one group can be approximately viewed as the same. Then, zeroforcing beamforming (ZFBF) can be utilized to cancel interference among groups. Let $\mathbf{g}_{S,1}, \mathbf{g}_{S,2}, \dots, \mathbf{g}_{S,M}$ be the channel from the satellite to the satellite users of different groups, $\mathbf{G} = [\mathbf{g}_{S,1}, \mathbf{g}_{S,2}, \dots, \mathbf{g}_{S,M}]^H$. The ZFBF vectors can be calculated by

$$[\mathbf{v}_1, \dots, \mathbf{v}_M] = \mathbf{G}^{-1} \mathbf{D}, \quad (2.5)$$

where D is the normalization diagonal matrix, and $\mathbf{D}^2 = \text{diag}\{\frac{1}{(\mathbf{G}^{-H}\mathbf{G}^{-1})_{1,1}}, \dots, \frac{1}{(\mathbf{G}^{-H}\mathbf{G}^{-1})_{N,N}}\}$, where $(\mathbf{H})_{n,n}$ is the n th element of the diagonal of \mathbf{H} .

Then the received signal of the BS user K in group J of BS I is

$$\begin{aligned} y_{B,I,J,K} &= \mathbf{h}_{I,J,K}^H \boldsymbol{\omega}_{I,J} \sqrt{P_{B,I,J}} s_{B,I,J} + n \\ &+ \mathbf{h}_{I,J,K}^H \sum_{j=1, j \neq J}^N \boldsymbol{\omega}_{I,j} \sqrt{P_{B,I,j}} s_{B,I,j} + \mathbf{g}_{B,I,J,K}^H \sum_{j=1}^M \mathbf{v}_j \sqrt{P_{S,j}} s_{S,j}, \end{aligned} \quad (2.6)$$

where $\mathbf{g}_{B,I,J,K}$ is the channel from the satellite to the BS users, and n is the additive white Gaussian noise (AWGN). The SINR can then be calculated as

$$\gamma_{B,I,J,K} = \frac{|\mathbf{h}_{I,J,K}^H \boldsymbol{\omega}_{I,J}|^2 P_{B,I,J}}{\sum_{\substack{j=1, \\ j \neq J}}^N |\mathbf{h}_{I,J,K}^H \boldsymbol{\omega}_{I,j}|^2 P_{B,I,j} + \sum_{j=1}^M |\mathbf{g}_{B,I,J,K}^H \mathbf{v}_j|^2 P_{S,j} + \sigma_n}, \quad (2.7)$$

where σ_n is the AWGN power.

The received signal of the satellite user is

$$\begin{aligned} y_{S,J,K} &= \mathbf{g}_{S,J}^H \sum_{j=1}^M \mathbf{v}_j \sqrt{P_{S,j}} s_{S,j} + n \\ &= \mathbf{g}_{S,J}^H \mathbf{v}_J \sqrt{P_{S,J}} s_{S,J} + n. \end{aligned} \quad (2.8)$$

Since the satellite users are located in areas without coverage of BSs, we ignore the interference from the BSs. The SINR can then be calculated as

$$\gamma_{S,J,K} = \frac{|\mathbf{g}_{S,J}^H \mathbf{v}_J|^2 P_{S,J}}{\sigma_n} \quad (2.9)$$

Based on the Shannon's theorem, the capacity of the whole system can be calculated as

$$\begin{aligned} C_B + C_S &= \sum_{I=1}^L \sum_{J=1}^N \sum_{K=1}^{|U_{B,I,J}|} C_{B,I,J,K} + \sum_{J=1}^M |U_{S,J}| C_{S,J,1} \\ &= \sum_{I=1}^L \sum_{J=1}^N \sum_{K=1}^{|U_{B,I,J}|} \log_2(1 + \gamma_{B,I,J,K}) + \sum_{J=1}^M |U_{S,J}| \log_2(1 + \gamma_{S,J,1}). \end{aligned} \quad (2.10)$$

Due to the different channel conditions of users as well as the co-channel interference among users, it is of great importance to allocate the power reasonably to achieve optimal system capacity performance. However, since the satellite will cause interference to all the BSs users within its coverage, it may lead to a relative small capacity for the satellite if we simply maximize the total capacity of the system. Thus, taking fairness into consideration, we introduce the minimum capacity constraint for the satellite to protect the performance of the satellite. Then, the optimization problem can be formulated as

$$\max_{\mathbf{P}_B, \mathbf{P}_S} C_B + C_S \quad (2.11)$$

$$C1 : C_S \geq C_{S,0},$$

$$C2 : \sum_{J=1}^N P_{B,I,J} \leq P_{B,I,\max}, \forall I,$$

$$C3 : \sum_{J=1}^M P_{S,J} \leq P_{S,\max},$$

$$C4 : P_{B,I,J}, P_{S,J} \geq 0,$$

where C1 is the minimum capacity constraint for the satellite, C2 is the maximum transmit power constraint for the BSs, and C3 is the maximum transmit power constraint for the satellite.

2.2.3 *Optimal Power Allocation Algorithm*

We have formulated the maximum capacity optimization problem based on the minimum satellite capacity constraint as (2.11). However, problem (2.11) is non-convex due to the non-convex objective function C_B . In this section, by means of the successive convex approximation (SCA) approach [26], we transform the non-convex problem into a series of convex subproblems, which are then solved using the Lagrangian dual method.

2.2.3.1 Transformation of Optimization Problem

The original optimization problem in (2.11) is a non-convex problem of high complexity. To overcome this problem, we adopt the successive convex approximation (SCA) approach proposed in [26], which transforms the non-convex problem into a series convex subproblems by approximating the non-convex function using some convex function around the feasible point and then solves the subproblem iteratively.

While constraints C1–C4 are all concave or linear, problem (2.11) is non-convex because of the non-convex function $C_{B,I,J,K} = \log_2(1 + \gamma_{B,I,J,K})$ in the objective function. We approximate this non-convex function by logarithmic approximation [27]:

$$\ln(1 + \gamma_{B,I,J,K}) \geq \theta_{B,I,J,K} \ln \gamma_{B,I,J,K} + \beta_{B,I,J,K}, \quad (2.12)$$

which is tight at $\gamma_{B,I,J,K} = \bar{\gamma}_{B,I,J,K}$ if the approximation parameters are selected as:

$$\theta_{B,I,J,K} = \frac{\bar{\gamma}_{B,I,J,K}}{1 + \bar{\gamma}_{B,I,J,K}}, \quad (2.13)$$

$$\beta_{B,I,J,K} = \ln(1 + \bar{\gamma}_{B,I,J,K}) - \frac{\bar{\gamma}_{B,I,J,K}}{1 + \bar{\gamma}_{B,I,J,K}} \ln \bar{\gamma}_{B,I,J,K}.$$

Apply the logarithmic approximation to both C_B and C_S , and change the variables by $\hat{\mathbf{P}}_S = \ln \mathbf{P}_S$, $\hat{\mathbf{P}}_B = \ln \mathbf{P}_B$, the lower bound of the objective function is obtained as follows:

$$C_B + C_S \geq C_B(e^{\hat{\mathbf{P}}_B}, \boldsymbol{\theta}_S, \boldsymbol{\beta}_S) + C_S(e^{\hat{\mathbf{P}}_S}, \boldsymbol{\theta}_S, \boldsymbol{\beta}_S) \quad (2.14)$$

$$= \sum_{I=1}^L \sum_{J=1}^N \sum_{K=1}^{|U_{B,I,J}|} \left[\frac{1}{\ln 2} (\theta_{B,I,J,K} \ln \gamma_{B,I,J,K}(e^{\hat{P}_{B,I,J}}) + \beta_{B,I,J,K}) \right]$$

$$+ \sum_{J=1}^M |U_{S,J}| \left[\frac{1}{\ln 2} (\theta_{S,J,1} \ln \gamma_{S,J,1}(e^{\hat{P}_{S,J}}) + \beta_{S,J,1}) \right],$$

in which

$$\gamma_{B,I,J,K}(e^{\hat{P}_{B,I,J}}) = \frac{|\mathbf{h}_{I,J,K}^H \boldsymbol{\omega}_{I,J}|^2 e^{\hat{P}_{B,I,J}}}{\sum_{j=1, j \neq J}^N |\mathbf{h}_{I,J,K}^H \boldsymbol{\omega}_{I,j}|^2 e^{\hat{P}_{B,I,j}} + \sum_{j=1}^M |\mathbf{g}_{B,I,J,K}^H \mathbf{v}_j|^2 e^{\hat{P}_{S,J}} + \sigma_n}, \quad (2.15)$$

$$\gamma_{S,J,1}(e^{\hat{P}_{S,J}}) = \frac{|\mathbf{g}_{S,J}^H \mathbf{v}_J|^2 e^{\hat{P}_{S,J}}}{\sigma_n}.$$

Then, substituting the objective function with the lower bound as well as doing the variable transformation, we can obtain the approximate subproblem as

$$\min_{\hat{\mathbf{P}}_B, \hat{\mathbf{P}}_S} - \left[C_B(e^{\hat{\mathbf{P}}_B}, \boldsymbol{\theta}_S, \boldsymbol{\beta}_S) + C_S(e^{\hat{\mathbf{P}}_S}, \boldsymbol{\theta}_S, \boldsymbol{\beta}_S) \right] \quad (2.16)$$

$$C1 : C_S(e^{\hat{\mathbf{P}}_S}, \boldsymbol{\theta}_S, \boldsymbol{\beta}_S) - C_{S,0} \geq 0,$$

$$C2 : P_{B,I,\max} - \sum_{J=1}^N e^{\widehat{P}_{B,I,J}} \geq 0, \forall I,$$

$$C3 : P_{S,\max} - \sum_{J=1}^M e^{\widehat{P}_{S,J}} \geq 0.$$

Note that we have transformed the problem into the standard form of convex optimization. According to [28], the log-sum-exp function is convex, and thus it is easy to prove that the subproblem (2.16) is a standard convex optimization problem. However, problem (2.16) is only the lower bound approximation of the original problem. To obtain the solution of the original problem, we update the approximate parameters in (2.13) using the results of the subproblem. Then, the updated parameters will be used for the calculation of the next iteration until the results converge.

2.2.3.2 Lagrangian Dual Method

In the last section, we have transformed the original non-convex optimization problem into a series convex subproblems by utilizing the SCA approach and logarithmic approximation. Then, in each iteration of the SCA approach, we solve the transformed subproblem in (2.16) by means of the Lagrangian dual method. The Lagrangian function of problem (2.16) is as follows:

$$\begin{aligned} L(e^{\widehat{\mathbf{P}}_B}, e^{\widehat{\mathbf{P}}_S}, \eta, \boldsymbol{\mu}, \lambda) \\ = -C_B(e^{\widehat{\mathbf{P}}_B}, \boldsymbol{\theta}_S, \boldsymbol{\beta}_S) - C_S(e^{\widehat{\mathbf{P}}_S}, \boldsymbol{\theta}_S, \boldsymbol{\beta}_S) \\ - \eta \left[\sum_{J=1}^M |U_{S,J}| C_{S,J,1}(e^{\widehat{P}_{S,J}}, \theta_{S,J,1}, \beta_{S,J,1}) - C_{S,0} \right] \\ - \sum_{I=1}^L \mu_I (P_{B,I,\max} - \sum_{J=1}^N e^{\widehat{P}_{B,I,J}}) \\ - \lambda (P_{S,\max} - \sum_{J=1}^M e^{\widehat{P}_{S,J}}), \end{aligned} \quad (2.17)$$

where $\eta, \boldsymbol{\mu}$ and λ are the Lagrange multipliers of constraints C1, C2 and C3 in (2.16).

The dual function is

$$D(\eta, \boldsymbol{\mu}, \lambda) = \inf_{\widehat{\mathbf{P}}_B, \widehat{\mathbf{P}}_S} \{L(e^{\widehat{\mathbf{P}}_B}, e^{\widehat{\mathbf{P}}_S}, \eta, \boldsymbol{\mu}, \lambda)\}. \quad (2.18)$$

Then the Lagrangian dual problem is

$$\max_{\eta, \mu, \lambda} D(\eta, \mu, \lambda) \quad (2.19)$$

$$s.t. \quad \eta, \mu, \lambda \geq 0.$$

By solving $\frac{\partial L}{\partial P_{B,I,J}} = 0$ and $\frac{\partial L}{\partial P_{S,J}} = 0$, we can obtain the optimal solutions as

$$P_{B,I,J} = e^{\widehat{P}_{B,I,J}} = \left[\frac{\sum_{K=1}^{|U_{B,I,J}|} \theta_{B,I,J,K}}{\mu_I \ln 2 + \sum_{j=1}^N \sum_{\substack{k=1 \\ j \neq J}}^{|U_{B,I,j}|} \theta_{B,I,j,k} \frac{|\mathbf{h}_{I,j,k}^H \boldsymbol{\omega}_{I,J}|^2}{I_{B,I,j,k}[t]}} \right]^+,$$

$$P_{S,J} = e^{\widehat{P}_{S,J}} = \left[\frac{(1 + \eta) |U_{S,J}| \theta_{S,J,1}}{\lambda \ln 2 + \sum_{i=1}^L \sum_{j=1}^N \sum_{k=1}^{|U_{B,i,j}|} \theta_{B,i,j,k} \frac{|\mathbf{g}_{B,i,j,k}^H \mathbf{v}_J|^2}{I_{B,i,j,k}[t]}} \right]^+, \quad (2.20)$$

where $(x)^+ = \max(0, x)$, and we define

$$I_{B,i,j,k}[t] = \sum_{l=1, l \neq j}^N |\mathbf{h}_{i,j,k}^H \boldsymbol{\omega}_{i,l}|^2 e^{\widehat{P}_{B,i,l}[t]} + \sum_{l=1}^M |\mathbf{g}_{B,i,j,k}^H \mathbf{v}_l|^2 e^{\widehat{P}_{S,l}[t]}, \quad (2.21)$$

which is calculated using the results of last iteration.

The optimal solution of the power allocation scheme is in the form of the Lagrange multipliers. Since $D(\eta, \mu, \lambda)$ in (2.18) is not differentiable. We calculate the Lagrange multipliers using the subgradient method:

$$\eta[t_\delta + 1] = [\eta[t_\delta] - \delta_\eta[t_\delta + 1](C_S(\boldsymbol{\theta}_S, \boldsymbol{\beta}_S) - C_{S,0})]^+, \quad (2.22)$$

$$\mu_I[t_\delta + 1] = \left[\mu_I[t_\delta] - \delta_{\mu_I}[t_\delta + 1](P_{B,I,\max} - \sum_{J=1}^N P_{B,I,J}) \right]^+, \forall I,$$

$$\lambda[t_\delta + 1] = \left[\lambda[t_\delta] - \delta_\lambda[t_\delta + 1](P_{S,\max} - \sum_{J=1}^M P_{S,J}) \right]^+,$$

where t_δ is the iteration step, and $\delta[t_\delta + 1]$ is the step size in each iteration of subgradient method.

Algorithm 1 Optimal power allocation algorithm

```

1: Initialize  $t = 1$ ,  $\theta_B = \theta_S = 1$ ,  $\beta_B = \beta_S = 0$  and  $\mathbf{P}_B[1] = \mathbf{P}_S[1] = 0$ 
2: repeat
3:   Initialize  $t_\delta = 1, \eta > 0, \mu > 0, \lambda > 0$ 
4:   Initialize  $\mathbf{I}_B$  referring to (2.21)
5:   repeat
6:     for  $I = 1$  to  $L$  do
7:       for  $J = 1$  to  $N$  do
8:         Update  $P_{B,I,J}$  referring to (2.20)
9:       end for
10:      end for
11:      for  $J = 1$  to  $J = M$  do
12:        Update  $P_{S,J}$  referring to (2.20)
13:      end for
14:      Update  $\eta, \mu, \lambda$  referring to (2.22)
15:      Update  $\mathbf{I}_B$  referring to (2.21)
16:      Set  $t_\delta = t_\delta + 1$ 
17:    until  $\mathbf{P}_B, \mathbf{P}_S$  converge
18:    Set  $\mathbf{P}_{B,I}[t] = \mathbf{P}_{B,I}[t + 1]$ 
19:    Update  $\theta, \beta$  referring to (2.13)
20:    Set  $t = t + 1$ 
21: until  $\mathbf{P}_B, \mathbf{P}_S$  converge

```

The optimal power allocation algorithm is summarized as Algorithm 1. We initiate the algorithm from a feasible point $\mathbf{P}_B[1], \mathbf{P}_S[1]$. In each iteration of the outer loop, we calculate the approximate parameters based on the results of last iteration and transform the original problem into a convex subproblem by logarithmic approximation. Then, in the inner loop, we solve the convex subproblem by means of the Lagrangian dual method. By solving the transformed subproblems iteratively, the results will converge to the optimal solution of problem (2.11).

2.2.4 Performance Evaluation

In this section, we provide the simulation results to evaluate the performance of the proposed power allocation algorithm. The satellite is assumed to be a LEO with a orbit of 1000 km. For simplification, we assume the total user number in each group is the same, and all users are uniformly distributed in the network. The carrier frequency is set as 2 GHz while the bandwidth B is set as 10 MHz. The AWGN power can then be calculated by $\sigma_n = BN_0$, in which $N_0 = -174$ dBm/Hz is the AWGN power spectral density. The maximum transmit power of all BSs are uniformly set as $P_{B,max} = 43$ dBm. The radio frequency (RF) power of the satellite is 80 W, and the transmit antenna gain is assume to be 50 dBi. The channels from BSs to users experience Rayleigh fading, and are modeled according to [29], while

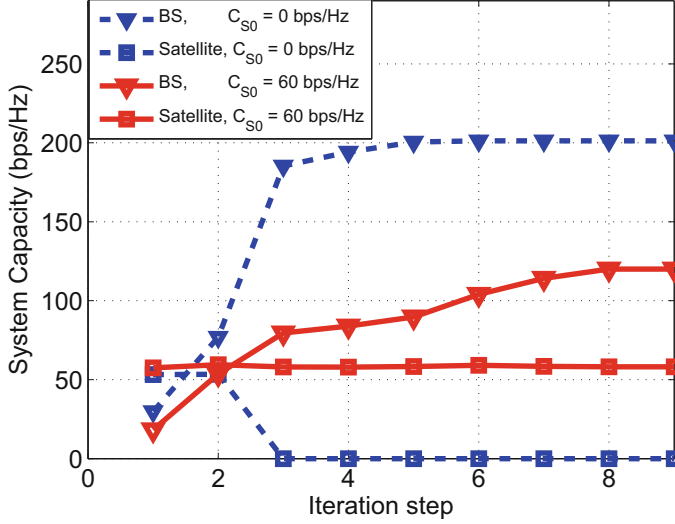


Fig. 2.5 The convergence process over iterations

the channels from the satellite to users are modeled as Rician channel according to [30]. Also, two other power allocation strategies are considered for comparison in the simulation, which are referred to as “Suboptimal Searching Algorithm” and “Greedy Algorithm”.

Figure 2.5 shows the convergence process of the proposed Algorithm 1, in which the BS number is set as $L = 3$, the group size is set as $|U_{S,J}| = 3$, the antenna numbers are set as $N = 2$ and $M = 2$. We can observe that for different settings of minimum capacity constraints $C_{S,0}$, the algorithm converges fast within ten steps. Also, since the satellite will cause interference to all BS users, the satellite capacity converges to almost zero if we set the minimum satellite capacity $C_{S,0} = 0$ bps/Hz.

Figure 2.6 gives the total capacity of the system of different BS numbers, in which we set the minimum satellite capacity constraint $C_{S,0} = 60$ bps/Hz, and the group size $|U_{S,J}| = 3$. We can observe that the total capacity almost increases linearly as BS number increases in all the cases, which indicates that introducing new BS to the system will not deteriorate the system performance. Also, with more transmit antennas, the system capacity will be improved, and we can see that increasing the antennas of either BSs or the satellite can achieve similar improvements. The system capacity increases by about 31.7% when both the BSs antennas and the satellite antennas increase from 2 to 4.

In Fig. 2.7, the influence of different group size on the system capacity is illustrated, in which the BS number is set as $L = 5$, the minimum satellite capacity constraint is set as $C_{S,0} = 60$ bps/Hz, and the group size is set as $|U_{S,J}| = 3$. Similar to the case of BS numbers, the total capacity also increases almost linearly with the group size. In the satellite system, since ZFBF is executed among groups, the satellite capacity is proportional to the group size. However, in the BSs system,

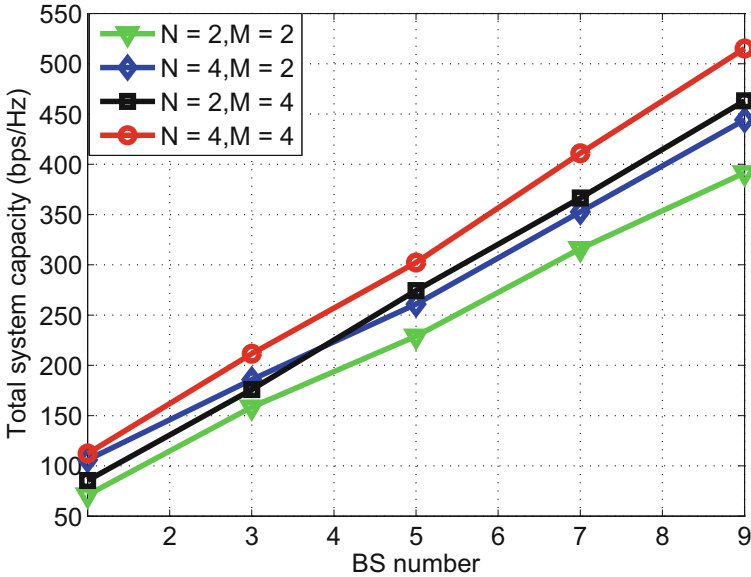


Fig. 2.6 Total system capacity of different interference temperature limit and antennas

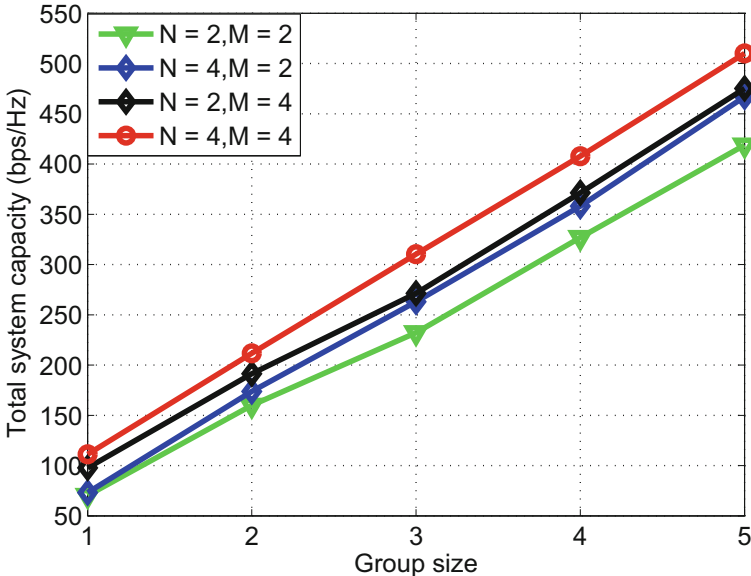


Fig. 2.7 Total system capacity of different group size

larger group size may cause larger inter-group interference, since the designing of beamforming vectors need to balance among all the users. On the other hand, larger group size also provides larger multi-user diversity gaining, which compensates

for the loss from inter-group interference. In multimedia multicast networks, the main system performance gaining comes from multicast transmission to groups. The linear increasing system performance indicates the potentials of multimedia multicast networks.

Finally, with $L = 3$, $N = 3$, $M = 3$, $C_{S,0} = 60$ bps/Hz, and $|U_{S,J}| = 4$, the comparison results with two other strategies are illustrated in Fig. 2.8. In the “Suboptimal Searching Algorithm”, a capacity-maximizing based searching is executed separately for each group to obtain the suboptimal power allocation scheme, while the water filling algorithm is adopted according to the channel conditions under the satellite capacity constraint in the “Greedy Algorithm”. We can observe that for different maximum BS transmit power, our proposed algorithm can achieve higher capacity performance, outperforming the two algorithms quite well. Due to the inter-group performance, the water filling algorithm cannot achieve satisfying performance, in which there is about 70% capacity loss compared to the optimal algorithm. The “Suboptimal Searching Algorithm” can achieve much better performance than the greedy strategy, since each group is optimized separately taking the inter-group interference into consideration. However, since only the suboptimal results are obtained, there is still about 15% loss of performance compared with the optimal algorithm.

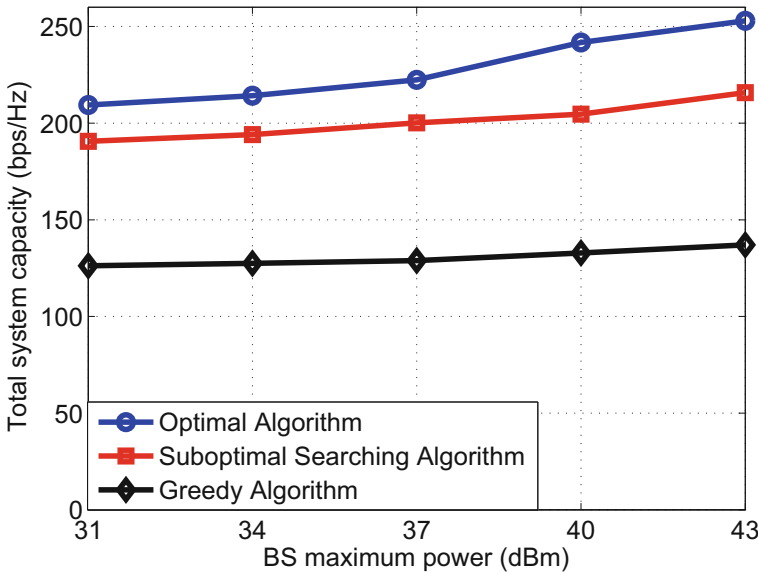


Fig. 2.8 Comparison of system performance with the heuristic strategy

2.3 Smart Communication Satellite

The satellite internet provides for both terrestrial and space users the communication and internet access services via communication satellites on different orbits. In the past few years, the satellite internet has evolved into a hot topic that captures the attention of both scientific research and industry operation all over the world. Google, SpaceX, and some other giants have all initiated their own satellite internet plan aiming to provide internet coverage, globally or specifically, using space network nodes such as medium earth orbit (MEO) satellite, e.g., O3b plan, and low earth orbit (LEO) satellite.

Satellites on various kinds of orbits, high, medium, and low, all can be used as transmission nodes in the satellite internet. Generally, high earth orbit (HEO) and MEO satellites cover the ground area through beamforming using multiple spot beams. However, due to their long distance (a few thousand to tens of thousands of kilometers) to the earth, HEO and MEO satellite systems suffer from high link loss, thus imposing high G/T and EIRP requirements on the ground terminals. For LEO communication satellite, e.g., Iridium and Globalstar, the distance between the earth and satellite is greatly reduced, and hence the link loss is low, so that direct communication between the satellite and small ground terminals can be supported. Nevertheless, the low orbit altitude limits the coverage area of one single LEO satellite. To meet the wide coverage requirement, multiple LEO satellites are usually arranged in accordance with a certain shape and rule to form a LEO satellite constellation, each satellite serving the ground in a uniform-coverage way. With the development of internet services, it is more and more difficult for LEO satellites with uniform coverage to meet the continually increasing requirements on communication rate. Though the energy of spot beams is more concentrated, using them naively would significantly reduce the coverage area. As such, under the limited energy constraint, the contradiction between coverage area and communication rate for LEO satellite becomes increasingly prominent.

Smart Communication Satellite (SCS), the first low earth orbit (LEO) mobile communication experimental satellite of China, developed by Tsinghua University and Beijing Xinwei Telecom Technology Inc., was launched on September 4, 2014 [31]. In order to solve the contradiction between data rate and cover range of LEO satellite communication, SCS exploits smart antennas on the LEO satellite, which produce fast-switched dynamic spot-beam, to meet the requirement of large coverage and high communication rate. In line with the current developing trends of small satellites, SCS makes a lot of efforts in communication-oriented satellite design. Through tackling a series of challenges under the constraints of size, cost, and energy, SCS developed a payload centric technique and accomplished the 100 kg-class weighted micro-satellite applicable to communication and navigation services. Firstly, SCS demonstrates the concept of smart beamforming for small satellite. Secondly, by using large numbers of industrial-grade components, SCS achieves low-cost facilities from altitude determination to the house-keeping system, as well as the communication payload. Finally, SCS accomplishes the file management, software upgrading and Internet access by a Linux operating system, making it naturally with the ability for evolution with Internet development.

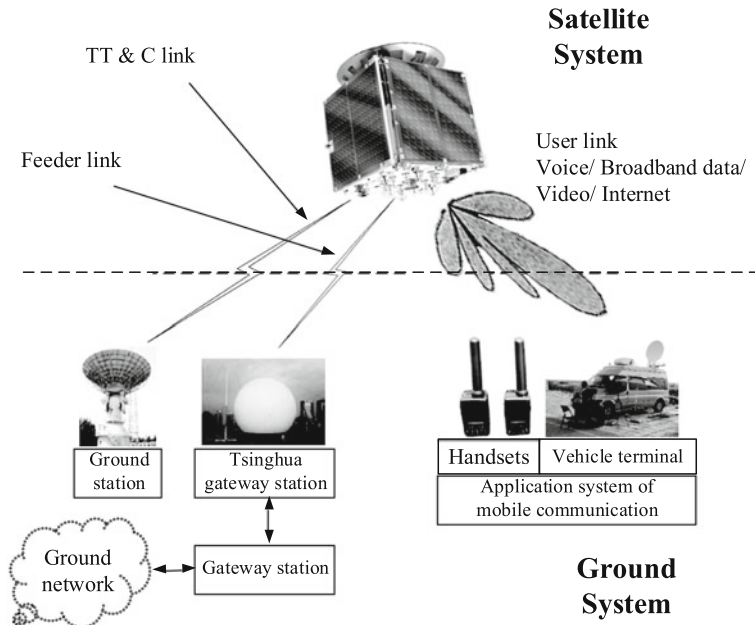


Fig. 2.9 The composition of SCS experiment system

2.3.1 System Design

The composition of SCS experiment system is presented in Fig. 2.9. The entire experiment system can be divided into two parts: the satellite system and the ground system. The satellite system contains the platform system and the payload system, while the ground system contains the application system of payloads, ground station and gateway station. There are three links between the satellite and ground: S band TT&C link, C band feeder link and S band user link. TT&C link carries the tele-control and telemetry information. Feeder link produces the high speed data download passageway for the flight logs and experimental data. Meanwhile, the feeder link connects the mobile communication payload and Tsinghua gateway station. The customer link employs smart beam, which is created by the mobile communication payload, to build a smart space communication system. If there is no support from ground station, the satellite forms communication links between users under its footprint through on-board switching.

The SCS is formed by payloads and platform. The payloads contains multi-media mobile communication payload based on smart antenna (with C band feeder link), and spectrum scan payload. The platform contains power subsystem, Tt&C subsystem (S band transponder and Tt&C unit), house-keeping subsystem (OBC and GPS), attitude determination and control subsystem (ADCS), structure subsystem and thermal subsystem.

2.3.2 Smart Beamforming

The satellite communication has the feature of non-uniform services and uncertainty in user distribution. In the vast sea, land and space, the user requests are relatively concentrated but area-uncertain. SCS does not adopt the uniform coverage scheme as in the traditional mobile satellite communication system. Instead, after the users initiate the service request, it would calculate and adjust the beam direction in real time according to the position information of the satellite and the user. Then, by allocating the time, space, and frequency resources, the on-demand beamforming in vast coverage area is achieved, which is called as the smart beamforming. The smart communication system can be described as “Smart beam, On-demand coverage”, by which the Internet access and communication between the handsets users and vehicle terminals users under coverage area can be built. By providing directional services, SCS effectively increases the user’s transmission rate, and meanwhile efficiently exploits the limited energy of small satellites. Table 2.2 gives the onboard experimental results of SCS.

The onboard mobile communication payload is composed of antenna, radio frequency subsystem, and baseband subsystem. The circular array, embedded on the side facing the ground, consists of twelve 4-arm helical antennas and is shared by both the transmitter and receiver. By on board autonomic computing and adaptive digital phase control technique, SCS reduces the effect of orbit change and attitude deviation on the precise beam direction during the high-mobility process of satellite, and hence the signals in the user receiver can be coherently superposed exactly all the time. The spectrum resource applicable for LEO communication satellite is highly deficient at present. To address this problem, SCS uses spectrum scanning payload to acquire real-time information of the current electromagnetic spectrum environment, whereby it provides support for the future spectrum sensing communication.

Table 2.2 The onboard experimental results of SCS

Test project	Test results
Minimum elevation angle of devices	24°
Intranetwork call setup time of handheld devices	≤300 ms
Internet network call setup time of handheld devices	≤400 ms
Delay of vehicle devices	≤100 ms
Uplink rate of handheld devices with single code channel	8 kbps
Uplink rate of handheld devices with double code channel	16 kbps
Downlink rate of handheld devices	Max 56 kbps
Uplink rate of vehicle devices	1024 kbps
Downlink rate of vehicle devices	1024 kbps

2.4 Summary

In this chapter, we discuss the main challenges when applying beamforming to satellite communication systems and introduced several prospective applications of satellite beamforming technology. Then, a multimedia multicast beamforming method for the integrated terrestrial-satellite network is proposed. Finally, a practical work of Smart Communication Satellite (SCS), the Chinese first low-earth-orbit communication satellite, is presented briefly.

References

1. Q. Yu, W. Meng, M. Yang, L. Zheng, Z. Zhang, Virtual multi-beamforming for distributed satellite clusters in space information networks. *IEEE Wirel. Commun.* **23**(1), 95–101 (2016)
2. G. Zheng, S. Chatzinotas, B. Ottersten, Generic optimization of linear precoding in multibeam satellite systems. *IEEE Trans. Wirel. Commun.* **11**(6), 2308–2320 (2012)
3. L.C. Godara, Application of antenna arrays to mobile communications. II. Beam-forming and direction-of-arrival considerations. *Proc. IEEE* **85**(8), 1195–1245 (1997)
4. H. Xu, J. Wang, J. Yuan, C. Jiang, C. Zhang, Generalized RQ minimization with applications in array transmit beamforming. *IEEE Antennas Wirel. Propag. Lett.* **16**(1), 177–180 (2017)
5. J. Du, C. Jiang, Q. Guo, M. Guizani, Y. Ren, Cooperative earth observation through complex space information networks. *IEEE Wirel. Commun.* **23**(2), 136–144 (2016)
6. C. Jiang, X. Wang, J. Wang, H. Chen, Y. Ren, Security in space information networks. *IEEE Commun. Mag.* **53**(8), 82–88 (2015)
7. S. Timotheou, I. Krikidis, G. Zheng, B. Ottersten, Beamforming for MISO interference channels with QoS and RF energy transfer. *IEEE Trans. Wirel. Commun.* **13**(5), 2646–2658 (2014)
8. J. Yang, H. Xi, F. Yang, Y. Zhao, Fast adaptive blind beamforming algorithm for antenna array in CDMA systems. *IEEE Trans. Veh. Technol.* **55**(2), 549–558 (2006)
9. P. Svedman, S.K. Wilson, L.J. Cimini, B. Ottersten, Opportunistic beamforming and scheduling for OFDMA systems. *IEEE Trans. Commun.* **55**(5), 941–952 (2007)
10. D. Christopoulos, S. Chatzinotas, B. Ottersten, Multicast multigroup precoding and user scheduling for frame-based satellite communications. *IEEE Trans. Wirel. Commun.* **14**(9), 4695–4707 (2015)
11. D. Kim, G. Lee, Y. Sung, Two-stage beamformer design for massive MIMO downlink by trace quotient formulation. *IEEE Trans. Commun.* **63**(6), 2200–2211 (2015)
12. S. Maleki, S. Chatzinotas, B. Evans, K. Liolis, J. Grotz, A.V. Coralli, N. Chuberre, Cognitive spectrum utilization in Ka band multibeam satellite communications. *IEEE Commun. Mag.* **53**(3), 24–29 (2015)
13. A.H. Khan, M.A. Imran, B.G. Evans, Semi-adaptive beamforming for OFDM based hybrid terrestrial-satellite mobile system. *IEEE Trans. Wirel. Commun.* **11**(10), 3424–3433 (2012)
14. Cisco Visual Networking Index: Global Mobile Data Traffic Forecast, 2015–2020, White Paper, Cisco, Feb 2016
15. H. Liu, Z. Chen, X. Tian, X. Wang, M. Tao, On content-centric wireless delivery networks. *IEEE Wirel. Commun.* **21**(6), 118–125 (2014)
16. E. Karipidis, N.D. Sidiropoulos, Z.-Q. Luo, Quality of service and max-min fair transmit beamforming to multiple cochannel multicast groups. *IEEE Trans. Signal Process.* **56**(3), 1268–1279 (2008)
17. Z. Xiang, M. Tao, X. Wang, Coordinated multicast beamforming in multicell networks. *IEEE Trans. Wirel. Commun.* **12**(1), 12–21 (2013)

18. J. Choi, Minimum power multicast beamforming with superposition coding for multiresolution broadcast and application to NOMA systems. *IEEE Trans. Commun.* **63**(3), 791–800 (2015)
19. M. Tao, E. Chen, H. Zhou, W. Yu, Content-centric sparse multicast beamforming for cache-enabled cloud RAN. *IEEE Trans. Wirel. Commun.* **15**(9), 6118–6131 (2016)
20. D. Christopoulos, S. Chatzinotas, B. Ottersten, Multicast multigroup precoding and user scheduling for frame-based satellite communications. *IEEE Trans. Wirel. Commun.* **14**(9), 4695–4707 (2015)
21. Y. Shen, C. Jiang, T. Quek, Y. Ren, Location-aware device communication design: exploration and exploitation on energy. *IEEE Wirel. Commun.* **23**(2), 46–52 (2016)
22. L. Xu, C. Jiang, Y. Shen, T. Quek, Z. Han, Y. Ren, Energy efficient D2D communications: a perspective of mechanism design. *IEEE Trans. Wirel. Commun.* **15**(11), 7272–7285 (2016)
23. 3rd Generation Partnership Project (3GPP), Feasibility study on new services and markets technology enablers – enhanced mobile broadband, Sept 2016
24. E. Lagunas, S.K. Sharma, S. Maleki, S. Chatzinotas, B. Ottersten, Resource allocation for cognitive satellite communications with incumbent terrestrial networks. *IEEE Trans. Cogn. Commun. Netw.* **1**(3), 305–317 (2015)
25. K. An, M. Lin, T. Liang, J. Wang, J. Wang, Y. Huang, A.L. Swindlehurst, Performance analysis of multi-antenna hybrid satellite-terrestrial relay networks in the presence of interference. *IEEE Trans. Commun.* **63**(11), 4390–4404 (2015)
26. B.R. Marks, G.P. Wright, A general inner approximation algorithm for nonconvex mathematical programs. *Oper. Res.* **26**(4), 681–683 (1978)
27. J. Papandriopoulos, J.S. Evans, SCALE: a low-complexity distributed protocol for spectrum balancing in multiuser DSL networks. *IEEE Trans. Inf. Theory* **55**(8), 3711–3724 (2009)
28. S. Boyd, L. Vandenberghe, *Convex Optimization* (Cambridge University Press, Cambridge, 2004)
29. 3rd Generation Partnership Project (3GPP), Further advancements for E-UTRA physical layer aspects, Dec 2016
30. E. Lutz, D. Cygan, M. Dippold, F. Dolainsky, W. Papke, The land mobile satellite communication channel-recording, statistics, and channel model. *IEEE Trans. Veh. Technol.* **40**(2), 375–386 (1991)
31. J. Jin, L. Kuang, J. Yan, X. Chen, Z. Ni, X. You, D. Sun, J. Lu, Smart Communication Satellite (SCS) project overview, in *29th Annual AIAA/USU Conference on Small Satellites*, pp. 1–6, 2015

Chapter 3

Interference Cancelation Reception

The integrated and/or hybrid satellite and terrestrial network has become more and more important because of its broad application prospect and has received considerable attention. At the same time, the integrated network also brings many challenges, especially the problem of interference. Due to the lack of frequency spectrum, frequency reuse is considered in the satellite network and the terrestrial network for enhancing spectral efficiency. However, this will cause considerable Co-Channel Interference (CCI) and thus interference coordination is imperative. In this chapter, we propose an interference coordination scheme for the integrated satellite and terrestrial network. The satellite sends pilots for channel estimation at terrestrial base-stations, and transmits the received data to the terrestrial gateway. Then interference coordination is performed at the terrestrial gateway, where the interference channel is updated according to both the estimated information and the predicted change based on the positions. Furthermore, based on the scheme, we analyze the precision that needs to be reached and obtain a direct view on how the precision may influence the system performance.

A new vision of next-generation networks (NGN) has been proposed by International telecommunication union (ITU), in which the integrated and/or hybrid satellite and terrestrial network is supposed to play important roles [1]. Also, in the European Technology platform NETWORLD2020, a Satellite Working Group produced a White Paper for the role of satellites in 5G [2]. The frame of the integrated network is attractive and promising since the satellite network can provide the best and most comprehensive coverage for low-density populations, while the terrestrial network or the ground component can provide the highest bandwidth and lowest cost coverage for high-density populations in urban environments [3].

While the integrated satellite and terrestrial network may bring lots of benefits in the development of communication, it also leads to many new challenges, especially the problem of interference and congestion [4]. The rapid development of wireless communication has led to increasing demand of frequency resources, and the problem of spectrum scarcity is becoming more and more serious.

Due to the lack of frequency spectrum, frequency reuse is considered in the satellite network and the terrestrial network for enhancing spectral efficiency. However, this will cause considerable Co-Channel Interference (CCI) when satellite terminals and base stations transmit signals at the same time with the same frequency [5, 6]. Thus interference coordination is imperative to mitigate the interference at the satellite. Over the past few years, there have been some meritorious works on interference modeling and interference coordination [7–10], which are referable in the development of the integrated networks. Sharma analyzed the interference model of different transmission modes in the integrated satellite and terrestrial network [7]. Khan proposed a novel semi-adaptive beamformer at the satellite to mitigate interference, which consumes less computing power without compromising on system performance [8]. Deslandes and Kang adopt the concept of the exclusive zone (EZ), where the terrestrial network is not allowed to use satellite frequencies [9, 10].

Generally, if we can obtain both the interference signal and the channel information, it is possible to subtract the interference signal from the mixed signal to mitigate the interference. Since the interference signal can be obtained directly from terrestrial base-stations, the main problem is to do the channel estimation for the interference signal. In this chapter, we propose an interference coordination scheme for the integrated satellite and terrestrial network [11]. The satellite sends pilots for channel estimation at terrestrial base-stations, and transmits the received data to the terrestrial gateway. Then interference coordination is performed at the terrestrial gateway, where the interference channel can be updated according to both the estimated information and the predicted change based on the positions.

3.1 Position-Assisted Interference Coordination

3.1.1 System Model

Consider an space-ground communication system, as shown in Fig. 3.1, where the user and the base stations transmit signals to the satellite with the same frequency F_1 [12]. Due to the frequency reuse, there exists interference at the satellite. As a result, the mixed signal is transmitted from the satellite to the terrestrial gateway. At the same time when the signals are transmitted from the base stations to the satellite, the base stations will also transmit their signals directly to the terrestrial gateway. Assume that the channel state information is available at the gateway, and the interference of the base stations may be mitigated by subtracting the signals of the direct link from the mixed signal.

As depicted in Fig. 3.1, we consider the case of multiple base stations and the position of base stations i is represented by constant P_{zi} and the position of the terrestrial gateway is represented by constants P_e , respectively. As the user is randomly moving, the position of the user is a function of time t , and is denoted by $P_u(t)$. Similarly, the position of satellite is function $O(t)$, which can be calculated

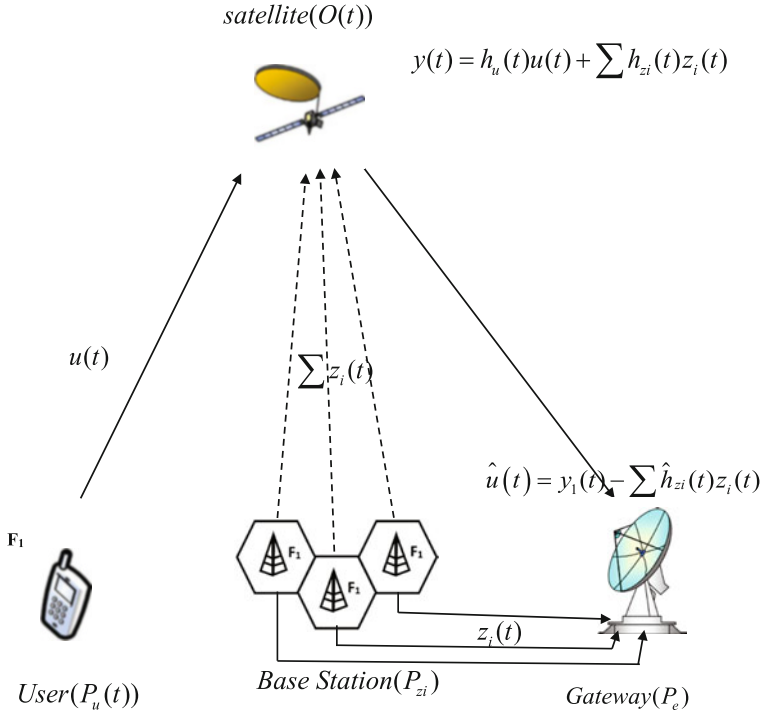


Fig. 3.1 Space ground communication system

from its orbit at the terrestrial gateway. The signals of base station i and the user are represented by $z_i(t)$ and $u(t)$, respectively. Assume the channel state information is known and the channel between base station i and the satellite is $h_{zi}(t)$, while the channel between the user and the satellite is $h_u(t)$. The received mixed signal at satellite can be expressed as

$$y(t) = h_u(t)u(t) + \sum_{i=1}^N h_{zi}(t)z_i(t). \quad (3.1)$$

Then the satellite transmits the mixed signal to the terrestrial gateway through channel $h_e(t)$, and the signal received at the gateway is $y_1(t)$. At the same time when base station i transmits $z_i(t)$ to the satellite, base station i also transmits $z_i(t)$ to the terrestrial gateway directly and the channel is h_{zi} . Using $z_i(t)$ from the base station and the channel state information, the gateway can subtract the interference signal $z_i(t)$ from $y_1(t)$, obtaining the user signal

$$u(t) = y_1(t) - \sum_{i=1}^N \hat{h}_{zi}(t)z_i^*(t), \quad (3.2)$$

where $z_i^*(t) = h_{zie}z_i(t)$ is the signal received from base station i and $\hat{h}_{zi}(t)$ is the equivalent combined channel for interference signal $z_i^*(t)$.

This is the general framework of this system, where the exact signal and channel are not defined yet. An important assumption in the system is that the channel state information is available, and thus we can subtract the interference signals to cancel the interference.

3.1.2 Scheme of Interference Coordination

Based on the general framework, we now give the exact scheme of interference coordination with some assumptions of the signal and channel. For simplification, we use equivalent baseband for our derivations, which is a reasonable approximation. The baseband signal $\phi(t)$ of base stations is

$$\phi(t) = \sin c\left(\frac{t}{T_s}\right) = \frac{\sin \pi f_s t}{\pi f_s t}. \quad (3.3)$$

We set the bandwidth as $B_w = 2W$, and then we have the symbol period $T_s = \frac{1}{2W}$ since the baseband signal is $\text{sinc}(t)$. The signal $z_i(t)$ can then be expressed as

$$z_i(t) = \sum_{n_i} A_i \phi(t - n_i T_s). \quad (3.4)$$

Assuming that the channel $h_u(t)$ and $h_{zi}(t)$ is additive white Gaussian noise (AWGN) channel and use w_1 to represent the noise at satellite. Then we have

$$y(t) = h_u(t)u(t) + \sum_{i=1}^N h_{zi}(t)z_i(t) + w_1, \quad (3.5)$$

and the attenuation of the channel is

$$\beta = \frac{\lambda}{4\pi L_0}, \quad (3.6)$$

where L_0 is the distance. Based on reality, channel h_{zie} can be approximately regarded as ideal by means of wired transmission. Thus, the noise is zero and there is no attenuation. Also, assume that the transmission between the satellite and the gateway uses Ka-band with narrow beam, which can achieve high transmission gain. Thus we can assume that there is no attenuation in channel $h_e(t)$, but we still need to consider the AWGN noise w_2 at the gateway. Note that, our assumption is reasonable since the positions of the base station and gateway are changeless.

To obtain the channel information $h_{zi}(t)$, the satellite will periodically sends pilots for channel estimation at the terrestrial base-stations. The channel $h_{zi}(t_0)$ at time t_0 is derived as

$$h_{zi}(t_0) = \beta_{zi} e^{-j\theta_{zi}(t_0)}, \quad (3.7)$$

where β_{zi} is the attenuation of channel $h_{zi}(t_0)$ and $\theta_{zi}(t_0)$ is the initial phase. Similarly, we can also estimate channel $h_e(t_0)$ in the same way. However, as the satellite randomly moves, the delays of channel $h_{zi}(t)$ and $h_e(t)$ at any time t are not constants due to the changing of the position, and the phases of the channels will change by time consequently. Without lose of generality, we can consider the transmission of one symbol period, during which period we can approximately think the position of the satellite is fixed. Then the delay of $h_{zi}(t)$ can be derived as

$$\tau_{zio}(t) = \frac{D(P_z, O(t))}{c}. \quad (3.8)$$

where $D(P_z, O(t))$ represents the distance between the base station i and the satellite. Use $\Delta\tau_{zio}(t) = \tau_{zio}(t) - \tau_{zio}(t_0)$ to represent the change of delay of channel $h_{zi}(t)$ at time t compared with time t_0 , then the channel can be updated according to both the estimated information $h_{zi}(t_0)$ and the predicted change $\Delta\tau_{zio}(t)$ based on the positions. The updated channel $h_{zi}(t)$ can be derived as

$$h_{zi}(t) = \beta_{zi} e^{-j[\theta_{zi}(t_0) + 2\pi\Delta\tau_{zio}(t)]} = \beta_{zi} e^{-j\theta_{zi}(t)}. \quad (3.9)$$

Similarly, the delay of $h_e(t)$ can be derived as $\tau_{oe}(t)$ and also the updated channel $h_e(t)$. As stated before, it is assumed that the transmission between the satellite and the gateway uses Ka-band with narrow beam, which can achieve high transmission gain. Thus, we can approximately set $\beta = 1$ and only consider the influence of delay. Besides, the delay of h_{ze} is constant as the positions of the base stations and gateway are changeless, and denoted by τ_{ze} . Then the signal received by the gateway from the satellite is given by

$$y_1(t) = h_e(t)y(t) \quad (3.10)$$

$$= h_e(t)h_u(t)u(t) + \sum_{i=1}^N h_e(t)h_{zi}(t)z_i(t) + h_e(t)w_1 + w_2.$$

Firstly, we consider different base station separately. Assume the interference of all other base stations have been mitigated at the gateway except station k , and we only need to calculate $\hat{h}_{zk}(t)$ to make $\hat{u}(t)$ meet the expression

$$\begin{aligned} \hat{u}(t) &= y_1(t) - \hat{h}_{zk}(t)z_k^*(t) - \sum_{i=1, i \neq k}^N h_e(t)h_{zi}(t)z_i(t) \\ &= h_e(t)h_u(t)u(t) + h_e(t)w_1 + w_2. \end{aligned} \quad (3.11)$$

Then we have

$$\hat{h}_{zk}(t) = \frac{h_e(t)}{h_{zke}} h_{zk}(t). \quad (3.12)$$

Similarly, we can calculate $\hat{h}_{zi}(t)$ of all base stations. One can obtain

$$\begin{aligned} \hat{u}(t) &= y_1(t) - \sum_{i=1}^N \hat{h}_{zi}(t) z_i^*(t) \\ &= h_e(t) h_u(t) u(t) + h_e(t) w_1 + w_2. \end{aligned} \quad (3.13)$$

By using the signal received from the base station and the channel state information, we have mitigated the interference of signal $\sum_{i=1}^N z_i(t)$. The remaining signal only contains signal $u(t)$ and the noise, which cannot be mitigated since it is unknown. Our scheme is summarized as follows.

1. **Step 1:** Mixed signal at the terrestrial gateway,

$$y_1(t) = h_e(t) h_u(t) u(t) + \sum_{i=1}^N h_e(t) h_{zi}(t) z_i(t) + h_e(t) w_1 + w_2.$$

2. **Step 2:** Estimated channel using pilots,

$$h_{zi}(t_0) = \beta_{zi} e^{-j\theta_{zi}(t_0)}.$$

3. **Step 3:** Delay predicted according to positions,

$$\tau_{zio}(t) = \frac{D(P_z, O(t))}{c}.$$

4. **Step 4:** Change of delay,

$$\Delta\tau_{zio}(t) = \tau_{zio}(t) - \tau_{zio}(t_0).$$

5. **Step 5:** Updated channel based on positions

$$\begin{aligned} h_{zi}(t) &= \beta_{zi} e^{-j[\theta_{zi}(t_0) + 2\pi\Delta\tau_{zio}(t)]} = \beta_{zi} e^{-j\theta_{zi}(t)} \\ h_e(t) &= e^{-j[\theta_e(t_0) + 2\pi\Delta\tau_{oe}(t)]} = e^{-j\theta_e(t)}. \end{aligned}$$

6. **Step 6:** Estimated equivalent combined channel,

$$\hat{h}_{zi}(t) = \frac{h_e(t)}{h_{zie}} h_{zi}(t).$$

7. **Step 7:** Interference coordination,

$$\begin{aligned}\widehat{u}(t) &= y_1(t) - \sum_{i=1}^N \widehat{h}_{zi}(t) z_i^*(t) \\ &= h_e(t) h_u(t) u(t) + h_e(t) w_1 + w_2.\end{aligned}$$

3.1.3 Precision Analysis

In the previous section, we have mitigated the interference of base stations from the user signal. However, this result is based on the ideal situation, where all parameters used are accurate. In fact, due to various reasons, the position information obtained is not ideal. In this case, when we use the same scheme proposed in the previous section, the interference cannot be completely mitigated. In this section, we will do the precision analysis and analyze the impact of the position inaccuracy.

As stated before, P_{zi} and P_e are constant, so the main position error comes from $O(t)$, which will cause error in the calculation of $\Delta\tau_{zio}(t)$ and $\Delta\tau_{oe}(t)$. We use $\bar{O}(t)$ to represent the actual position information we obtain, which is not accurate. The actual change of delay we calculate from the position is

$$\begin{aligned}\overline{\Delta\tau}_{zio}(t) &= \frac{D(P_{zi}, \bar{O}(t))}{c} - \frac{D(P_{zi}, \bar{O}(t_0))}{c} \\ \overline{\Delta\tau}_{oe}(t) &= \frac{D(P_e, \bar{O}(t))}{c} - \frac{D(P_e, \bar{O}(t_0))}{c}\end{aligned}\quad (3.14)$$

Then the estimated equivalent combined channel for interference signal $z_i^*(t)$ will be

$$\begin{aligned}\bar{h}_{zi}(t) &= \beta_{zi} e^{-j[\theta_{zio}(t_0) + \theta_{ze}(t_0)] - j2\pi[\overline{\Delta\tau}_{zio}(t) + \overline{\Delta\tau}_{oe}(t) - \tau_{zie}]} \\ &= \beta_{zi} e^{-j[\bar{\theta}_{zio}(t) + \bar{\theta}_{ze}(t) + 2\pi\tau_{zie}]}.\end{aligned}\quad (3.15)$$

Using the estimated $\bar{h}_{zi}(t)$, then $\widehat{u}(t)$ will be

$$\begin{aligned}\widehat{u}(t) &= y_1(t) - \sum_{i=1}^N \bar{h}_{zi}(t) z_i^*(t) \\ &= h_e(t) h_u(t) u(t) \\ &\quad + \sum_{i=1}^N \beta_{zi} \{ e^{-j[\theta_{zio}(t) + \theta_{oe}(t)]} - e^{-j[\bar{\theta}_{zio}(t) + \bar{\theta}_{oe}(t)]} \} z_i(t) \\ &\quad + e^{-j2\pi\tau_{oe}(t)} w_1 + w_2.\end{aligned}\quad (3.17)$$

The second item in the expression is the interference signal from the base stations, which is not completely mitigated due to the position inaccuracy. We now turn to analyze the impact of the interference signal.

Assume the power of the user signal on the ground is P_u , and then the user power at the gateway is $\beta_u^2 P_u$. We have defined the baseband signal of base stations as $\phi(t) = \sin c(\frac{t}{T_s})$ in the previous section, whose fourier spectrum is

$$H(f) = T_s, -\frac{1}{2}f_s \leq f \leq \frac{1}{2}f_s. \quad (3.18)$$

From (3.16) the fourier spectrum of the interference from base station i can be derived as

$$G_i(f) = H(f)(e^{-if[\theta_{zio}(t) + \theta_{oe}(t)]} - e^{-if[\bar{\theta}_{zio}(t) + \bar{\theta}_{oe}(t)]}), \quad (3.19)$$

and it is easy to obtain

$$|G_i(f)|^2 = |H(f)|^2 2\{1 - \cos[2\pi f \Delta \tau_i(t)]\} \quad (3.20)$$

$$\Delta \tau_i(t) = [\bar{\Delta \tau}_{zio}(t) + \bar{\Delta \tau}_{oe}(t)] - [\Delta \tau_{zio}(t) + \Delta \tau_{oe}(t)].$$

Assume the power of $z_i(t)$ on the ground is P_{zi} , and then power of base station i at the gateway is $P_{H_i} = \beta_{zi}^2 P_{zi}$. We use P_{G_i} to represent the interference power of base station i at the gateway and $\frac{P_{G_i}}{P_{H_i}}$ can be expressed as

$$\frac{P_{G_i}}{P_{H_i}} = \frac{\int_{-\infty}^{+\infty} |G_i(f)|^2 df}{\int_{-\infty}^{+\infty} |H(f)|^2 df} = 2(1 - \sin c(\Delta \tau_i(t) f_s)). \quad (3.21)$$

The total power of the interference from all base stations is given by

$$\begin{aligned} P_G &= \sum_{i=1}^N \frac{P_{G_i}}{P_{H_i}} P_{H_i} \\ &= \sum_{i=1}^N 2(1 - \sin c(\Delta \tau_i(t) f_s)) P_{H_i}. \end{aligned} \quad (3.22)$$

The delay error $[\bar{\Delta \tau}_{zio}(t) + \bar{\Delta \tau}_{oe}(t)] - [\Delta \tau_{zio}(t) + \Delta \tau_{oe}(t)]$ differs according to different base station. Generally, we expect to confirm the maximum position error of $O(t)$ that we can tolerate, expressed as $\Delta O(t)$. It is easy to prove that $\Delta \tau_i(t) \leq 2\frac{\Delta(O(t))}{c}$, so we can obtain

$$\begin{aligned} P_G &\leq 2(1 - \sin c(\frac{2f_s \Delta(O(t))}{c})) \sum_{i=1}^N P_{H_i} \\ &= 2(1 - \sin c(\frac{2f_s \Delta(O(t))}{c})) P_H, \end{aligned} \quad (3.23)$$

where $P_H = \sum_{i=1}^N P_{H_i} = \sum_{i=1}^N \beta_{zi}^2 P_{zi}$ is the total power of signals of all base stations at the gateway. For simplification, we approximately regard the β_{zi} of different base station as the same, expressed as β_z . Then we have $P_H = \beta_z^2 \sum_{i=1}^N P_{zi} = \beta_z^2 P_z$, where P_z is the total power of signals of all base stations on the ground.

Based on the above analysis, we now turn to analyze the *SIR* gain of our interference coordination scheme, where $SIR = \frac{P_s}{P_I}$ is the Signal to Interference Ratio at he gateway. Let SIR_0 and SIR_{co} represent the *SIR* without and with interference coordination. Then, we have the *SIR* gain G_{SIR}

$$G_{SIR} = \frac{SIR_{co}}{SIR_0} = \frac{\frac{\beta_u^2 P_u}{P_G}}{\frac{\beta_u^2 P_u}{P_H}} = \frac{P_H}{P_G} \geq \frac{1}{2[1 - \sin c(\frac{2f_s \Delta O(t)}{c})]}. \quad (3.24)$$

This expression gives the relation between the lower bound of *SIR* gain and the position error of satellite. It means that after implementing the interference coordination scheme at the terrestrial gateway, as long as the position error is less than $\Delta O(t)$, the *SIR* gain will be larger than G_{SIR} .

To obtain the exact curve, we need other assumption on the symbol rate f_s . For symbol rate $f_s = 1 \text{ MHz}/2 \text{ MHz}/3 \text{ MHz}$, we have Fig. 3.2. We can observe that after implementing the interference coordination scheme at the terrestrial gateway, we have obtained considerable *SIR* gain according to different position error. For

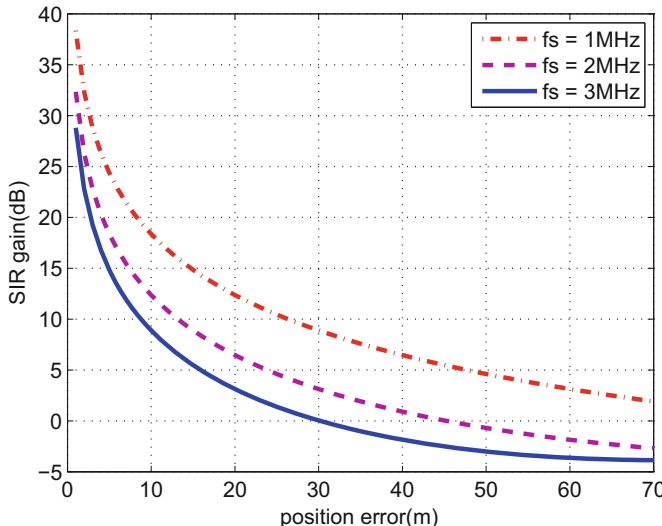


Fig. 3.2 Relation between the lower bound of *SIR* gain and the position error of different frequency

$f_s = 1$ MHz, when position error is less than 26 m, the *SIR* gain will be larger than 10 dB. To obtain more than 3 dB gain, the position error needs to be less than 60 m. However, when position error continues to increase, we cannot ensure gaining due to the too large inaccuracy of position. Also, we can observe that as symbol rate f_s increases, the *SIR* gain decreases because the same position error will cause larger residual error respectively. When symbol rate f_s increases from 1 to 3 MHz, there will be about 9 dB loss in the *SIR* gain.

3.1.4 Performance Evaluation

In the previous section, we analyzed the relation between the lower bound of *SIR* gain and the position error of satellite, and derived the curve of different symbol rate f_s . With the same assumption, we now turn to some simulations to research on the real system performance and compare it with our theoretical results.

As stated before, we set the baseband signal of base stations as $\phi(t) = \sin c(\frac{t}{T_s})$. Reference to Iridium, the height of the satellite is 780 km, and we can obtain $\beta_z = 1.9 \times 10^{-8}$. The signals of the user and base stations are randomly generated. The position error of the satellite is randomly generated at any direction, and we do the simulation repeatedly for $N = 100$ times to avoid accidental results. We calculate the mean results and worst results of *SIR* gain at the gateway for different position error and the results are shown in Fig. 3.3.

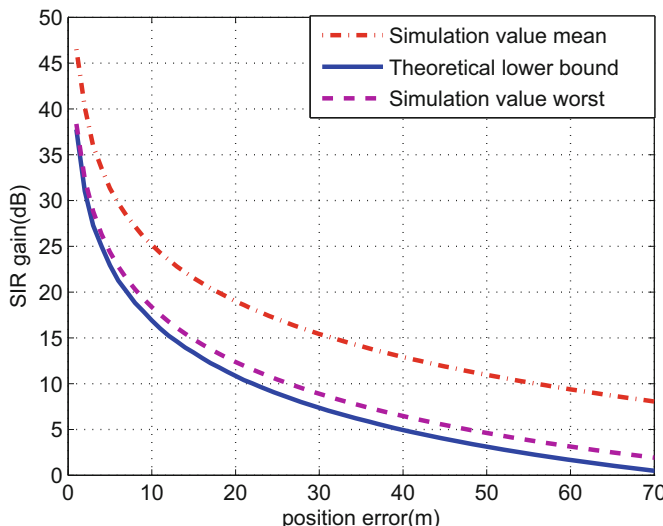


Fig. 3.3 Relation between SIR gain and the position error of theoretical and simulation results

We can observe that the mean results is better than the theoretical lower bound by about 8 dB since the position error will not always cause the maximum delay error for different direction. Also, we can see that the worst results coincide with the theoretical analysis quite well, although the simulation result is a little higher than the theoretical analysis. Since what we obtained in the previous section is the lower bound of the *SIR* gain, the result is reasonable and it also proves that the theoretical analysis is close to the real result.

3.2 Channel State Information Based Interference Coordination

3.2.1 Model and Formulation

We consider the scenario of one satellite user and N BSs as depicted in Fig. 3.4. In the ground, BSs and the Gateway are connected by wire, which is convenience to perform interference coordination [13, 14, 17]. Moreover, it is considered the scenario that the uplink of the satellite and the downlink of BSs share the same frequency band, and vice versa. The bandwidth of the system is assumed to be B . In this section, we focus on the situation of the uplink of the satellite and the downlink of BSs, and the downlink of the satellite and the uplink of BSs can readily extended with same analytical method.

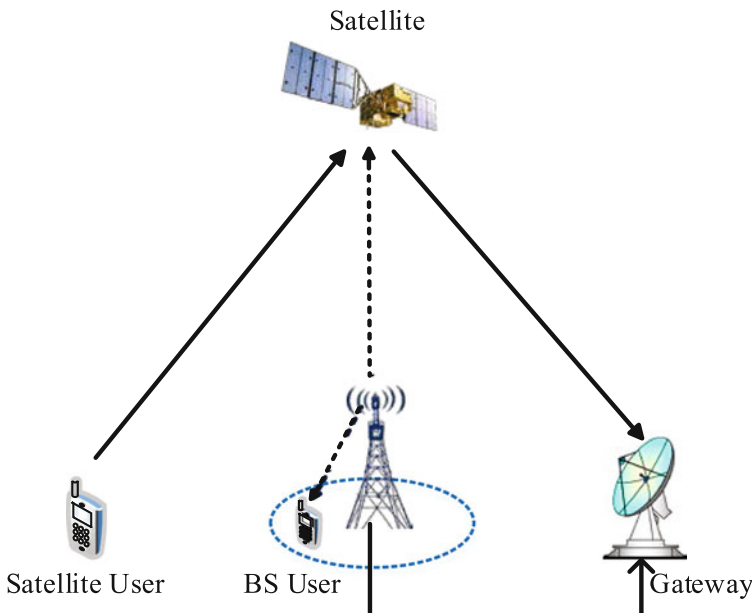


Fig. 3.4 System model of the integrated network

Table 3.1 Parameter definition

Notation	Physical meaning
s	The signal of the satellite user
u_i	The signal of BS
h_u	The channel state information between the satellite and its user
h_b	The channel state information between BS and the satellite
g_i	The channel state information between BS and its user
h_g	The channel state information between the satellite and the gateway

According to the system model, various types of information are required [15, 16], including different channel state information (CSI) and signals information, to realize interference mitigation for the terrestrial-satellite system. Therefore, the relevant parameters are defined at Table 3.1. Signals from the satellite users and BSs are mixed at the satellite which is first transmitted to the gateway, and then the interference is mitigated at the ground. Through utilizing the CSI and signals information, the interference of BSs can be efficiently subtracted from the mixed signal, i.e., the interference is restrained and the original signal of the satellite user can be obtained. The mix signal can be written as follow

$$y = h_u s + \sum_{i=1}^N h_b u_i + n_1, \quad (3.25)$$

where n_1 is gaussian noise with variance of σ_{n_1} . Meanwhile, the signal received by the gateway can be expressed by

$$\begin{aligned} y_e &= h_g (h_u s + \sum_{i=1}^N h_b u_i + n_1) + n_2 \\ &= h_g h_u s + \sum_{i=1}^N h_g h_b u_i + n_1 h_g + n_2. \end{aligned} \quad (3.26)$$

Different CSIs are estimated by utilizing pilot signals. Let \bar{h}_b and \bar{h}_g be the CSI obtained from BSs and the gateway, as well as ϵ_b and ϵ_g which are called the error factors of the CSIs. Obviously, the part of BS's signals for the mix signal can be easily formulated by

$$y_b = h_u s + \sum_{i=1}^N h_g h_b u_i + n_1 \quad (3.27)$$

Thus, we can obtain the signal after canceling the interference of BSs as follows

$$s = y_e - y_b \quad (3.28)$$

$$\begin{aligned} &= h_g h_u s + \sum_{i=1}^N (\overline{h_b h_g} - h_b h_g) u_i + n_1 h_g + n_2 \\ &= h_g h_u s + \sum_{i=1}^N \Delta h_{bg} u_i + h_g n_1 + n_2, \end{aligned}$$

where Δh_{bg} is error of channel estimation.

If the channel state estimation is inaccurate, the interference of BSs cannot be canceled completely. The precision of estimation error directly impacts the level of residual interference, and thus the power control of BSs should be applied to avoid excessive interference. Considering this problem, we can further calculate the error of channel estimation as follows

$$\Delta h_{bg} = (\epsilon_i + \epsilon_g - \epsilon_i \epsilon_g) h_b h_g \quad (3.29)$$

$$\approx (\epsilon_b + \epsilon_g) h_b h_g, \quad (3.30)$$

where $\epsilon_b \sim N(0, \kappa_b)$ and $\epsilon_g \sim N(0, \kappa_g)$ follow the normal distribution that

$$E(|\Delta h_{bg}|^2) = (\kappa_b + \kappa_g) |h_g|^2 |h_b|^2. \quad (3.31)$$

Then, the interference power can be written by

$$P_s = \sum_{i=1}^N (\kappa_b + \kappa_g) |\Delta h_{bg}|^2 p_i. \quad (3.32)$$

In order to guarantee the QoS of the satellite user, the interference power should be constrained within the maximum tolerable interference level P^c .

$$P_s = \sum_{i=1}^N (\kappa_b + \kappa_g) |\Delta h_{bg}|^2 p_i \leq P^c. \quad (3.33)$$

Meanwhile, the power of each BS should be less than a certain maximum value, i.e.,

$$0 \leq P_i \leq P_{max}, \quad (3.34)$$

where P_i is the transmission power of each BS, and P_{max} is the maximum transmission power of the BS.

To evaluate the performance of the terrestrial systems, we compute the downlink capacity of BSs by Shannon's theorem as follows

$$\sum_{i=1}^N C_i = \sum_{i=1}^N \log_2 \frac{1 + |g_b|^2 p_i}{\sigma_{nB}}. \quad (3.35)$$

To avoid the interference of BSs, the transmit power has to be controlled in BS to satisfy the interference constraint, which also needs to be satisfied by the power constraint for each BS. In such a case, the objective of power control can be described as follows

$$\text{Max} \sum_{i=1}^N C_i \quad (3.36)$$

$$\text{s.t. } C_1 : \{p_i \geq 0, \forall i\}, \quad (3.37)$$

$$C_2 : p_i \leq P_{max}, \forall i, \quad (3.38)$$

$$C_3 : \sum_{i=1}^N (\kappa_b + \kappa_g) |h_{bg}|^2 p_i \leq P^c. \quad (3.39)$$

3.2.2 Lagrangian Multiplier Method and Algorithm

In the previous section, we formulate the optimization problem in (3.36), which is a standard convex problem with the objective function being a convex function and all constraint conditions being convex sets. In this section, we solve the optimization problem by means of the Lagrangian multiplier method. The Lagrangian function is

$$L(p_i, \lambda_i, \mu) = \sum_{i=1}^N C_i - \sum_{i=1}^N \lambda_i (P_{max} - p_i) - \mu (P^c - \kappa_b + \kappa_g) |h_{bg}|^2 p_i, \quad (3.40)$$

where λ_i and μ are the Lagrange multipliers vectors for the constraints C_2 and C_3 . Thus, the Lagrangian dual function can be given as

$$\theta(\lambda, \mu) = \inf_{p_i \geq 0, \forall i} \left\{ L(p_i, \lambda, \mu) \right\}, \quad (3.41)$$

Then the dual problem can be written as

$$\max_{\lambda, \mu} \theta(\lambda, \mu), \quad (3.42)$$

$$\text{s.t. } \lambda, \mu \geq 0, \quad (3.43)$$

$$p_i \geq 0, \forall i. \quad (3.44)$$

Algorithm 2 Power allocation algorithm

```

1: Initialize  $N$  Iterations and Lagrangian variables vectors  $\lambda, \mu$ , set  $j = 0$ ;
2: Initialize  $p_i$  with power distribution for each BS;
3: repeat
4:   for  $i = 1$  to  $N$  do
5:     Update  $\lambda_i$  according to (3.47);
6:     Update  $p_i$  according to (3.46);
7:   end for
8: until Convergence or  $j = N$  Iterations

```

For this optimization, we can solve the dual problem iteratively, in which the optimal solution p_i^* should satisfy the condition

$$\frac{\partial L}{\partial p_i^*} = -\frac{1}{\ln 2} \left(\frac{|g_b|^2}{|g_b|^2 p_i^* + \sigma_{n_B}} \right) + \lambda_i + \mu(\kappa_b + \kappa_g) |h_{bg}|^2 \begin{cases} = 0, p_i^* > 0, \\ \geq 0, p_i^* = 0. \end{cases} \quad (3.45)$$

From (3.36), we can obtain the optimal power allocated from BS i to user as

$$p_i^* = \left(\frac{1}{\ln 2} \left(\frac{1}{\lambda + \mu(\kappa_b + \kappa_g) |h_{bg}|^2} - \frac{\sigma_{n_B}}{|g_b|^2} \right) \right)^+. \quad (3.46)$$

where $(x)^+ = \max(0, x)$. Note that the optimal solution of p_i is in the form of λ and μ . Since $\theta(\lambda, \mu)$ of (3.41) is not differentiable, we use the subgradient method to obtain λ and μ iteratively, i.e.,

$$\lambda^{(j+1)} = [\lambda^{(j)} - \gamma_1^{(j)} (P_m a x - p_i)]^+, \quad (3.47)$$

$$\mu^{(j+1)} = [\mu^{(j)} - \gamma_2^{(j)} (P^c - \sum_{i=1}^N (\kappa_b + \kappa_g) |h_{bg}|^2 p_i)]^+, \quad (3.48)$$

where $j \in \{1, 2, \dots, N \text{ iterations}\}$ represents the iteration step, and $\gamma_1^{(j)}, \gamma_2^{(j)}$ are the step sizes of iteration j . Upon each iteration, the Lagrange multipliers λ and μ are updated according to (3.47), and then p_i is updated according to (3.46). We summarize the algorithm in Algorithm 2.

3.2.3 Performance Evaluation

In this section, we simulate Algorithm 2 to evaluate the performance of system in the aforementioned scenario. The satellite is assumed to be on the orbit of 10,000 km. The carrier frequency is 2 GHz in the S frequency band and the bandwidth B is set as

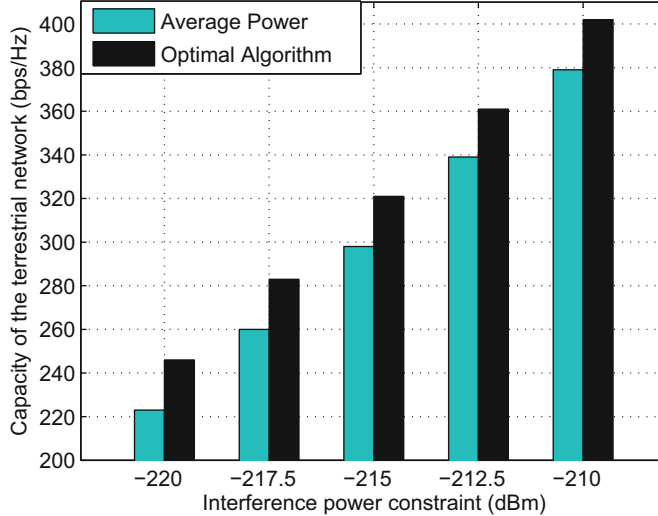


Fig. 3.5 Capacity of the terrestrial network with different interference constraints

10 MHz. The number of BS i is 50, and each BS has the maximum transmit power P_B^{max} . The satellite channel is modeled as Rician channel and the channel from BS to user is modeled as Rayleigh channel. The error factors of channel estimation are set as $\kappa_b = 0.01$ and $\kappa_g = 0.1$, respectively. We compare our optimal power allocation algorithm with the average power algorithm, and the comparison results are shown in Fig. 3.5. We can observe that the proposed algorithm outperforms the average algorithm quite well, and can significantly improve the capacity of the terrestrial network.

3.3 Summary

In this chapter, we propose an interference coordination scheme for the integrated satellite and terrestrial network. The interference coordination is performed at the terrestrial gateway, where the interference channel is updated according to both the estimated information and the predicted change based on the positions. Then, two interference coordination examples based on position information and channel state information are analyzed.

References

1. S. Kim, Evaluation of cooperative techniques for hybrid/integrated satellite systems, in *2011 IEEE International Conference on Communications (ICC)* (IEEE, New York, 2011)
2. B.G. Evans, The role of satellites in 5G, in *2014 7th Advanced Satellite Multimedia Systems Conference and the 13th Signal Processing for Space Communications Workshop (ASMS/SPSC)* (IEEE, New York, 2014)
3. K. Sastri, G. Giambene, S. Kim, Satellite component of NGN: integrated and hybrid networks. *Int. J. Satell. Commun. Netw.* **29**(3), 191–208 (2011)
4. J. Wang, C. Jiang, H. Zhang, V. Leung, Y. Ren, Aggressive congestion control mechanism for space systems. *IEEE Aerosp. Electron. Syst. Mag.* **31**(3), 28–33 (2016)
5. Y. Zhang, C. Jiang, Z. Han, S. Yu, J. Yuan, Interference-aware coordinated power allocation in autonomous wi-fi environment. *IEEE Access* **4**(1), 3489–3500 (2016)
6. H. Zhang, C. Jiang, J. Chen, V. Leung, Cooperative interference mitigation and handover management for heterogeneous cloud small cell networks. *IEEE Wirel. Commun.* **22**(3), 92–99 (2015)
7. S.K. Sharma, S. Chatzinotas, B. Ottersten, Satellite cognitive communications: interference modeling and techniques selection, in *6th Advanced Satellite Multimedia Systems Conference (ASMS) and 12th Signal Processing for Space Communications Workshop (SPSC)* (IEEE, New York, 2012)
8. A.H. Khan, M.A. Imran, B.G. Evans, Semi-adaptive beamforming for OFDM based hybrid terrestrial-satellite mobile system. *IEEE Trans. Wirel. Commun.* **11**(10), 3424–3433 (2012)
9. V. Deslandes, J. Tronc, A. Beylot, Analysis of interference issues in integrated satellite and terrestrial mobile systems, in *2010 5th Advanced Satellite Multimedia Systems Conference (ASMA) and the 11th Signal Processing for Space Communications Workshop (SPSC)* (IEEE, New York, 2010)
10. K. Kang et al., Analysis of interference and availability between satellite and ground components in an integrated mobile-satellite service system. *Int. J. Satell. Commun. Netw.* **33**(4), 351–366 (2015)
11. X. Zhu, R. Shi, W. Feng, N. Ge, Position-assisted interference coordination for integrated terrestrial-satellite networks, in *IEEE PIMRC*, 2015, pp. 971–975
12. Y. Shen, C. Jiang, T. Quek, Y. Ren, Device-to-device-assisted communications in cellular networks: an energy efficient approach in downlink video sharing scenario. *IEEE Trans. Wirel. Commun.* **15**(2), 1575–1587 (2016)
13. C. Jiang, Y. Chen, K.J.R. Liu, Distributed adaptive networks: a graphical evolutionary game theoretic view. *IEEE Trans. Signal Process.* **61**(22), 5675–5688 (2013)
14. F. Luo, C. Jiang, J. Du, J. Yuan, Y. Ren, S. Yu, M. Guizani, A distributed gateway selection algorithm for UAV networks. *IEEE Trans. Emerg. Top. Comput.* **3**(1), 22–33 (2015)
15. X. Zhao, Y. Zhang, C. Jiang, J. Yuan, J. Cao, Mobile-aware topology control potential game: equilibrium and connectivity. *IEEE Internet Things J.* **3**(6), 1267–1273 (2016)
16. J. Guo, X. Liu, C. Jiang, J. Cao, Y. Ren, Distributed fault-tolerant topology control in cooperative wireless ad hoc networks. *IEEE Trans. Parallel Distrib. Syst.* **26**(10), 2699–2710 (2015)
17. W. Feng et al., Virtual MIMO in multi-cell distributed antenna systems: coordinated transmissions with large-scale CSIT. *IEEE J. Sel. Areas Commun.* **31**(10), 2067–2081 (2013)

Chapter 4

Spectrum Sharing

In the fifth-generation (5G) networks, millimeter-wave (mmWave) bands have drawn great attention for the large amount of possible bandwidth. Meanwhile, satellite communications have also shown great interest in the mmWave bands, especially the Ka band. Under such a circumstance, the spectrum sharing between the satellite and terrestrial communication systems becomes prominent. In this chapter, we analyze the interference caused by terrestrial cellular systems to the geostationary (GEO) system in two transmission modes. In order to protect the GEO system, we construct a protection radius where the terrestrial transmitters must locate outside. Then, in the scenario of spectrum coexistence between geostationary (GEO) and non-geostationary (NGEO) satellite systems, we discover and investigates the issue of blind spot where the spectrum awareness techniques may fail to identify the spectrum holes. Both the uplink and downlink transmissions are analyzed and three key parameters, i.e. altitude of NGEO satellites and antenna patterns of NGEO and GEO earth stations, are considered.

4.1 Spectrum Coexistence Between GEO and Terrestrial Systems

4.1.1 *Interference Analysis and Network Mode*

There are two transmission modes in the spectrum coexistence between GEO and terrestrial systems, as shown in Figs. 4.1 and 4.2 [1], respectively. The normal mode means the downlink link of the GEO and the downlink of the cellular are in the same frequency band, and vice versa; while the reverse mode means the downlink link of the GEO and the uplink of the cellular are in the same frequency band, and

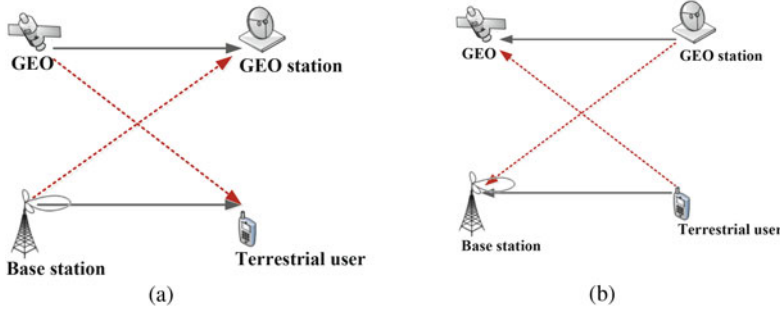


Fig. 4.1 Normal mode. (a) Downlink link. (b) Uplink link

vice versa. Note that in this chapter, we mainly consider the interference received by the satellite system and the downlink/uplink in the remainder of this chapter all represent those links of the satellite system.

In the normal mode, the interference from the terrestrial terminals to the GEO satellite can be neglected due to the limited transmission power of the terrestrial terminals versus the long distance, as described in Fig. 4.1b, while the interference from the terrestrial BSs to the GEO earth station should be the principal concern, as shown in Fig. 4.1a. In the reverse mode, the interference experienced at the GEO system is from two aspects: in the downlink link, the terrestrial terminals can cause interference to the GEO earth station, as shown in Fig. 4.2a; while in the uplink link, the aggregate interference from a number of terrestrial BSs can also interfere with the GEO satellite, as shown in Fig. 4.2b. By comparing the two modes, although the GEO satellite would be disturbed by the terrestrial BSs in the reverse mode, the GEO earth station experiences less interference from the terrestrial terminals than that from the terrestrial BSs in the normal mode, which is more favorable in practical. Since the analytical method in the downlink link of the reverse mode is similar to that in the downlink link of the normal mode, we mainly study two scenarios in this chapter, i.e., the downlink link of the normal mode as expressed in Fig. 4.1a, and the uplink link of the reverse mode as expressed in Fig. 4.2b.

We consider the cognitive network as follows: the GEO system regarded as the primary user and the terrestrial system regarded as the secondary user [2, 3]. As shown in Fig. 4.3, it is assumed that the GEO system consists of a GEO satellite and a GEO earth station located at the center of the network. In general, the location of GEO earth station can be known through the ITU database. In order to ensure an outage capacity of the GEO system, any terrestrial BS is at least R_0 radium away from the GEO earth station. There are n terrestrial BSs randomly and uniformly distributed with density ρ in the circle between the radius R_0 and R .

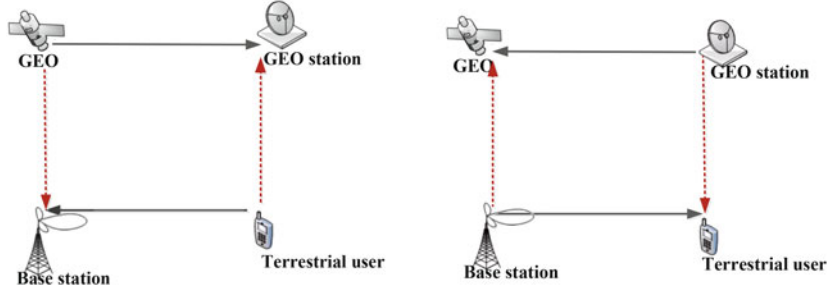


Fig. 4.2 Reverse mode. (a) Downlink link. (b) Uplink link

4.1.2 Channel and Signal Model

For the downlink link of the normal mode, the interference from a terrestrial BS to the GEO earth station can be calculated by [4]

$$I_{bs \rightarrow es} = P_{bs} G_{be} G_{es} \left(\frac{c}{4\pi f} \right)^2 (d_{bs \rightarrow es})^{-\alpha} \phi_{\sigma}^2, \quad (4.1)$$

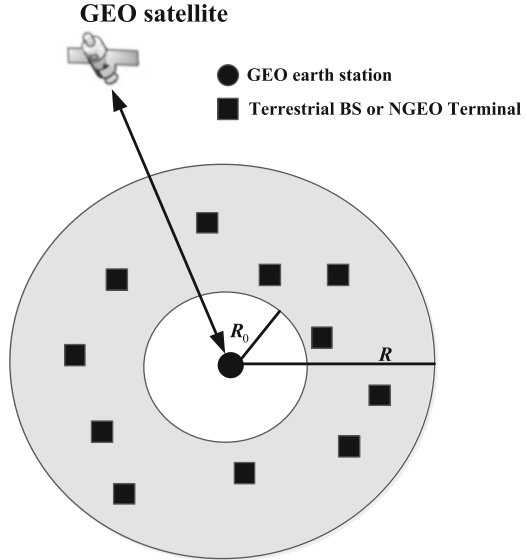
where P_{bs} is the transmission power of the terrestrial BS, G_{be} is the transmission antenna gain of the terrestrial BS at the direction towards the GEO earth station, G_{es} is the GEO earth station antenna gain at the direction of the terrestrial BS, c is the light speed, f is the center frequency of the spectrum band, $d_{bs \rightarrow es}$ is the distance between the terrestrial BS and the GEO earth station, α is the path-loss exponent which depends on different environment [5], and ϕ_{σ} is a Rayleigh parameter. Due to the direction of the GEO earth station antenna is concentrated at the satellite, it is reasonable to assume that the GEO earth station's antenna gain at the direction of terrestrial BS G_{es} is a small constant. However, the terrestrial BSs are located randomly around the GEO earth station and the antenna direction of the terrestrial BS is normally horizontal, and thus the BSs' transmission gain towards the GEO station G_{be} is relatively high.

For the uplink link of the reverse mode, the interference from the terrestrial BS to the GEO satellite can be calculated by [5, 6]

$$I_{bs \rightarrow sa} = P_{bs} G_{bs} G_{sa}(\theta) \left(\frac{c}{4\pi f d_{bs \rightarrow sa}} \right)^2 \phi_k^2, \quad (4.2)$$

where P_{bs} is the transmission power at the terrestrial BS, G_{bs} is the terrestrial BS antenna gain at the direction of GEO satellite, $G_{sa}(\theta)$ is the GEO satellite antenna gain to direction of θ , ϕ_k is a Ricean parameter, $d_{bs \rightarrow sa}$ is the distance between terrestrial BS and the GEO satellite. Due to the direction of the terrestrial BS is

Fig. 4.3 The spectrum coexistence between GEO and other systems



normally horizontal, it could be assumed that the terrestrial BS antenna gain G_{bs} at the direction of GEO satellite is a small constant.

4.1.3 Outage Constraint of the GEO System

The outage constraint of the GEO system is given as follows

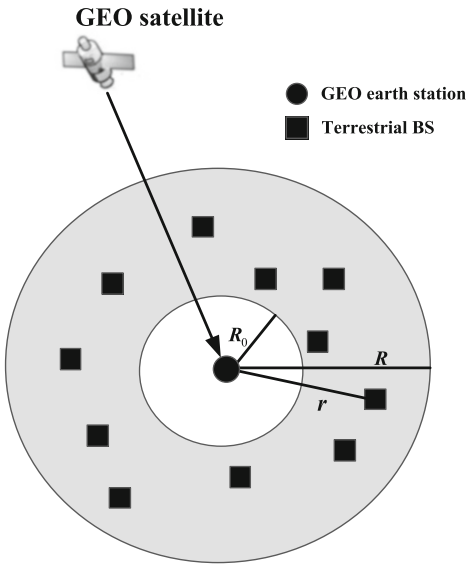
$$Pr[T_0 \leq C_0] \leq \eta, \quad (4.3)$$

where T_0 is the data rate of GEO system, η is the outage probability, and C_0 is the minimal rate required for the GEO service. This constraint ensures that the GEO system rate is at least C_0 for all but η fraction of the time. With the Shannon capacity, the GEO system achievable rate can be written by

$$T_0 = \log \left(1 + \frac{P_{gr}}{I + N} \right), \quad (4.4)$$

where I represents the aggregated interference power experienced by the GEO receiver, P_{gr} represents the received power of the GEO system, and N denotes the noise that can be calculated by $N = KT\ln(2)$, with K being the Boltzman's constant, T being the temperature of the GEO system, and W being the bandwidth. In such a case, the outage constraint (4.3) is equivalent to the following

Fig. 4.4 The spectrum coexistence in the downlink link of the normal mode



$$Pr \left[I \geq \frac{P_{gr}}{2^{C_0} - 1} - N \right] \leq \eta. \quad (4.5)$$

4.1.4 Downlink Link of the Normal Mode

Based on the interference analysis between GEO and terrestrial systems, we in this section further derive respectively the closed-form expression for the expected interference experienced at the GEO satellite and earth station, and then calculate the GEO earth station protection radius R_0 in downlink link of the normal mode.

4.1.4.1 Expected Interference at the GEO Earth Station

In the downlink link of the normal mode, any terrestrial BS is at least R_0 radius away from the GEO earth station, as described in Fig. 4.4. As terrestrial BSs are assumed to be uniformly distributed, r has the distribution of

$$f(r) = \frac{2r}{R^2 - R_0^2}, \quad (4.6)$$

where r is the distance from the GEO earth station to the terrestrial BS, and $R_0 \leq r \leq R$. The interference received by the GEO earth station originates from all $n = \rho\pi(R^2 - R_0^2)$ terrestrial BSs, and thus the expected interference in (4.1) can be written and derived as follows

$$\begin{aligned}
E[I_{bs \rightarrow es}] &= P_{bs} G_{be} G_{es} \left(\frac{c}{4\pi f} \right)^2 \int_{R_0}^R \frac{2\pi \rho r}{r^\alpha} dr \cdot E[\phi_\sigma^2] \\
&= \frac{c^2 \rho P_{bs} G_{be} G_{es}}{8\pi f^2 (2 - \alpha)} \left(\frac{1}{R^{(\alpha-2)}} - \frac{1}{R_0^{(\alpha-2)}} \right) E[\phi_\sigma^2].
\end{aligned}$$

Since ϕ_σ is a Rayleigh parameter, we have $E(\phi_\sigma^2) = 2\sigma^2$, where σ is the shadow fading of Rayleigh channel. In such a case, the value of $E[I_{bs \rightarrow es}]$ can be given as

$$E[I_{bs \rightarrow es}] = \frac{c^2 \sigma^2 \rho P_{bs} G_{be} G_{es}}{4\pi f^2 (2 - \alpha)} \left(\frac{1}{R^{(\alpha-2)}} - \frac{1}{R_0^{(\alpha-2)}} \right). \quad (4.7)$$

Considering an infinite network, i.e. $R \rightarrow \infty$, we have

$$E[I_{bs \rightarrow es}]_{R \rightarrow \infty} = \frac{c^2 \sigma^2 \rho P_{bs} G_{be} G_{es}}{4\pi f^2 (\alpha - 2)} \frac{1}{R_0^{(\alpha-2)}}. \quad (4.8)$$

For example, when the path-loss exponent α is chosen as 4 in our scenario [6], $E[I_{bs \rightarrow es}]$ can be re-written as follows

$$E[I_{bs \rightarrow es}]_{R \rightarrow \infty}^{\alpha=4} = \frac{c^2 \sigma^2 \rho P_{bs} G_{be} G_{es}}{8\pi f^2 R_0^2}. \quad (4.9)$$

4.1.4.2 GEO Earth Station Protection Radius

The definition of the GEO earth station protection area is to guarantee an outage performance for the GEO system. By applying Markov inequality, the GEO earth station outage constraint in (4.5) can be given as follows

$$Pr[I_{bs \rightarrow es} \geq \frac{P_{gre}}{2^{C_0} - 1} - N_e] \leq \frac{E[I_{bs \rightarrow es}]}{\frac{P_{gre}}{2^{C_0} - 1} - N_e}, \quad (4.10)$$

where P_{gre} is the reception power of the GEO earth station from the satellite and N_e is the noise at the GEO earth station. By imposing the outage constraint η in (4.5) on the right-hand-side of (4.10), we can have the bound of $E[I_{bs \rightarrow es}]$ as

$$E[I_{bs \rightarrow es}] \leq \eta \left(\frac{P_{gre}}{2^{C_0} - 1} - N_e \right) \triangleq E[I_{bs \rightarrow es}]_{max}. \quad (4.11)$$

Again, when $R \rightarrow \infty$, by substituting (4.8) into (4.11), the bound on the protection radius can be achieved as follows

Table 4.1 Simulation parameters

Parameter	Values
Frequency bands	18 GHz
Shadow fading σ	8.7 dB
BS transmit power P_{bs}	37/40/43 dBm
BS antenna gain G_{be}	16 dBi
BS antenna radiation pattern	ITU-R F.1336
Satellite EIRP	62.7 dBW
Earth station antenna diameter	0.75 m
Maximum earth station antenna gain	41 dB
Earth station antenna gain towards the BS G_{es}	-10 dB
Earth station antenna radiation pattern	ITU-R S.465-6
Earth station noise temperature	300 K

$$R_0 \geq \left(\frac{c^2 \sigma^2 \rho P_{bs} G_{be} G_{es}}{4\pi f^2 \eta (\alpha - 2) \left(\frac{P_{gre}}{2^{C_0-1}} - N_e \right)} \right)^{\frac{1}{(\alpha-2)}} \triangleq R_0^{\min}. \quad (4.12)$$

This equation indicates a minimum distance that ensuring the outage constraint for the GEO earth station. When the terrestrial BS is at least R_0^{\min} radium away from the GEO earth station, the harmful interference to the GEO earth station can be considered as negligible. For example, when $\alpha = 4$, Eq. (4.12) can be re-written by

$$R_0 \geq \left(\frac{c^2 \sigma^2 \rho P_{bs} G_{be} G_{es}}{8\pi f^2 \eta \left(\frac{P_{gre}}{2^{C_0-1}} - N_e \right)} \right)^{\frac{1}{2}}. \quad (4.13)$$

4.1.4.3 Simulations

In this section, we investigate the relationship between the GEO earth station protection radius R_0 and the expected interference $E[I_{bs \rightarrow es}]$ with the different terrestrial BS power P_{bs} . In the simulation, the system parameters are listed in Table 4.1. As we can see from Fig. 4.5, it is obvious that the greater transmission power of the terrestrial BS can lead to more interference at the GEO earth station. For the sake of guaranteeing the outage performance of the GEO earth station, the protection radius R_0 should be at least 8 km, 11.3 km and 16 km when terrestrial BS power is respectively 37 dBm, 40 dBm and 43 dBm. In other words, when the distance from the terrestrial BS to the GEO earth station is larger than the minimum protection radius R_0 above, terrestrial and GEO systems can be harmonious coexistence in the same spectrum band.

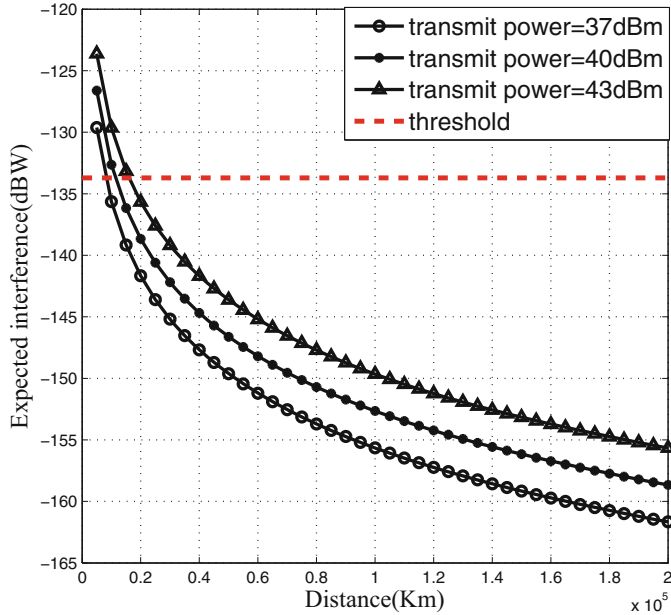


Fig. 4.5 The relationship between the expected interference $E[I_{bs \rightarrow es}]$ and the protection radius R_0 with the different BS power when $\alpha = 4$ and $\eta = 0.1$

4.1.5 Uplink Link of the Reverse Mode

Based on the interference analysis between GEO and terrestrial systems, we in this section further derive respectively the closed-form expression for the expected interference experienced at the GEO satellite and earth station, and then calculate the GEO earth station protection radius R_0 in uplink link of the reverse mode.

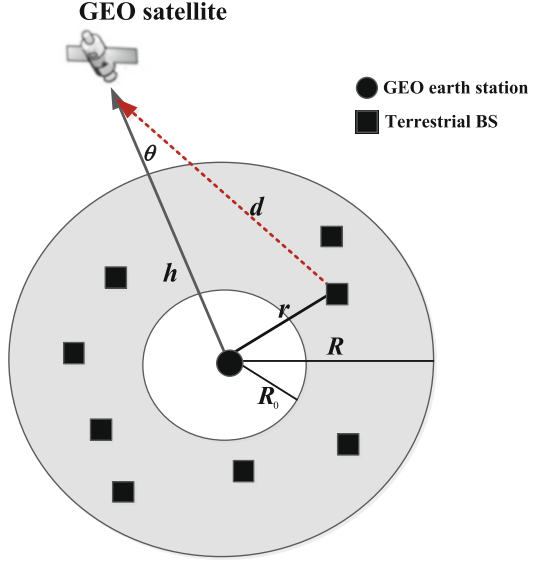
4.1.5.1 Expected Interference Experienced at the GEO Satellite

As illustrated in Fig. 4.6, let us use r to denote the distance between the terrestrial BS and the GEO earth station, and $d_{bs \rightarrow sa}$ to denote the distance between the GEO satellite and the terrestrial BS. Suppose that the GEO earth station is located at the substellar point of the GEO satellite and θ is the off bore-sight angle of the GEO satellite in the direction of the terrestrial BS. In such a case, $d_{bs \rightarrow sa}$ can be expressed by

$$d_{bs \rightarrow sa}(\theta) = h \sec \theta, \quad (4.14)$$

where h represents the altitude between the GEO satellite and the GEO earth station and usually assumed to be 35,786 km. Since all the terrestrial BSs are assumed to

Fig. 4.6 The spectrum coexistence in the uplink reverse link



be uniformly distributed, r has the distribution of

$$f(r) = \frac{2r}{R^2 - R_0^2}, \quad R_0 \leq r \leq R. \quad (4.15)$$

As $\theta = \arctan \frac{r}{h}$, θ has the distribution of

$$f(\theta) = \frac{2h^2 \tan \theta \sec^2 \theta}{R^2 - R_0^2}, \quad \arctan \frac{R_0}{h} \leq \theta \leq \arctan \frac{R}{h}. \quad (4.16)$$

The interference received by the GEO satellite is from all $n = \rho \pi (R^2 - R_0^2)$ terrestrial BSs, and the expected interference of (4.2) can be derived as follows

$$\begin{aligned} E[I_{bs \rightarrow sa}] &= E[P_{bs} G_{bs} G_{sa}(\theta) \left(\frac{c}{4\pi f d_{bs \rightarrow sa}(\theta)} \right)^2 \phi_k^2] \\ &= \frac{P_{bs} G_{bs} c^2 \rho}{8\pi f^2} \int_{\arctan \frac{R_0}{h}}^{\arctan \frac{R}{h}} G_{sa}(\theta) \tan \theta d\theta \cdot E[\phi_k^2]. \end{aligned} \quad (4.17)$$

Since the channel between the terrestrial BS and the satellite is considered to be Rician fading, we have $E(\phi_k^2) = 2\sigma^2 + \nu^2$, where ν is the Rice factor and σ is the shadow fading coefficient. In such a case, the expected interference in (4.17) can be re-written by

$$E[I_{bs \rightarrow sa}] = \frac{P_{bs} G_{bs} c^2 \rho (2\sigma^2 + \nu^2)}{8\pi f^2} \int_{\arctan \frac{R_0}{h}}^{\arctan \frac{R}{h}} G_{sa}(\theta) \tan \theta d\theta. \quad (4.18)$$

The reference antenna pattern $G_{sa}(\theta)$ for the GEO satellite can be referred to the standard in ITU-R S. 672-4 [7]. In addition, when considering the scenario of an infinite network, i.e. $R \rightarrow \infty$, the term $\int_{\arctan \frac{R_0}{h}}^{\arctan \frac{R}{h}} G_{sa}(\theta) \tan \theta d\theta$ can be derived as follows

$$\lim_{R \rightarrow \infty} \int_{\arctan \frac{R_0}{h}}^{\arctan \frac{R}{h}} G_{sa}(\theta) \tan \theta d\theta = 1.52 + 10^{\frac{G_{max}}{10}} \left(\ln \left(\left| \cos \left(\frac{\theta_b \pi}{180} \right) \right| \right) - \ln \left(\left| \cos \left(\arctan \frac{R_0}{h} \right) \right| \right) \right), \quad (4.19)$$

where G_{max} is the maximum antenna gain of the GEO satellite and θ_b is the one half the 3 dB beam width. Finally, by substituting (4.19) into (4.18), the value of $E[I_{bs \rightarrow sa}]$ can be obtained.

4.1.5.2 GEO Satellite Protection Radius

Similarly, by applying the Markov inequality, the GEO satellite outage constraint in (4.5) can be expressed by

$$Pr[I_{bs \rightarrow sa} \geq \frac{P_{grs}}{2^{C_0} - 1} - N_s] \leq \frac{E[I_{bs \rightarrow sa}]}{\frac{P_{grs}}{2^{C_0} - 1} - N_s} \leq \eta, \quad (4.20)$$

where P_{grs} is the reception power of the GEO satellite and N_s is the noise of GEO satellite. In such a case, the upper bound of $E[I_{bs \rightarrow sa}]$ can be obtained

$$E[I_{bs \rightarrow sa}] \leq \eta \left(\frac{P_{grs}}{2^{C_0} - 1} - N_s \right). \quad (4.21)$$

By substituting (4.18) and (4.19) into (4.21), the bound on the protection radius can be finally achieved.

4.1.5.3 Simulations

In this section, we investigate the relationship between the GEO system protection radius R_0 and the expected interference $E[I_{bs \rightarrow sa}]$ with the different BS power P_{bs} . In the simulation, the system parameters are listed in Table 4.2. As described in Fig. 4.7, the harmful interference can be ignored when the terrestrial BS power is 37 and 40 dBm. Whereas the protection radius R_0 is at least 60.29 km when the terrestrial BS power increases into 43 dBm. An alternative method to solve the interference problem is to control the transmission power of the terrestrial BSs, which should also ensure the terrestrial link working normally.

Table 4.2 Simulation parameters

Parameter	Values
Frequency bands	27.5 GHz
BS transmit power P_{bs}	37/40/43 dBm
BS antenna gain towards the satellite G_{bs}	1 dBi
BS antenna radiation pattern	ITU-R F.1336
Maximum satellite antenna gain	47 dBi
Earth station EIRP	63 dBW
Satellite noise temperature	500 K
Satellite antenna radiation pattern	ITU-R S.672-4

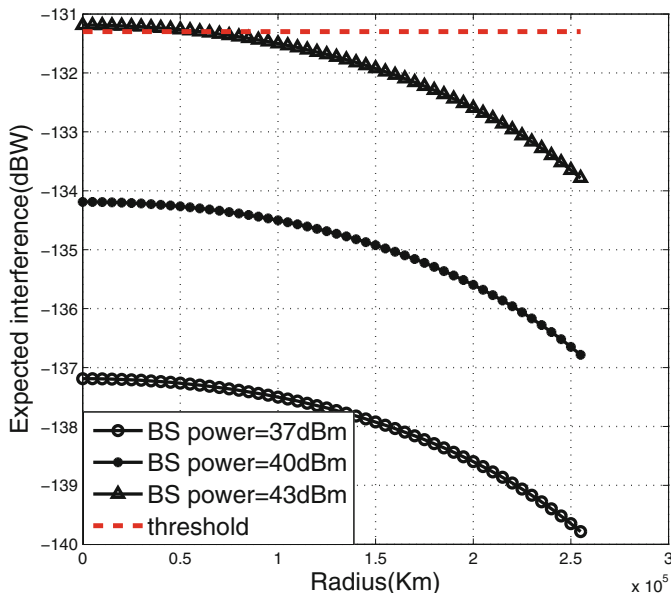


Fig. 4.7 The relationship between the expected interference $E[I_{bs \rightarrow sa}]$ and protection radius R_0 with the different BS power when $\beta = 0.1$

4.2 Spectrum Coexistence Between GEO and NGEO Systems

4.2.1 Interference Analysis and Network Mode

Depends on current ITU-R regulation, consider that the spectrum sharing between GEO and NGEO systems operating in downlink normal mode and uplink normal mode. As described in Fig. 4.8, the GEO earth station and GEO satellite will be interfered respectively by NGEO satellite and NGEO earth stations. We consider the cognitive network as follows: the GEO system regarded as the primary user and the NGEO system regarded as the secondary user. As shown in Fig. 4.9, it is assumed that the GEO system consists of a GEO satellite and a GEO earth station

Fig. 4.8 The spectrum coexistence between GEO and NGEO systems

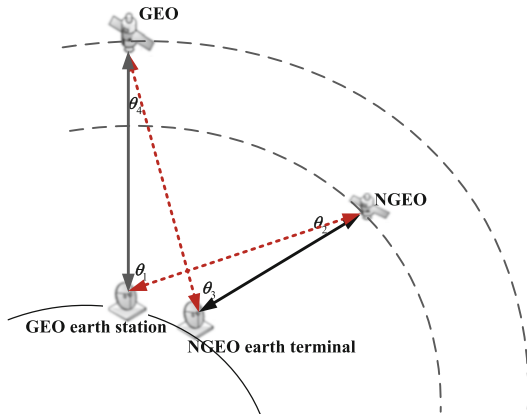
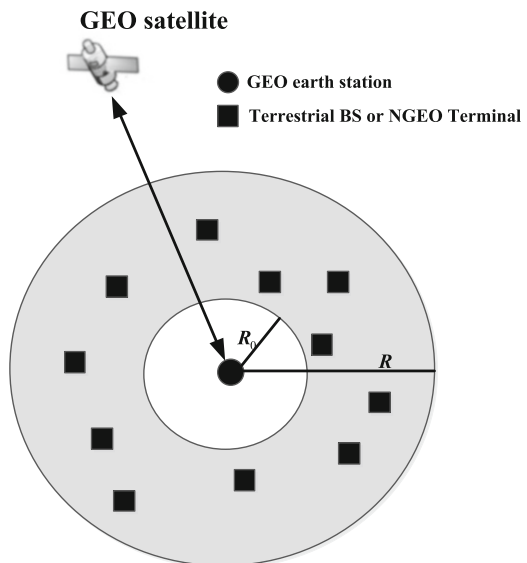


Fig. 4.9 The spectrum coexistence between GEO and other systems



located at the center of the network. In general, the location of GEO earth station can be known through the ITU database. In order to ensure an outage capacity of the GEO system, any NGEO earth terminal is at least R_0 radium away from the GEO earth station. There are n NGEO terminals randomly and uniformly distributed with density ρ in the circle between the radius R_0 and R .

4.2.2 Channel and Signal Model

As shown in Fig. 4.8, in the downlink normal link, the interference from the NGEO satellite to the GEO earth station can be expressed as

$$I_{ns \rightarrow es} = P_{ns} G_{ns}(\theta_2) G_{es}(\theta_1) \left(\frac{c}{4\pi f d_{ns \rightarrow es}} \right)^2 \phi_k^2, \quad (4.22)$$

where P_{ns} is the transmission power at the NGEO satellite, $G_{ns}(\theta_2)$ is the NGEO satellite gain at the direction of θ_2 , $G_{es}(\theta_1)$ is the GEO earth station antenna gain to direction of θ_1 , ϕ_k is a Ricean parameter, $d_{ns \rightarrow es}$ is the distance between the NGEO satellite and the GEO earth station.

For the uplink link, the interference from the NGEO terminal to the GEO satellite can be calculated as

$$I_{nt \rightarrow sa} = P_{nt} G_{nt}(\theta_3) G_{sa}(\theta_4) \left(\frac{c}{4\pi f d_{nt \rightarrow sa}} \right)^2 \phi_k^2, \quad (4.23)$$

where P_{nt} is the transmission power at the NGEO terminal, $G_{nt}(\theta_3)$ is the NGEO terminal antenna gain at the direction of θ_3 , $G_{sa}(\theta_4)$ is the GEO satellite antenna gain to the direction of θ_4 , ϕ_k is a Ricean parameter, $d_{nt \rightarrow sa}$ is the distance between NGEO earth terminal and the GEO satellite.

4.2.3 Downlink Normal Mode

Based on the interference analysis between GEO and NGEO systems in last section, we in this section derive the closed-form expression for the expected interference and then calculate the GEO system protection radius in the downlink normal link. Assume that the GEO earth station is located at the substellar point of the GEO satellite. The rectangular coordinate system is established in Fig. 4.10, the geocentre O is assumed to be the origin of coordinates, θ_1 is the off bore-sight angle of the GEO earth station in the direction of the NGEO satellite, θ_2 is the off bore-sight angle of the NGEO satellite in the direction of the GEO earth station, θ_3 is the off bore-sight angle of the NGEO earth station in the direction of the GEO satellite and θ_4 is the off bore-sight angle of the GEO satellite in the direction of the NGEO earth station. Let ψ denotes the included angle between GEO and NGEO satellites and ν denotes the included angle between GEO and NGEO earth stations. In addition, r also represents the distance between the GEO and NGEO earth stations, and $R_0 \leq r \leq R$.

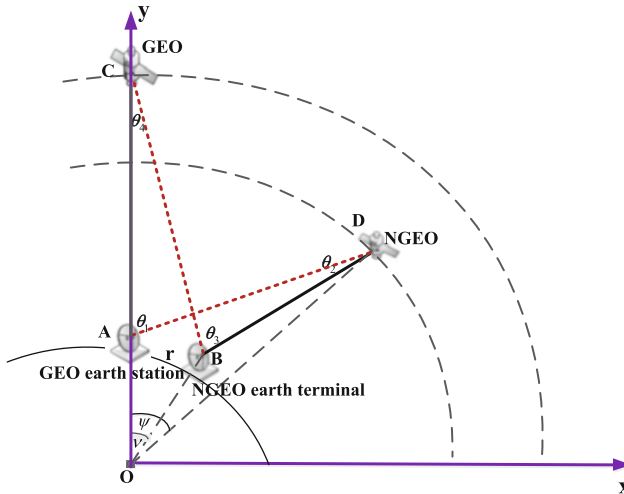


Fig. 4.10 The spectrum coexistence between GEO and NGEO systems

The vectors **AC**, **AD**, **BC**, **BD** can be expressed as following

$$\begin{aligned}
 \mathbf{AC} &= [0, 35,786], \\
 \mathbf{AD} &= [h_{ngeo} \sin \psi, h_{ngeo} \cos \psi - req], \\
 \mathbf{BC} &= [-req \sin \nu, (35,786 + req) - req \cos \nu], \\
 \mathbf{BD} &= [h_{ngeo} \sin \psi - req \sin \nu, h_{ngeo} \cos \psi - req \cos \nu],
 \end{aligned} \tag{4.24}$$

where $\nu = \frac{r}{req}$, req is the earth radius 6,378 km, h_{ngeo} denotes the altitude of NGEO satellite and 35,786 km is the altitude of the GEO satellite.

In Fig. 4.11, the contour maps depict the variation of θ_1 to θ_4 with the changes of angle ψ and distance r . It can be seen that, r has little influence on θ_1 and has a very tiny influence on θ_3 , in addition, both θ_1 and θ_3 increase when ψ is becoming larger; with the increasing of ψ , θ_2 first increases then decreases and θ_4 has little changes, and also larger value of r leads to greater θ_2 and θ_3 .

4.2.3.1 Expected Interference Experienced at the GEO Earth Station

As the analysis above, since all NGEO earth stations uniformly and randomly distribute in the circle between the radius R_0 and R , the distribution of r can be expressed as $f(r) = \frac{2r}{R^2 - R_0^2}$, $R_0 \leq r \leq R$. The interference received by the GEO satellite originates from all $n = \rho\pi(R^2 - R_0^2)$ NGEO earth stations, and thus the expected interference in (4.22) can be written and derived as follows

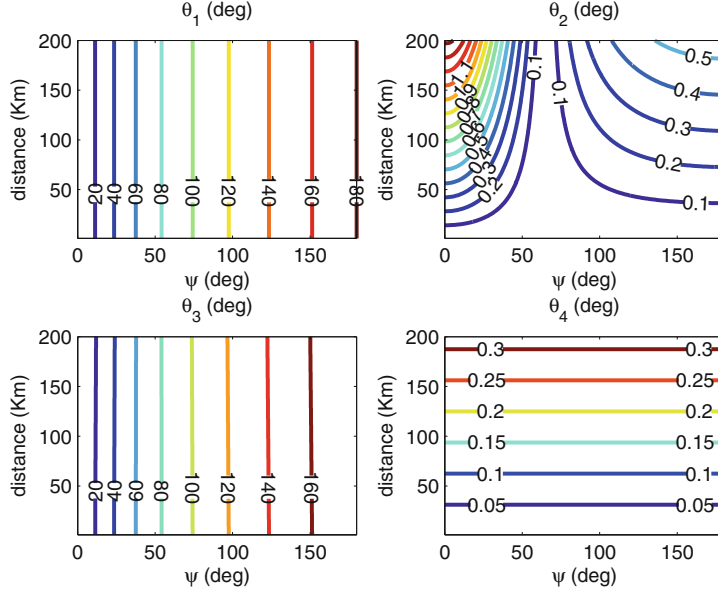


Fig. 4.11 Contour maps of θ_1 to θ_4 with respect to varying r and ψ

$$E[I_{ns \rightarrow es}] = (2\sigma^2 + v^2)\rho P_{ns} \int_{R_0}^R r \int_0^{2\pi} G_{ns}(\theta_2) G_{es}(\theta_1) \left(\frac{c}{4\pi f d_{ns \rightarrow es}} \right)^2 d\psi dr,$$

$$\theta_1 = \arccos\left(\frac{\mathbf{AC} \cdot \mathbf{AD}}{|\mathbf{AC}| |\mathbf{AD}|}\right), \theta_2 = \arccos\left(\frac{\mathbf{AD} \cdot \mathbf{BD}}{|\mathbf{AD}| |\mathbf{BD}|}\right), d_{ns \rightarrow es} = |\mathbf{AD}|.$$
(4.25)

The reference antenna pattern G_{ns} and G_{es} can be referred to the standard in ITU-R.S.1528 and ITU-R.S.456.

Substitute (4.24) into (4.25), the expected interference $E[I_{ns \rightarrow es}]$ becomes the function of R_0 and R . In the following simulations, we consider the NGEO earth stations distribute in the finite ranges.

4.2.3.2 GEO Satellite Protection Radius

By applying the Markov inequality, the GEO satellite outage constraint in (4.5) can be expressed by

$$Pr[I_{ns \rightarrow es} \geq \frac{P_{gre}}{2^{C_0} - 1} - N_s] \leq \frac{E[I_{ns \rightarrow es}]}{\frac{P_{gre}}{2^{C_0} - 1} - N_s} \leq \eta,$$
(4.26)

where P_{gre} is the reception power of the GEO earth station and N_s is the noise of GEO satellite. the upper bound of $E[I_{ns \rightarrow es}]$ can be obtained

$$E[I_{ns \rightarrow es}] \leq \eta \left(\frac{P_{gre}}{2^{C_0} - 1} - N_s \right). \quad (4.27)$$

By substituting (4.25) and into (4.27), the bound on the protection radius can be achieved.

4.2.3.3 Simulations

In this section, we investigate the relationship between the GEO system protection radius R_0 and the expected interference $E[I_{ns \rightarrow es}]$ in the downlink normal mode, with the different NGEO satellite heights. In order to ensure the NGEO system capacity, the higher altitude of NGEO satellite corresponds to the greater transmission power. The model of the NGEO satellite system refers to O3b system, and the detailed parameters of GEO and NGEO systems are given in Table 4.3. As described in Fig. 4.12, the higher altitude of NGEO satellite leads to more interference to GEO earth station. The reason is, with the increase of NGEO satellite height, the growth rate of NGEO satellite transmission power is faster than the distance between NGEO satellite and GEO earth station.

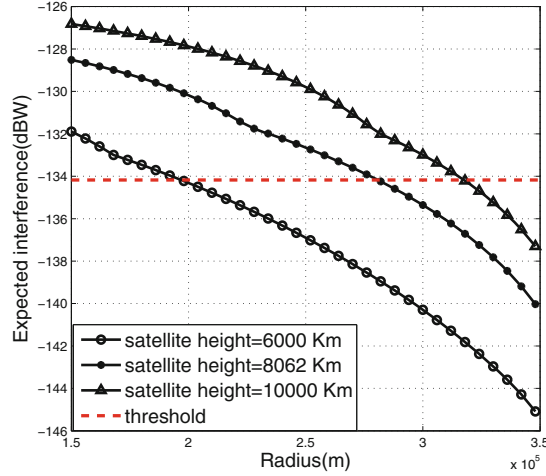
4.2.4 Uplink Normal Mode

Based on the interference analysis between GEO and NGEO systems, we in this section derive the closed-form expression for the expected interference and then calculate the GEO system protection radius in the uplink normal link.

Table 4.3 Simulation parameters

Satellite height/transmit power	
Downlink link parameter	Values
Frequency bands	18.48 GHz
Parameters for NGEO satellite	
Satellite height/transmit power P_{ns}	6000 km/7.8887 dBW 8062 km/10.4546 dBW 10,000 km/12.3257 dBW
Max satellite antenna gain G_{ns}	31.5 dBi
Half power beamwidth	3.2°
NGEO satellite antenna radiation pattern	ITU-R S.1528
Parameters for GEO system	
Satellite height	35,786 km
Satellite EIRP	62.7 dBW
Max station antenna gain G_{es}	41 dBi
Station antenna diameter	0.75 m
Station noise temperature	300 K
GEO station antenna radiation pattern	ITU-R S.465-6

Fig. 4.12 The relationship between the expected interference $E[I_{ns \rightarrow es}]$ and protection radius R_0 with the different NGEO satellite height when $\beta = 0.1$



4.2.4.1 Expected Interference Experienced at the GEO Satellite

Similar to the analysis in downlink normal mode, the expected interference in (4.23) can be written as follows

$$E[I_{nt \rightarrow sa}] = (2\sigma^2 + v^2)\rho P_{ns} \int_{R_0}^R r \int_0^{2\pi} G_{nt}(\theta_3) G_{sa}(\theta_4) \left(\frac{c}{4\pi f d_{nt \rightarrow sa}} \right)^2 d\psi dr,$$

$$\theta_3 = \arccos\left(\frac{\mathbf{BC} \cdot \mathbf{BD}}{|\mathbf{BC}| |\mathbf{BD}|}\right), \theta_4 = \arccos\left(\frac{\mathbf{AC} \cdot \mathbf{BC}}{|\mathbf{AC}| |\mathbf{BC}|}\right),$$

$$d_{nt \rightarrow sa} = |\mathbf{BC}|. \quad (4.28)$$

The reference antenna pattern G_{nt} and G_{sa} can be referred to the standard in ITU-R.S.1428 and ITU-R.S.672.

Substitute (4.24) into (4.28), the expected interference $E[I_{nt \rightarrow sa}]$ becomes the function of R_0 and R .

4.2.4.2 GEO Satellite Protection Radius

Similarly, by applying the Markov inequality, the upper bound of $E[I_{nt \rightarrow sa}]$ can be obtained

$$E[I_{nt \rightarrow sa}] \leq \eta \left(\frac{P_{grs}}{2^{C_0} - 1} - N_s \right). \quad (4.29)$$

where P_{grs} is the reception power of the GEO satellite and N_s is the noise of GEO satellite. By substituting (4.28) and (4.29), the bound on the protection radius can be achieved.

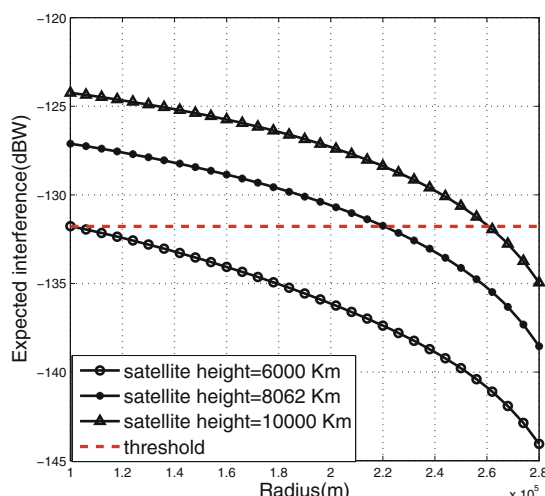
4.2.4.3 Simulations

In this section, we investigate the relationship between the GEO system protection radius R_0 and the expected interference $E[I_{nt \rightarrow sa}]$ with the different NGEO satellite heights in the reverse normal mode. The detailed parameters of GEO and NGEO systems are given in Table 4.4. It is obvious that the higher altitude of NGEO satellite corresponds to the greater transmission power. In addition, the distance between the NGEO earth station and the GEO satellite remain unchanged with the

Table 4.4 Simulation parameters

Satellite height/transmit power	
Uplink link parameter	Values
Frequency bands	28.28 GHz
<i>Parameters for NGEO earth station</i>	
Satellite height/transmit power of earth station P_{nt}	6000 km/17.4341 dBW 8062 km/20 dBW 10,000 km/21.87 dBW
Station antenna diameter	0.3 m
Max earth station antenna gain G_{nt}	36.7 dBi
NGEO earth station antenna radiation pattern	ITU-R S.1428-1
<i>Parameters for GEO system</i>	
Satellite height	35,786 km
Earth station EIRP	63 dBW
Max satellite antenna gain G_{sa}	47 dBi
Satellite noise temperature	500 K
Half power beamwidth	0.82°
GEO satellite antenna radiation pattern	ITU-R S.672-4

Fig. 4.13 The relationship between the expected interference $E[I_{ns \rightarrow es}]$ and protection radius R_0 with the different NGEO satellite height when $\beta = 0.1$



different NGEO satellite heights. Therefore, the higher NGEO satellite height can cause the more interference from the NGEO earth station to the GEO satellite, and the protection radius R_0 needed is greater, as described in Fig. 4.13.

4.3 Blind Spot of Spectrum Awareness Techniques

Compared with geostationary (GEO) satellite systems, non-geostationary (NGEO) satellite systems have certain advantages, such as low space attenuation, low propagation delay and less cost of in-orbit injection per satellite etc. As the number of NGEO satellites in space has been continuously increasing, the requirement for frequency coexistence between the NGEO and GEO satellite networks also arises rapidly, which means more interference may occur between two satellite systems. Moreover, new NGEO satellite systems have to protect the existing GEO satellite systems in the shared spectrum according to the policy of the Radio Regulations (RR) [8].

In order to reduce the interference caused by spectrum coexistence and improve the spectrum utilization, cognitive radios (CR) techniques have been proposed as a promising solution to improve current situation [9–14]. The main functions of CR can be classified as spectrum sensing [15–18], spectrum management [19–21], spectrum sharing [22–25] and spectrum mobility [26, 27]. Among them, as the basis function of CR, spectrum awareness techniques allow the cognitive systems to be aware of the vacant or unused bands for the utilization of sparing bands. The effectiveness of the spectrum awareness methods have been presented for terrestrial communication systems in [28–33]. Nevertheless, the spectrum awareness techniques in the satellite communications area have not been well investigated and the existing works mainly focus on the analysis of application scenarios and the interference studies between NGEO and GEO satellite systems. In the earlier stage, Fortes et al. presented an analytical approach to assess interference involving two or more NGEO satellite networks [34]. Later, the contribution in [35] discussed the application prospects of spectrum awareness in NGEO systems. Meanwhile, Park et al. [36] analyzed the interference effect from NGEO system to GEO system by BER (bit-error-rate) performance, according to varying the angular separation and the number of NGEO satellites. The interference characteristics between an NGEO satellite MSS (mobile satellite services) gateway station and a GEO satellite FSS (fixed satellite services) earth station under the reverse band sharing was researched in [37]. Recently, Sharma et al. [38] proposed an adaptive power control technique for both the uplink and downlink scenarios in order to mitigate the in-line interference between GEO and MEO satellite systems.

Among the existing literature, few papers have discussed concretely the feasibility of spectrum awareness techniques in the coexistence scenario between GEO and NGEO satellite systems. In this context, the general method of spectrum awareness is that, if the NGEO system receivers detect the signals from the GEO system, the shared spectrum is considered to be occupied; otherwise, it is regarded as an idle

and can be accessed by the NGEO satellite systems. However, as the mobility of NGEO satellite, there can be an area where the NGEO system could not receive the signals from the GEO transmitters but the GEO system may be disturbed by the NGEO transmitters. In this area, i.e. the blind spot of spectrum awareness, the spectrum awareness techniques would fail to identify accurately the spectrum holes across the shared spectrum for NGEO systems. Considering this problem, we introduce a method to investigate whether there exists the situation of blind spot in the spectrum coexistence of the GEO system as a primary user and the NGEO system as a cognitive user. Both uplink and downlink transmissions are analyzed and three key parameters, i.e. altitude of NGEO satellites and antenna patterns of NGEO and GEO earth terminals, are considered. Moreover, we propose several classical application scenarios and study the performance of spectrum awareness methods numerically.

4.3.1 System Model

In order to analyze the probability of the blind spot, the essence is to identify the region where the NGEO system could detect the signals from GEO transmitters (we call it as detection area in this article) and the region where the GEO system could be interfered by NGEO transmitters (we call it as interference area). If the interference area is not contained by the detection area, the blind spot of spectrum awareness would be existent. To simplify the theoretical analysis but without loss of generality, we study a single NGEO satellite operating in the same frequency bands as that of the GEO satellite. Meanwhile, the worst interference scenario is considered by assuming that both the GEO and NGEO earth stations are located in the equatorial plane.

As described in Fig. 4.14, the NGEO system coexists with the GEO system. θ_1 is the off bore-sight angle of the GEO earth station along the direction of the NGEO satellite, θ_2 is the off bore-sight angle of the NGEO satellite along the direction of the GEO earth station, θ_3 is the off bore-sight angle of the NGEO earth station along the direction of the GEO satellite and θ_4 is the off bore-sight angle of the GEO satellite along the direction of the NGEO earth station. Moreover, $d_{ge \rightarrow ns}$ represents the distance between the GEO earth station and the NGEO satellite, $d_{ne \rightarrow gs}$ represents the distance between the NGEO earth station and GEO satellite, r is the distance between GEO and NGEO earth stations. Let β denote the included angle between the GEO and NGEO satellites, and α denote the included angle between the GEO and NGEO earth stations. As the locations of GEO and NGEO earth stations is assumed to be fixed, the angle α and θ_4 are also constants. In addition, since the NGEO satellite moves over the time, the values of β also varies over the time.

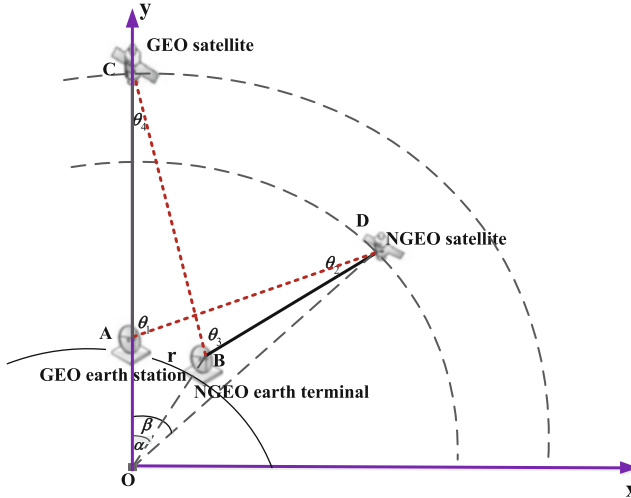


Fig. 4.14 The spectrum coexistence between GEO and NGEO systems

4.3.2 *Blind Spot Analysis of Uplink Scenario*

In this section, we conduct theoretic analysis on the blind spot based on the aforementioned system model of the uplink scenario. In the uplink, the blind spot is the area where the NGEO satellite could not detect the signals from the GEO earth station while the NGEO earth station would cause interference to the GEO satellite, i.e. when the detection area cannot cover the interference area, the blind spot appears.

4.3.2.1 **The Area of the NGEO Satellite Detecting the Signals from the GEO Earth Station (Detection Area)**

The uplink transmission from the GEO earth station to the GEO satellite can be received by the NGEO satellite, if the power of received signals exceeds the level of detection threshold. The power of signals received by the NGEO satellite from the GEO earth station can be written as follow

$$P_{ge \rightarrow ns} = P_{get} G_{get}(\theta_1) G_{nsr}(\theta_2) \left(\frac{c}{4\pi f d_{ge \rightarrow ns}} \right)^2 \geq P_{th}, \quad (4.30)$$

where P_{get} is the transmission power of the GEO earth station, G_{get} is the gain of the transmit antenna at the GEO earth station, G_{nsr} is the gain of the receive antenna at the NGEO satellite, P_{th} is the detection threshold, c is the light speed and f is the center frequency of the spectrum bands.

It can be seen from Fig. 4.14, the vectors **AC**, **AD**, **BD** can be expressed as

$$\begin{aligned}\mathbf{AC} &= [0, 35, 786], \\ \mathbf{AD} &= [h_{ngeo} \sin \beta, h_{ngeo} \cos \beta - req], \\ \mathbf{BD} &= [h_{ngeo} \sin \beta - req \sin \alpha, h_{ngeo} \cos \beta - req \cos \alpha],\end{aligned}\quad (4.31)$$

where $\alpha = \frac{r}{req}$, req is the earth radius 6378 km, h_{ngeo} denotes the altitude of NGEO satellite and 35,786 km is the altitude of the GEO satellite. In addition, θ_1 , θ_2 and $d_{ge \rightarrow ns}$ in (4.30) can be presented by β and h_{ngeo} :

$$\theta_1 = \arccos\left(\frac{\mathbf{AC} \cdot \mathbf{AD}}{|\mathbf{AC}| |\mathbf{AD}|}\right) = \arccos\left(\frac{h_{ngeo} \cos \beta - req}{\sqrt{c_2 - 2c_1 \cos(\beta)}}\right), \quad (4.32)$$

$$\begin{aligned}\theta_2 &= \arccos\left(\frac{\mathbf{AD} \cdot \mathbf{BD}}{|\mathbf{AD}| |\mathbf{BD}|}\right) \\ &= \arccos\left(\frac{h_{ngeo}^2 - c_1 \cos(\beta - \alpha) - c_1 \cos(\beta) + req^2 \cos(\alpha)}{\sqrt{(c_2 - 2c_1 \cos(\beta))(c_2 - 2c_1 \cos(\beta - \alpha))}}\right),\end{aligned}\quad (4.33)$$

$$d_{ge \rightarrow ns} = |\mathbf{AD}| = \sqrt{c_2 - 2c_1 \cos(\beta)}, \quad (4.34)$$

where $c_1 = h_{ngeo} * req$, $c_2 = h_{ngeo}^2 + req^2$, $c_3 = req^2 + (req + 35,786)^2$, $c_4 = 2req * (req + 35,786)$.

The reference antenna pattern G_{get} and G_{ns} can be referred to the standard in ITU-R.S.1428 and ITU-R.S.1528. In such a case, the detection area can be evaluated by β and h_{ngeo} .

4.3.2.2 The Area of the NGEO Earth Station Generating the Interference to GEO Satellite (Interference Area)

The uplink transmission from the NGEO earth station to the NGEO satellite may cause interference to the GEO satellite. In order to protect the GEO system, the equivalent power flux-density (epfd) is introduced to estimate the interference from the NGEO to the GEO system according to RR. Let us use $epfd_{th}$ to represent the limits of $epfd$ given in RR, i.e., if the value of $epfd$ exceeds the threshold, it is assumed that the GEO satellite will be disturbed by the NGEO system

$$epfd = \frac{P_{net} G_{net}(\theta_3) G_{gsr}(\theta_4)}{4\pi d_{ge \rightarrow gs}^2 G_{gsr,max}} \geq epfd_{th}, \quad (4.35)$$

where P_{net} is the transmit power of the NGEO earth station, G_{net} is the gain of the transmit antenna at the NGEO earth station, G_{gsr} is the gain of the receive antenna at the GEO satellite and $G_{gsr,max}$ represents the maximum gain of the receive antenna of the GEO satellite. In addition, the reference antenna pattern G_{net} and G_{gsr} can be referred to the standard in ITU-R.S.1428 and ITU-R.S.672-4.

Similarly, we can find that $d_{ne \rightarrow gs}$, $G_{gsr,max}$ and θ_4 are constants, while θ_3 can be expressed by β and h_{ngeo} :

$$\begin{aligned}\theta_3 &= \arccos\left(\frac{\mathbf{BC} \cdot \mathbf{BD}}{|\mathbf{BC}| |\mathbf{BD}|}\right) \\ &= \arccos\left(\frac{req^2 - c_1 \cos(\beta - \alpha)}{\sqrt{(c_3 - c_4 \cos(\alpha))(c_2 - 2c_1 \cos(\beta - \alpha))}}\right) \\ &\quad + \frac{42164(h_{ngeo} \cos(\beta) - req \cos(\alpha))}{\sqrt{(c_3 - c_4 \cos(\alpha))(c_2 - 2c_1 \cos(\beta - \alpha))}},\end{aligned}\quad (4.36)$$

$$\theta_4 = \arccos\left(\frac{\mathbf{AC} \cdot \mathbf{BC}}{|\mathbf{AC}| |\mathbf{BC}|}\right) = \arccos\left(\frac{42164 - req \cos(\alpha)}{req^2 + c_3 - c_4}\right),\quad (4.37)$$

$$d_{ne \rightarrow gs} = |\mathbf{BC}| = \sqrt{c_3 - c_4 \cos(\alpha)},\quad (4.38)$$

where $\mathbf{BC} = [-req \sin \alpha, (35,786 + req) - req \cos \alpha]$. By substituting expressions above into (4.35), it can be found readily that the interference area also can be evaluated by β and h_{ngeo} .

4.3.2.3 Blind Spot

In this scenario, the blind spot is the region where the detection area fails to cover the detection area. The blind spot can be written as

$$\begin{cases} P_{ge \rightarrow ns} = P_{get} G_{get}(\theta_1) G_{nsr}(\theta_2) \left(\frac{c}{4\pi f d_{ge \rightarrow ns}}\right)^2 \leq P_{th}, \\ epfd = \frac{P_{net} G_{net}(\theta_3) G_{gsr}(\theta_4)}{4\pi d_{ne \rightarrow gs}^2 G_{gsr,max}} \geq epfd_{th}. \end{cases}\quad (4.39)$$

From the derivation above, the blind spot can be expressed by β and h_{ngeo} , and thus, the value of β and h_{ngeo} satisfying (4.39) is the scope of blind spot.

4.3.3 *Blind Spot Analysis of Downlink Scenario*

In this section, we conduct theoretic analysis on the blind spot based on the aforementioned system model of the downlink scenario. We consider the spectrum coexistence of GEO and NGEOP systems both operating in the downlink. The blind spot in the downlink is the area where the NGEOP earth station could not detect the signals from the GEO satellite while the NGEOP satellite would bring the interference into the GEO earth station, i.e. when the detection area cannot cover the

interference area, the blind spot appears. The same analytical method is introduced as described in the previous section.

4.3.3.1 The Area of the NGEO Earth Station Detecting the Signals from the GEO Satellite (Detection Area)

The power of signals received by the NGEO earth station from the GEO satellite can be written as follow

$$P_{gs \rightarrow ne} = P_{gs} G_{gst}(\theta_4) G_{ner}(\theta_3) \left(\frac{c}{4\pi f d_{ne \rightarrow gs}} \right)^2 \geq P_{th}, \quad (4.40)$$

where P_{gs} is the transmission power of the GEO satellite, G_{gst} is the gain of the transmit antenna at the GEO satellite, G_{ner} is the gain of the receive antenna at the NGEO satellite, P_{th} is the detection threshold, c is the light speed and f is the center frequency of the spectrum band. Moreover, the reference antenna pattern G_{gst} and G_{ner} can be referred to the standard in ITU-R.S.672-4 and ITU-R.S.1428. If the value of $P_{gs \rightarrow ne}$ exceeds P_{th} , the NGEO earth station can detect the signals from the GEO satellite. Based on the previous analysis, we know that the range of detection area depends on the value of β and h_{ngeo} .

4.3.3.2 The Area of NGEO Satellite Generating the Interference to GEO Earth Station (Interference Area)

Similarly, we have

$$epfd = \frac{P_{nst} G_{nst}(\theta_2) G_{ger}(\theta_1)}{4\pi d_{ge \rightarrow ns}^2 G_{ger,max}} \geq epfd_{th}, \quad (4.41)$$

where P_{nst} is the transmit power of the NGEO satellite, G_{nst} is the gain of the transmit antenna at the NGEO satellite, G_{ger} is the gain of the receive antenna at the GEO earth station and $G_{ger,max}$ represents the maximum gain of the receive antenna of the GEO earth station. In addition, the reference antenna pattern G_{nst} and G_{ger} can be referred to the standard in ITU-R.S.1528 and ITU-R.S.1428. Moreover, $epfd_{th}$ represents the limits of $epfd$ given in RR. If the value of $epfd$ exceeds the threshold, the GEO satellite will be disturbed by the NGEO. Similarly, the interference area can be evaluated by β and h_{ngeo} .

4.3.3.3 Blind Spot

Base on the analysis above, the β and h_{ngeo} in the blind spot satisfy the following formula

$$\begin{cases} P_{gs \rightarrow ne} = P_{gs} G_{gst}(\theta_4) G_{ner}(\theta_3) \left(\frac{c}{4\pi f d_{ne \rightarrow gs}} \right)^2 \leq P_{th}, \\ epfd = \frac{P_{nst} G_{nst}(\theta_2) G_{ger}(\theta_1)}{4\pi d_{ge \rightarrow ns}^2 G_{ger,max}} \geq epfd_{th}. \end{cases} \quad (4.42)$$

4.3.4 Simulations and Analysis

In the simulation setup, the detection region and interference region are analyzed by varying β and h_{ngeo} , where h_{ngeo} varies from 500 to 30,000 km. The model of the NGEO satellite system refers to O3b system, and the detailed parameters of O3b and GEO system are given in [38]. Moreover, the distance between the GEO and the NGEO earth stations is supposed to be 3.31 km. Furthermore, we analyze the gain patterns of the GEO/NGEO earth stations and the GEO/NGEO satellites using relevant ITU-R recommendations [7, 39, 40].

4.3.4.1 Uplink Simulation Results

In the uplink simulation scenario, the carrier frequency is set as 28.28 GHz. The detection threshold is supposed to be $N - 10$ dB tentatively and N is the noise of NGEO system. In addition, the threshold of $epfd$ is -162 dBW/m 2 in 28.28 GHz according to RR. The contour maps are used to analyze the performance of $P_{ge \rightarrow ns}$ and $epfd$ with varying NGEO satellite altitudes and the values of β . The horizontal axis presents the altitude of NGEO satellite, and the vertical axis presents the values of β in following figures.

The antenna diameters of GEO earth station and NGEO earth station both are 7 m. In Fig. 4.15, the contour maps depict the power of signals received by NGEO satellite with different levels. The area below the detection threshold is that where the NGEO satellite can sense the signals from GEO earth station. It can be seen that, only when the value of β is close to zero, the signals from GEO earth station can be received. For instance of $h_{ngeo} = 10,000$ km, the NGEO satellite could detect the signals only when $|\beta| \leq 0.2^\circ$. In Fig. 4.16, the contour maps present the values of $epfd$ with different levels. The area below the threshold is that where the NGEO earth station could bring interference into the GEO satellite.

In order to conduct a clear comparison, both the detection area and the interference area are illustrated in Fig. 4.17, where the detection area is below the dot line and the interference area is below the solid line. With the increasing altitudes of the NGEO satellite, the tendency of the detection area and interference area are opposite to each other. Specifically, when $h_{ngeo} \geq 8000$ km, the detection area cannot cover the detection area, i.e., there exists the blind spot of spectrum awareness in the uplink.

Fig. 4.15 Contour maps of received signals by NGEO satellite with respect to varying NGEO altitude and β

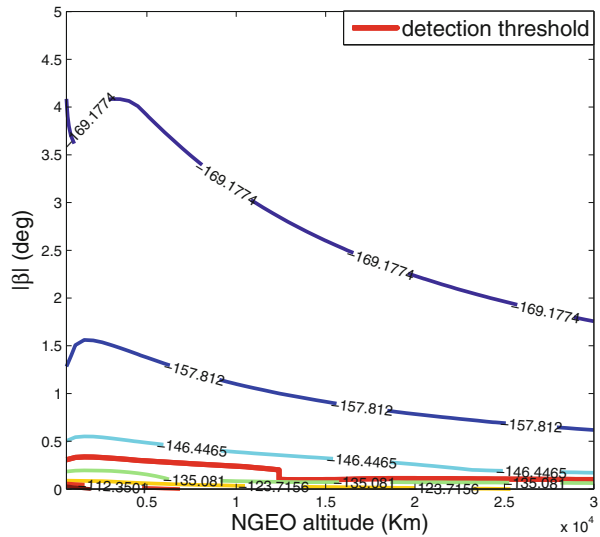
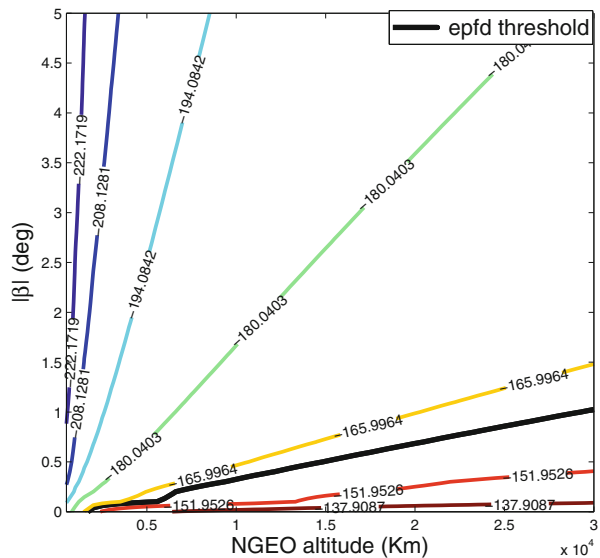


Fig. 4.16 Contour maps of equivalent power flux-density with respect to varying NGEO altitude and β



The antenna patterns are chosen as 0.7 m, 2.4 m and 7 m, respectively, as described in Figs. 4.18 and 4.19. It can be found that the smaller antenna corresponds to the larger detection area and also the larger interference area in the uplink scenario. This can be ascribed to the fact that the width of the side lobe in the smaller antenna is wider, therefore the regions disturbed by GEO and NGEO earth stations are wider in the smaller antenna.

Fig. 4.17 The detection area and interference area in the uplink

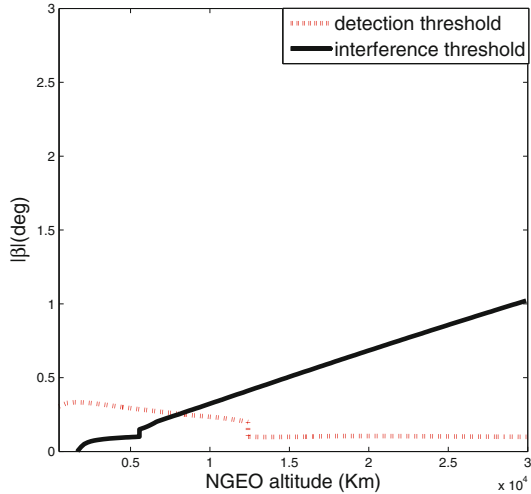
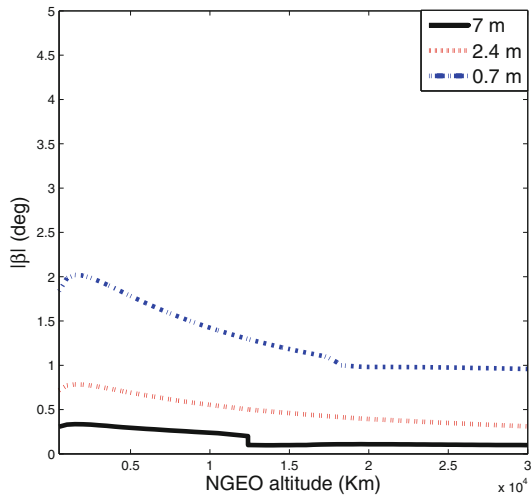


Fig. 4.18 The detection area in different antenna patterns of GEO earth stations



The reason of generating the blind spot is that the detection area could not cover the interference area. Reducing the value of detection threshold can enlarge the range of detection area so that the blind spot can be removed or reduced. The required level of the detection threshold can be acquired by the following steps:

- when h_{ngeo} is fixed, the range of β corresponding to the interference area (β_{inter}) can be obtained through (4.35);
- if the detection area cover the interference area, the range of β corresponding to the detection area (β_{det}) should be equal to β_{inter} at least;
- therefore, substituting the maximum value of β_{inter} and h_{ngeo} into (4.30) yields the value of P_{th} .

Fig. 4.19 The interference area in different antenna patterns of NGEO earth stations

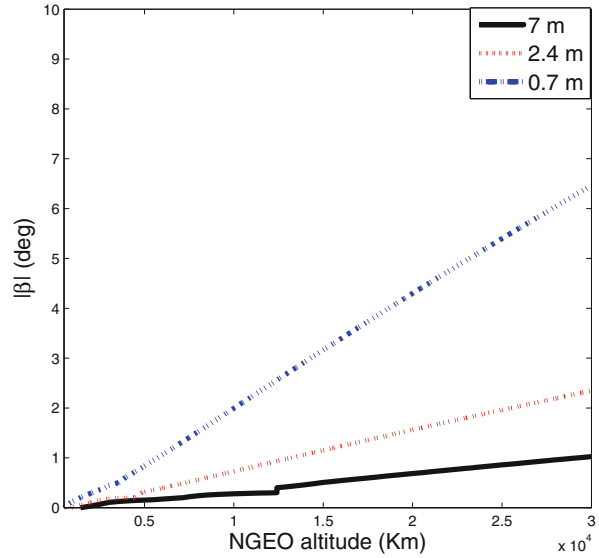


Table 4.5 Detection threshold needed

h_{ngeo} (km)	β_{inter} (deg)	Detection threshold (dB)
20,000	[-0.6 0.6]	N-25
15,000	[-0.5 0.5]	N-21
8062	[-0.2 0.2]	N-8
5000	Only when $\beta = 0^\circ$	N+22

Table 4.5 listed the detection threshold needed corresponding to different h_{ngeo} in order to remove the blind spot. As shown in Fig. 4.17 and Table 4.1, the higher altitude of NGEO means the larger blind spot, also requires the lower detection threshold, i.e. the detection methods should have a satisfied performance in low SNR.

4.3.4.2 Downlink Simulation Results

In the downlink simulation scenario, the carrier frequency is set as 18.48 GHz. The detection threshold is considered to be N-10 dB tentatively. In addition, the threshold of epfd is -161.4 dBW/m^2 in 18.48 GHz according to RR. The contour map is also used to analyze the performance of $P_{gs \rightarrow ne}$ and $epfd$ with different NGEO satellite altitudes and different values of β . The horizontal axis presents the altitude of NGEO satellite, and the vertical axis presents the values of β .

The antenna diameters of GEO earth station and NGEO earth station are 0.75 m and 2.4 m respectively. In Fig. 4.20, the contour maps present the power of signals received by NGEO earth station with different levels. The area below the detection threshold is that where the NGEO earth station can sense the signals from the GEO

Fig. 4.20 Contour maps of received signals by NGEO earth station with respect to varying NGEO altitude and β

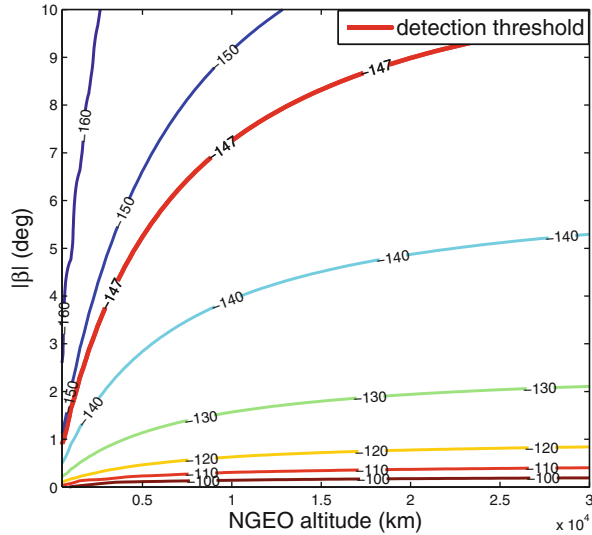
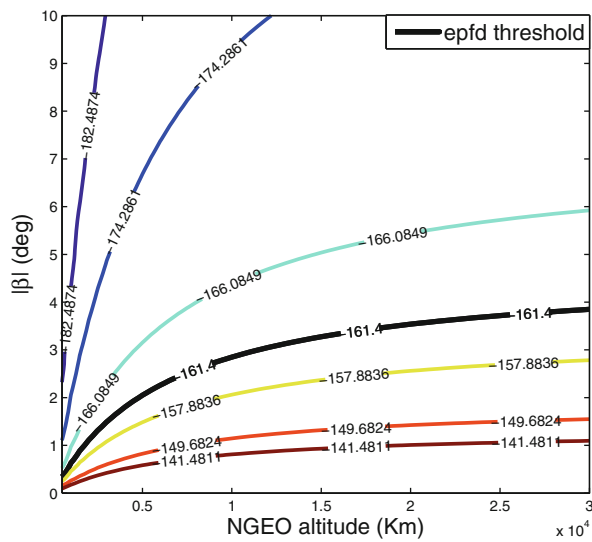


Fig. 4.21 Contour maps of equivalent power flux-density with respect to varying NGEO altitude and β



satellite. For instance, when $h_{ngeo} = 10,000$ km and $|\beta| \leq 7^\circ$, the NGEO earth station could detect the signals. In Fig. 4.21, the contour maps denote the values of $epfd$. The area below the threshold is that where the NGEO satellite could bring interference into GEO earth station. For instance, when $h_{ngeo} = 10,000$ km, $|\beta| \leq 2.8^\circ$, the GEO earth station will be disturbed by the NGEO satellite.

Similarly, both the detection area and the interference area are expressed in Fig. 4.22, where the detection area is below the dot line and the interference area is below the solid line. It can be found that both detection area and interference area

Fig. 4.22 The detection area and interference area in the downlink

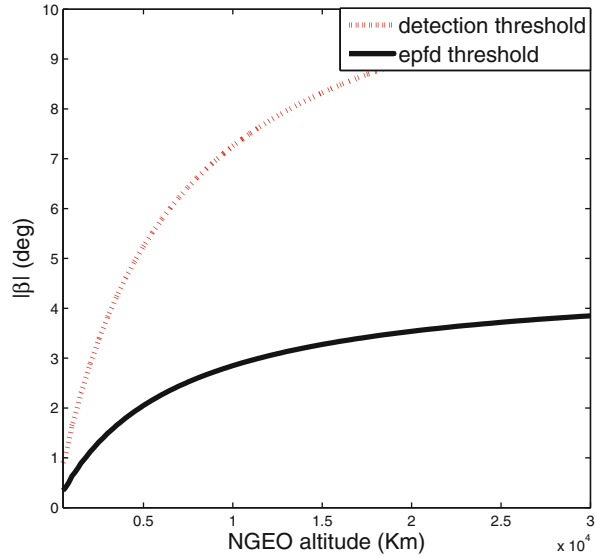
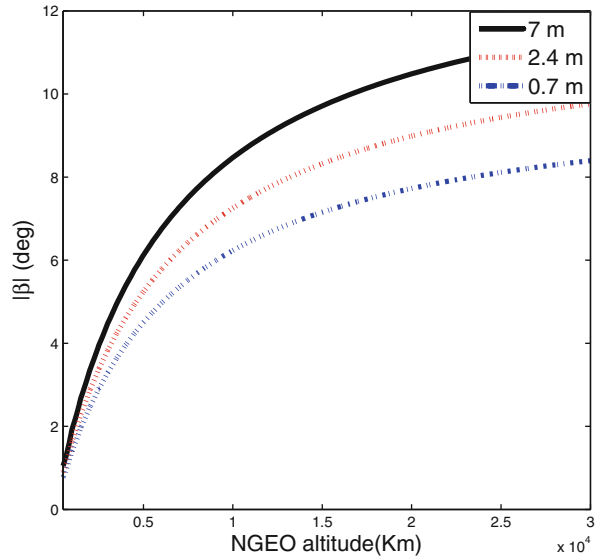


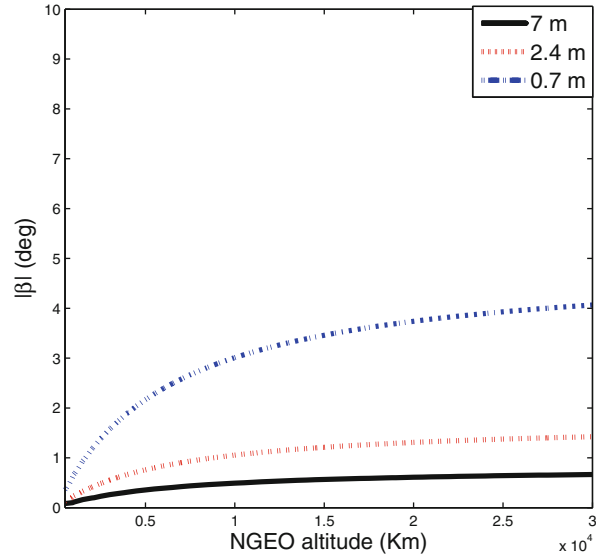
Fig. 4.23 The detection area in different antenna patterns of NGEO earth station



increase with the h_{ngeo} increasing. As the detection area contains the interference area, the blind spot of spectrum awareness is not existent in this situation.

The antenna patterns are chosen respectively 0.7 m, 2.4 m and 7 m, as described in Figs. 4.23 and 4.24. It can be found in Fig. 4.23 that the smaller antenna size of NGEO station corresponds to the smaller detection area. In the downlink, the NGEO earth stations detect the signals from GEO satellite. Since the antenna diameter of NGEO earth station is smaller, the noise level of the NGEO system is higher so that

Fig. 4.24 The interference area in different antenna patterns of GEO earth station



the required detection threshold is higher. For an instance, the noise of 7 m antenna is -138 dB, while that of 2.4 and 0.7 m antenna is -136 and -134 dB. As expressed in Fig. 4.24, the interference area is larger in smaller antenna. This can be explicated that the width of side lobe is wider and the maximum antenna gain is smaller in the smaller GEO station antenna, and thus, the area where the GEO earth station is disturbed by NGEO satellite is wider in the smaller antenna.

4.4 Summary

In this chapter, we analyze the interference caused by terrestrial cellular systems to the geostationary (GEO) system in two transmission modes. Then, in the scenario of spectrum coexistence between geostationary (GEO) and non-geostationary (NGEO) satellite systems, we discovers and investigates the issue of blind spot where the spectrum awareness techniques may fail to identify the spectrum holes. Both the uplink and downlink transmissions are analyzed and three key parameters, i.e. altitude of NGEO satellites and antenna patterns of NGEO and GEO earth stations, are considered.

References

1. S. Sharma, S. Chatzinota, B. Ottersten, Satellite cognitive communications: interference modeling and techniques selection, in *IEEE ASMA and 12th SPSC*, July 2012, pp. 111–118

2. C. Jiang, Y. Chen, Y.H. Yang, C.Y. Wang, K.J.R. Liu, Dynamic Chinese restaurant game: theory and application to cognitive radio networks. *IEEE Trans. Wirel. Commun.* **13**(4), 1960–1973 (2014)
3. C. Jiang, Y. Chen, K.J.R. Liu, Multi-channel sensing and access game: Bayesian social learning with negative network externality. *IEEE Trans. Wirel. Commun.* **13**(4), 2176–2188 (2014)
4. V. Abhayawardhana, I. Wassell, D. Crosby, M. Sellars, M. Brown, Comparison of empirical propagation path loss models for fixed wireless access systems. *IEEE VTC* **1**, 73–77 (2005)
5. ITU-R P.526-8, Series of ITU recommendations propagation by diffraction (2013)
6. 3GPP TR 36.814 v9.0.0, 3rd generation partnership project; Technical specification group radio access network; Evolved universal terrestrial radio access (E-UTRA); Further advancements for E-UTRA physical layer aspects (2010)
7. ITU-R S.672-4, Satellite antenna radiation pattern for use as a design objective in the fixed-satellite service employing geostationary satellites (2010)
8. ITU, Radio Regulations (2012)
9. Q. Mahmoud (ed.), *Cognitive Networks: Towards Self-Aware Networks* (Wiley, New York, 2007)
10. K.E. Baddour, O. Ureten, T.J. Willink, A distributed message-passing approach for clustering cognitive radio networks. *Wirel. Pers. Commun.* **57**(1), 119–133 (2011)
11. C. Jiang, Y. Chen, K.J.R. Liu, Y. Ren, Renewal-theoretical dynamic spectrum access in cognitive radio network with unknown primary behavior. *IEEE J. Sel. Areas Commun.* **31**(3), 406–416 (2013)
12. C. Jiang, Y. Chen, Y. Gao, K.J.R. Liu, Joint spectrum sensing and access evolutionary game in cognitive radio networks. *IEEE Trans. Wirel. Commun.* **12**(5), 2470–2483 (2013)
13. C. Jiang, Y. Chen, K.J.R. Liu, Y. Ren, Optimal pricing strategy for operators in cognitive femtocell networks. *IEEE Trans. Wirel. Commun.* **13**(9), 5288–5301 (2014)
14. C. Jiang, H. Zhang, Y. Ren, H. Chen, Energy-efficient non-cooperative cognitive radio networks: micro, meso and macro views. *IEEE Commun. Mag.* **52**(7), 14–20 (2014)
15. T. Yucek, H. Arslan, A survey of spectrum sensing algorithms for cognitive radio applications. *IEEE Commun. Surv. Tutorials* **11**(1), 116–130 (2009)
16. M. Nekovee, T. Irnich, J. Karlsson, Worldwide trends in regulation of secondary access to white spaces using cognitive radio. *IEEE Trans. Wirel. Commun.* **19**(4), 32–40 (2012)
17. M. Sansoy, A.S. Buttar, Spectrum sensing algorithms in cognitive radio: a survey, in *Electrical, Computer and Communication Technologies (ICECCT)*, 2015, pp. 1–5
18. T.J. Willink, A belief-based approach to spectrum occupancy mapping. *EURASIP J. Wirel. Commun. Netw.* **12**(1), 112 (2013)
19. I.F. Akyildiz, W.Y. Lee, M.C. Vuran, A survey on spectrum management in cognitive radio networks. *IEEE Commun. Mag.* **46**(4), 40–48 (2008)
20. Y.F. Liu, Dynamic spectrum management: a complete complexity characterization. *IEEE Trans. Inf. Theory* **63**(1), 392–403 (2017)
21. M. Rajarshi, Spectrum management framework in next generation wireless networks, in *2016 IEEE Annual IEEE*, 2016, pp. 1–6
22. F. Hessar, S. Roy, Spectrum sharing between a surveillance radar and secondary wi-fi networks. *IEEE Trans. Aerosp. Electron. Syst.* **52**(3), 1434–1448 (2016)
23. O.T. Hines, 14.5–14.8 GHz frequency sharing by data relay satellite uplinks and broadcasting-satellite uplinks. *IEEE Trans. Aerosp. Electron. Syst.* **3**, 401–409 (1981)
24. H. Deng, B. Himed, Interference mitigation processing for spectrum-sharing between radar and wireless communication systems. *IEEE Trans. Aerosp. Electron. Syst.* **49**(3), 1911–1919 (2013)
25. J.A. Mahal, A. Khawar, A. Abdelhadi, Spectral coexistence of MIMO radar and MIMO cellular system. *IEEE Trans. Aerosp. Electron. Syst.* **53**(2), 655–668 (2017)
26. Z. Qin, L. Lu, B. Wang, A novel approach for spectrum mobility games with priority in cognitive radio networks, in *2014 IEEE International Conference on Communications (ICC)* (IEEE, New York, 2014), pp. 1416–1421
27. I. Christian, B. Lu, L. Wang, Spectrum mobility in cognitive radio networks. *IEEE Commun. Mag.* **50**(6), 114–121 (2012)

28. Y.F. Liu, Dynamic spectrum management: a complete complexity characterization. *IEEE Trans. Inf. Theory* **58**(4), 1804–1815 (2009)
29. D. Cabric, A. Tkachenko, R. Brodersen, Spectrum sensing measurements of pilot, energy, and collaborative detection, in *Proceedings IEEE Military Communication Conference*, 2006, pp. 1–7
30. K. Challapali, S. Mangold, Z. Zhong, Spectrum agile radio: detection spectrum opportunities, in *Symposium on Advanced Radio Technologies* (2004)
31. C. Jiang, Y. Chen, K.J.R. Liu, Y. Ren, Network economics in cognitive networks. *IEEE Commun. Mag.* **53**(5), 75–81 (2015)
32. C. Jiang, Y. Chen, K.J.R. Liu, Data-driven optimal throughput analysis for route selection in cognitive vehicular networks. *IEEE J. Sel. Areas Commun.* **32**(11), 2149–2162 (2014)
33. H. Zhang, C. Jiang, Q. Hu, Y. Qian, Self-organization in disaster resilient heterogeneous small cell networks. *IEEE Netw.* **30**(2), 116–121 (2016)
34. J.M.P. Fortes, An analytical method for assessing interference in interference environments involving NGSO satellite networks. *Int. J. Sat. Commun.* **17**(6), 399–419 (1999)
35. L. Ma, H. Liu, X. Liag, The application of cognitive radio technology in LEO satellite systems, in *Telecommunications Techniques*, 2010, pp. 49–51
36. C. Park, Interference analysis of geostationary satellite networks in the presence of moving non-geostationary satellites, in *ITCS 2010*, 2010, pp. 1–5
37. H. Kobayashi, H. Shinonaga, N. Araki, Y. Ito, Study on interference between non-GSO MSS gateway station and GSO FSS earth station under reverse band operation, in *1995 Tenth International Conference on Digital Satellite Communications*, vol.1 (Brighton, 1995), pp. 282–289
38. S.K. Sharma, S. Chatzinotas, B. Ottersten, In-line interference mitigation techniques for spectral coexistence of GEO and NGEO satellite. *Int. J. Sat. Commun. Netw.* **34**, 11–39 (2016)
39. ITU-R S.1428, Reference FSS earth station radiation patterns for use in interference assessment involving non-GSO satellite in frequency bands between 10.7 GHz and 30 GHz (2000)
40. ITU-R S.1528, Satellite antenna radiation patterns for non-geostationary orbit satellite antennas operating in the fixed-satellite service below 30 GHz (2001)

Chapter 5

Spectrum Sensing

Cognitive radio has emerged as an efficient approach to implement reuse of the licensed spectrums. Among the cognitive radio technologies, cooperative spectrum sensing has been corroborated to be an effective approach to counter channel fading. In this chapter, we consider the terrestrial system as secondary user (SU) and the satellite system as primary user (PU), where secondary terrestrial users attempt to sense and access the primary satellite systems' licensed spectrum. We first advance a strategy for SUs to search available spectrums with asynchronous MAC-layer sensing. With this method, the SUs do not need to know the communication mechanisms in satellite network when dynamically accessing. Then, we discuss the asynchronous cooperative sensing situation, and derive the optimal sensing parameters under such asynchronous scenario. Finally, we propose a density control mechanism for managing number of terrestrial secondary transmitters around one satellite ground station in order to guarantee that the primary communications are not interfered. Note that in the remaining of this section, all the "SUs" refer to the terrestrial unlicensed users and all the "PUs" refer to the licensed satellite systems.

5.1 Asynchronous MAC-Layer Spectrum Sensing

With the development of communication satellites in recent years, mobile satellite communication system is becoming more and more mature, which becomes an important part of mobile communication system. The remarkable feature of the system is the utilization of multiple access mode, for the global users with large span, wide range, long distance roaming and mobile, flexible communication services, as well as the terrestrial cellular mobile communication system expansion. It was launched on August 6, 2016, called Tiantong No. 01 satellite, which is the first satellite of communication system in China, and becomes an important part of China's spatial information infrastructure.

On the other hand, with the development of radio technology, limited spectrum resources and demands for broadband service become the contradiction of restricting the development of mobile communication technology. In the authorized band, such as mobile satellite communication system in the required frequency band, its utilization efficiency is quite low, and the occupied bands at different times and locations are usually free, the phenomenon of which is caused by the mode of fixed spectrum allocation. In order to improve the utilization ratio of the spectrum in mobile satellite communication system and meet the communication needs of the wireless mobile communication between the mobile terminal without affecting the normal communication in the authorized frequency band, we propose a spectrum sharing system in which unauthorized terrestrial terminals perceive the satellite system and use idle spectrum resources for data transmission [48]. However, since the communication protocols of the satellite systems are usually restricted to the public, the terrestrial users may have no access to the MAC layer communication mechanism of the mobile satellite communication system. Therefore, we propose an asynchronous system aiming to complete the process of spectrum sensing in the case of non-slotted scenario. In the following, the terrestrial systems is referred as SU and the satellites system is referred as PU, without loss of generality.

Current methods of searching available channels incline to analyze the slot-based situations, which we call as synchronous scheme. In such cases, communications in PU's network are based on time slot. At the beginning of each slot, SUs who want to access primary spectrum will check the availability of current channels. However, if SUs have no idea about the time table in PU's network, such synchronous schemes will not work. Otherwise, their arbitrary accesses will inevitably bring lots of interference to PU [45–47], violating the essence of DSA. Moreover, it is also possible that communications among PUs are not based on synchronous scheme at all. Considering these problems, we designed an interference-aware strategy to discover available spectrums with asynchronous MAC-layer spectrum sensing [39, 40], which can help SU cognitively and asynchronously access available channels even without knowing the communication protocol of PU's network. In this section, we will focus on four points as listed below:

- *Strategy for Searching Available Channels*

For SU, it is true that the most important thing is to discover available channels effectively and quickly. However, the potential interference caused by them should not be overlooked. In this section, we present an asynchronous interference-aware strategy for searching available channels. The strategy holds that SUs should dynamically allocate total finite search time to sense existing channels according to different parameters of different channels, in order to bring minimal interference to PU [41–43].

- *Vacating Strategy*

When PUs emerge at the channel which secondary network is occupying, SU must vacate current channel and look for a new opportunity with minimum delay so that they can resume their communication as soon as possible. Therefore, it is

important for SU to minimize the delay in discovering a new available channel when vacating. We also present a vacating strategy in this section. For time saving, the strategy holds that SU should re-sense remaining channels in part instead of researching all channels. Meanwhile, it also gives the re-sense sequence in order to achieve high success rate, taking advantage of previous search results.

- *Estimation of Channel Parameters*

In our model, channel usage model is considered as an Interrupted Poisson Process (IPP). Hence, the key is to precisely estimate parameters of IPP to formulate our expressions. We adopt the moment matching estimator in this section, which shows good performance in simulations and also well tracks time-varying channels.

- *Impact on PU's Achievable Rate*

How many SUs can one primary receiver bear without degrading the achievable data rate of PU? Hence, it is also necessary to analyze the impact of interference caused by SUs on PU's capacity. Thus, we can reckon the deterioration of PU's performance under potential interference brought by SUs' access, to estimate allowed number of SUs according to PU's tolerability.

In [1–4], some synchronous schemes for discovering available spectrums are discussed, among which [1] is representative. In that section, Q. Zhao assumed that all channels are synchronous and slotted. Through partially observing each channel's history of Markov process, SUs dynamically sense and access available channels. Considering that the complexity of optimization exponentially increases along with the linear increase of channel numbers, a sub-optimal greedy algorithm was proposed, which can achieve fairly low complexity, as well as good performance. However, as aforementioned, such schemes rest on two premises: (1) The primary network is based on synchronous schemes; (2) Secondary users are aware of PU's time table.

References [5–7] proposed an asynchronous access method, which regarded the channel usage pattern as ON-OFF alternating periods. In order to maximize discovery of opportunities, the author analyzed two unfavorable cases: unexplored opportunity and sensing overhead. Through minimizing the probability of such two cases, optimized sense period of each channel was obtained, as well as the sense sequence. Unlike them, the basis of our search strategy is to avoid interference to PU caused by SU's dynamic access. Moreover, the scheme discussed in this section analyzes the interference in packet level, which is more practical than these two papers where only period level was illustrated.

In [8] and [9], IPP model was first imported to illustrate the traffic model of PU. Similarly, our search strategy also hired IPP model as the basic channel model. However, [8] aimed at addressing the fairness problem and proposed a fair multiple access method; while [9] mainly discussed a cooperative way to access channels for SU. Both of them are totally different from the problem discussed in this section.

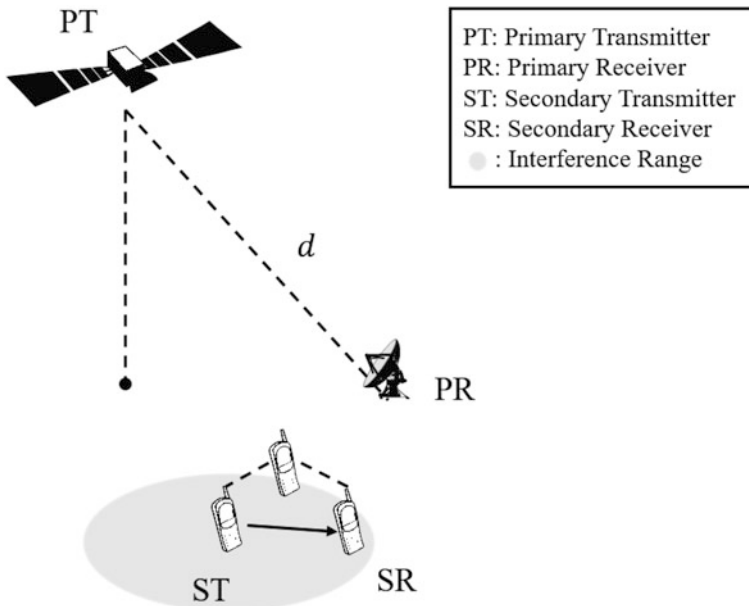


Fig. 5.1 System model of the network

5.1.1 System Model

5.1.1.1 Network Entity

Figure 5.1 shows the scenario we will discuss in this section. The primary transmitter (i.e. the satellite) is at the top of the center of the region. The supposed receiver (PR) is d meters away from the satellite. In the secondary network, SUs use IEEE 802.11 RTS/CTS mechanism to avoid collision and interference. Once a pair of SUs discover that some channel has been occupied by their network, they will not try to access this channel. Therefore, with such competitive mechanism, it is reasonable to assume that within the interference range of ST, only one pair of SUs communicate with each other at one moment, as ST and SR in Fig. 5.1.

5.1.1.2 Channel Model

According to the essence of DSA, PUs have no obligation to know the presence of SU. They always have priority to access their licensed spectrums. In the eyes of one SU, each channel alternatively switches between FREE period and BUSY period. The BUSY period means the channel is being occupied by some PUs, while the FREE period is just a “spectrum hole” for SU. Therefore, the channel usage model

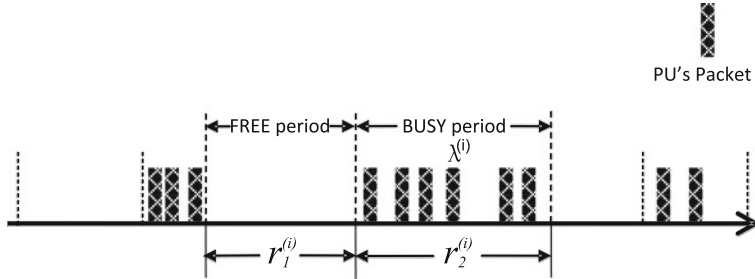


Fig. 5.2 Channel's IPP model

is equal to the traffic model of PUs. For instance, in digital TV broadcast system, one broadcast from base station means one BUSY period in channel. For a more general case, different BUSY periods are regarded as memoryless and mutually independent, as in [5] and [9]. This quality is also true for FREE periods. Therefore, we can respectively assume that the lengths of FREE/BUSY period $T_{FR}^{(i)}/T_{BU}^{(i)}$ obey negative exponential distribution with parameter $r_1^{(i)}/r_2^{(i)}$ (hereafter the headnote “(i)” of all parameters means the i th channel).

In BUSY period of each channel, it is assumed that PU's packets arrive by Poisson process. That means the arrival interval $T_{in}^{(i)}$ obeys negative exponential distribution with rate $\lambda^{(i)}$. Thus, the channel usage by PU can be modeled as an IPP [10], as Fig. 5.2 shows. The FREE period and BUSY period alternatively appear. Additionally, communications among PU are all in packets with some constant average length and holding time in channel.

5.1.1.3 Activity of Secondary Users

SUs who are intent to access primary spectrums will search all channels in advance, which is so-called “Listen before Talk”. As each SU is only equipped with one antenna, it is assumed that SU can just sense one channel at one time, no instance of simultaneously sensing two or multi-channels. If no PU is discovered in this search period, SU will regard the status of current channel as a FREE period.

The proposed strategy setups four states for SU's activity: observation state, search state, transmission state and vacating state. Figure 5.3 illustrates the state transition diagram. In observation state, SU will alternatively sleep and wake up to listen up all channels, estimating and updating the IPP parameters of them. Once there are packets need to be transmitted, SU will jump out of the observation state and switch to search state. Then SU begins to search all channels in turn within some finite search time. According to the search result, one channel will be determined at last. After accessing the determined channel, SU will begin transmitting data packets and keep sensing current channel. Once a new PU is discovered, SU will immediately vacate the current channel. Then, through analyzing total already

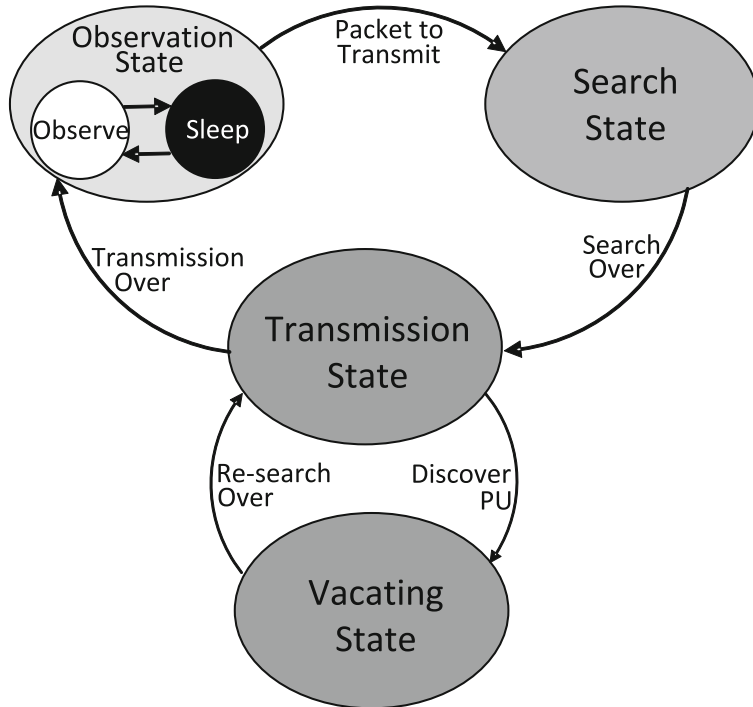


Fig. 5.3 State transition diagram of SU

access time and previous searched results of each channel, SU will choose new channels to re-sense and access. The circulation will not finish until all packets are transmitted.

5.1.2 Searching Available Channels

Based on the aforementioned channel model, this section will explicitly analyze how to obtain the optimal strategy of searching available channels for secondary users. Firstly, two questions should be explained:

- What does the “strategy” mean?
- What is the standard of “optimal”?

We define the first as that within finite total search time, SU dynamically allocates this limited time to sense N channels according to different parameters of different channels. And the standard of “optimal” is defined as SU bringing minimal probability of interference to PU. It is obvious that more total search time will help SU obtain more information about current channels, in turn achieving lower

probability of interference to PU. However, more search time will also bring more energy consumption and inevitably limit the total transmission time. Therefore, it is a complicated trade-off problem, which needs to establish constrained optimization equations so as to seek for the optimal solutions.

In order to illustrate interference probability P_{inf} , we here define two variables: *SEER* (Sense Error) and *SEES* (Sense Excess). The former refers to the probability of SU mistaking a “fake” spectrum hole for an opportunity. The latter is due to the overlong total search time. *SEER* and *SEES* constitute P_{inf} and following two sections will explicitly discuss their mathematical expressions. Here assumes that the allocation of total search time is vector $\vec{\Theta} = (\theta^{(1)}, \theta^{(2)}, \dots, \theta^{(N)})$, which means for the i th channel, the length of search period is $\theta^{(i)}$. If the relationship between interference probability P_{inf} and allocation vector $\vec{\Theta}$ can be found, the optimization equation will be established as Eq. (5.1). The finite total search time C_s is a constrain condition. And it also should be assured that search period of each channel $\theta^{(i)} \geq 0$.

$$\begin{aligned} \text{Min. } P_{inf} &= \frac{1}{N} \left(\sum_{i=1}^N \text{SEER}^{(i)} + \sum_{i=1}^N \text{SEES}^{(i)} \right) \\ &= \mathcal{F}(\vec{\Theta}) \\ \text{s.t. } & \begin{cases} \vec{\Theta} \cdot \vec{E}^T = C_s \\ \vec{\Theta} \cdot \vec{I}_N \geq \vec{0}_N \end{cases} \end{aligned} \quad (5.1)$$

in which $\vec{E} = (1, 1, \dots, 1)_N$, \vec{I}_N is N dimensional identity matrix and $\vec{0}_N$ is N dimensional zero matrix.

5.1.2.1 Analysis of *SEER*

If SU arrives in channel’s BUSY period and senses a short period end with no discovery of PU’s existence, sense error will happen. *SEER* is defined as probability of such circumstance, as Fig. 5.4 shows. In other words, it is the probability of SU’s search period falling into the arrival interval of PU’s two adjacent packets. As assumed above, the arrival interval $T_{in}^{(i)}$ obeys the negative exponential distribution with *p.d.f.*:

$$f_{T_{in}^{(i)}}(t) = \frac{1}{\lambda^{(i)}} e^{-t/\lambda^{(i)}} \quad (5.2)$$

Therefore, once PU’s arrival interval is longer than the search period of this channel, sense error will appear. Thus, we can obtain the sense error probability $\text{SEER}^{(i)}$ of each channel. According to the assumption that PUs’ packets are in some constant average length, we use τ to express the average holding time.

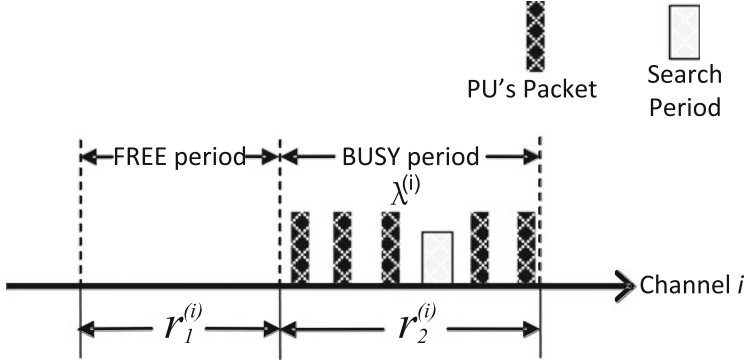


Fig. 5.4 Illustration of SEER

$$\begin{aligned}
 SEER^{(i)} &= \text{Prob}\left(T_{in}^{(i)} \geq \theta^{(i)}\right) \\
 &= \frac{r_2^{(i)}}{r_1^{(i)} + r_2^{(i)}} \frac{\lambda^{(i)}}{\tau + \lambda^{(i)}} \int_{\theta^{(i)}}^{+\infty} f_{T_{in}^{(i)}}(t) dt \\
 &= \epsilon^{(i)} \int_{\theta^{(i)}}^{+\infty} \frac{1}{\lambda^{(i)}} e^{-t/\lambda^{(i)}} dt \\
 &= \epsilon^{(i)} e^{-\theta^{(i)} / \lambda^{(i)}}
 \end{aligned} \tag{5.3}$$

where $\epsilon^{(i)} = \frac{r_2^{(i)}}{r_1^{(i)} + r_2^{(i)}} \frac{\lambda^{(i)}}{\tau + \lambda^{(i)}}$. $\epsilon^{(i)}$ has its physical significance: occurrence probability of PU's arrival interval. From the expression of $SEER^{(i)}$, we can see that it is relevant with arrival rate of PU's packets $\lambda^{(i)}$ and occurrence probability of PU's arrival interval $\epsilon^{(i)}$, as well as the search period of current channel.

5.1.2.2 Analysis of SEES

Considering the feasibility of hardware designation, it is assumed that every SU can only sense one channel at one time. Thus, although SU arrives in channel's FREE period and discovers no PU during the search period, it is possible that the channel switches into BUSY period when SU is searching other existing channels. We define such instance as SEES (Sense Excess), as Fig. 5.5 shows. Therefore, for channel i , if the *forward recurrence time* of its FREE period $T_{fw-FR}^{(i)}$ is longer than current search period $\theta^{(i)}$ but shorter than total remaining search time $\sum_{j=i}^N \theta^{(j)}$, $SEES^{(i)}$ will appear, as Eq. (5.4) shows below.

$$SEES^{(i)} = \text{Prob}\left(\theta^{(i)} \leq T_{fw-FR}^{(i)} \leq \sum_{j=i}^N \theta^{(j)}\right) \tag{5.4}$$

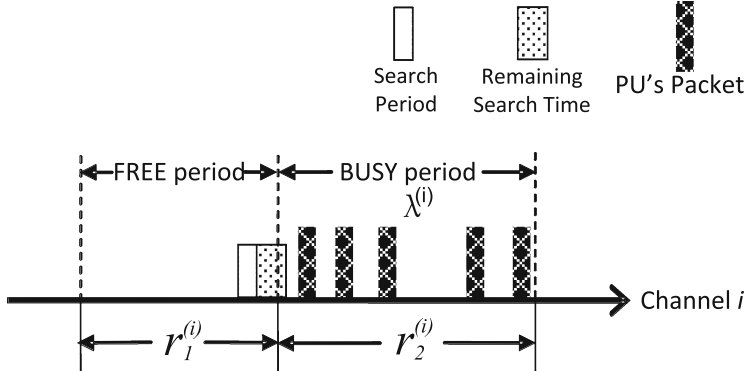


Fig. 5.5 Illustration of SEES

The *forward recurrence time* of FREE period $T_{fw_FR}^{(i)}$ refers to the duration from SU's search point (the time point when SU begins to sense current channel) to the end of FREE period, as Fig. 5.6 shows. According to the renewal theory [11], for a renewal process with average renewal interval α , its distribution of *forward recurrence time* is

$$F_H(t) = P(T_{fw} \leq t) = \frac{1}{\alpha} \int_0^t (1 - H(y)) dy \quad (5.5)$$

where $H(y)$ is the distribution of renewal interval. As aforementioned, the lengths of FREE periods form a Poisson process, which means the distribution of FREE period's renewal interval $F_{T_{FR}^{(i)}}(y)$ is a negative exponential distribution with parameter $r_1^{(i)}$. Thus, the distribution of FREE period's *forward recurrence time* $F_{T_{fw_FR}^{(i)}}(t)$ is:

$$\begin{aligned} F_{T_{fw_FR}^{(i)}}(t) &= \frac{1}{r_1^{(i)}} \int_0^t (1 - F_{T_{FR}^{(i)}}(y)) dy \\ &= \frac{1}{r_1^{(i)}} \int_0^t (1 - (1 - e^{-y/r_1^{(i)}})) dy \\ &= 1 - e^{-t/r_1^{(i)}} \end{aligned} \quad (5.6)$$

From the result, it can be seen that the *forward recurrence time* of FREE period still obeys the negative exponential distribution with parameter $r_1^{(i)}$ and *p.d.f.* $f_{T_{fw_FR}^{(i)}}(t)$.

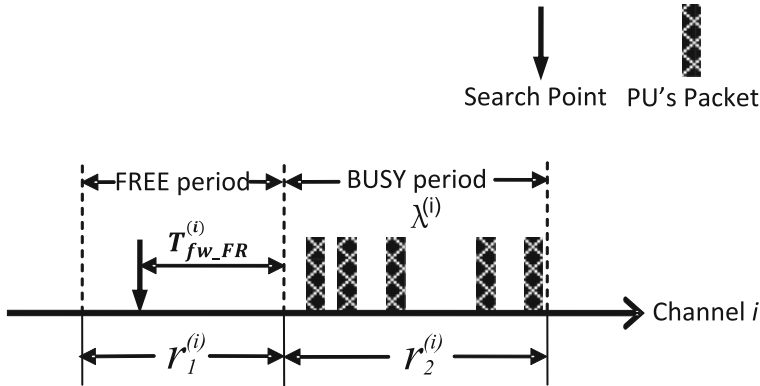


Fig. 5.6 Forward recurrence time of FREE period

Thus, according to the Eq. (5.4), we can obtain the expression of $SEES^{(i)}$:

$$\begin{aligned}
 SEES^{(i)} &= \frac{r_1^{(i)}}{r_1^{(i)} + r_2^{(i)}} \int_{\theta^{(i)}}^{\sum_{j=i}^N \theta^{(j)}} f_{T_{fw-FR}^{(i)}}(t) dt \\
 &= \eta^{(i)} \int_{\theta^{(i)}}^{\sum_{j=i}^N \theta^{(j)}} \frac{1}{r_1^{(i)}} e^{-t/r_1^{(i)}} dt \\
 &= \eta^{(i)} \left(e^{-\theta^{(i)}/r_1^{(i)}} - e^{-\sum_{j=i}^N \theta^{(j)}/r_1^{(i)}} \right)
 \end{aligned} \tag{5.7}$$

where $\eta^{(i)} = r_1^{(i)} / (r_1^{(i)} + r_2^{(i)})$. $\eta^{(i)}$ means occurrence probability of FREE period. It depends on the average renewal interval of FREE/BUSY period $r_1^{(i)}/r_2^{(i)}$.

5.1.2.3 Overall Analysis

After the analysis of $SEER$ and $SEES$, interference probability P_{inf} can be expressed as Eq. (5.8) below.

$$\begin{aligned}
 P_{inf} &= \frac{1}{N} \left(\sum_{i=1}^N SEER^{(i)} + \sum_{i=1}^N SEES^{(i)} \right) \\
 &= \frac{1}{N} \sum_{i=1}^N \left(\epsilon^{(i)} e^{-\theta^{(i)}/\lambda^{(i)}} + \eta^{(i)} \left(e^{-\theta^{(i)}/r_1^{(i)}} - e^{-\sum_{j=i}^N \theta^{(j)}/r_1^{(i)}} \right) \right)
 \end{aligned} \tag{5.8}$$

There are some different situations about P_{inf} as discussed below. In this section, we will only focus on the third situation in respect that the first two situations are sub-problems of the third.

1. When $\lambda^{(i)} \ll r_1^{(i)}$, which means PU's packets nearly occupy whole BUSY period with extremely short intervals or the channel's occupation are relatively sparse with extremely long FREE period. Under such condition, sense error caused by $SEER^{(i)}$ will be infinitesimal and can be ignored;
2. When $\lambda^{(i)} \cong r_1^{(i)}$, which means PU's arrival interval is almost same as the length of channel's FREE period. In this case, the channel will be modeled as a Poisson process instead of an IPP and PU's arrival intervals are all "spectrum holes" for SU. Thus, $SEER^{(i)}$ will not exist, leaving only $SEES^{(i)}$;
3. When $\lambda^{(i)} = \frac{1}{3}r_1^{(i)} \sim \frac{1}{20}r_1^{(i)}$, Eq. (5.8) holds.

5.1.2.4 Optimal Allocation Result

Combining Eqs. (5.1) and (5.8), we can acquire the optimal allocation vector $\vec{\Theta}^*$ through resolving the constrained optimization equation below. Φ^Θ means all allocation schemes.

$$\begin{aligned} \vec{\Theta}^* = \operatorname{Arg} \min_{\Theta \in \Phi^\Theta} P_{inf} \\ \text{s.t. } \begin{cases} \vec{\Theta} \cdot \vec{E}^T = C_s \\ \vec{\Theta} \cdot \vec{I}_N \geq \vec{0}_N \end{cases} \end{aligned} \quad (5.9)$$

where \vec{E} , \vec{I}_N , $\vec{0}_N$ and C_s are defined like in Eq. (5.1).

From Eq. (5.7), we can see that $SEES^{(i)}$ is related with the search sequence of all channels. And SU should sense channels with longer search period first to achieve less P_{inf} . The problem is which channel has longer search period. It is obvious that for each channel, longer search period will bring less P_{inf} . In channels with long FREE periods, the probability of sense error and excess is already low. Therefore, such channel should be assigned shorter search period. In other words, the busy channel (with shorter FREE period) needs longer search period and should be sensed first.

5.1.3 Vacating Strategy

After SU successfully accessed one available channel, it will keep monitoring it. Once some PUs appear, SU should immediately vacate current channel (we call it "PU-appeared" channel hereafter) and begin to look for other available ones. In order to decrease the latency caused by channel-switching, SU will re-sense other channels in part with some short constant search period. And once it discovers a FREE channel, it will not search other channels any more, which is unlike the comprehensive search strategy. However, the problem is what is the re-search

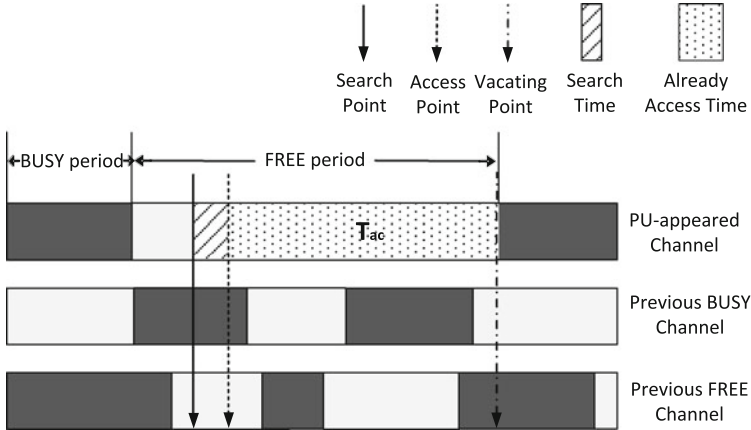


Fig. 5.7 Illustration of vacating

sequence of those remaining $N - 1$ channels in order to achieve high success rate, in which success means the channel is available when SU is re-sensing it. Apart from that PU-appeared channel, remaining $N - 1$ channels include some previous FREE channels and some previous BUSY channels. The “previous” FREE or BUSY here means the previous channel states when SU was searching those channels at the very beginning, instead of when SU is vacating the PU-appeared channel, as Fig. 5.7 shows.

In Fig. 5.7, T_{ac} is defined as “already access time”, which means the duration from successfully accessing to vacating. T_{ac} needs to be recorded by SUs themselves. It can be seen that after T_{ac} , the previous BUSY channel may turn into FREE when SU vacating; while the previous FREE channel may become BUSY. In order to re-discover other available channels promptly, there are two choices for SUs:

- Choose from previous BUSY channels which have shorter *forward recurrence time* of BUSY period?
- Choose from previous FREE channels which have longer *forward recurrence time* of FREE period?

The definition of *forward recurrence time* of BUSY period $T_{fw_BU}^{(i)}$ is same as $T_{fw_FR}^{(i)}$. According to the analysis in Sect. 5.1.2.2, we can get the expectation of $T_{fw_FR}^{(i)}$ and $T_{fw_BU}^{(i)}$:

$$\begin{cases} E(T_{fw_FR}^{(i)}) = E(T_{FR}^{(i)}) = r_1^{(i)} \\ E(T_{fw_BU}^{(i)}) = E(T_{BU}^{(i)}) = r_2^{(i)} \end{cases} \quad (5.10)$$

We here define a vector $\overrightarrow{T_{ex}} = (T_{ex}^{(1)}, T_{ex}^{(2)}, \dots, T_{ex}^{(N-1)})$ that contains expectations of access time of remaining $N - 1$ channels. Thus, SUs can re-search new available

Algorithm 3 Construct vector $(T_{ex}^{(1)}, T_{ex}^{(2)}, \dots, T_{ex}^{(N-1)})$

```

for previous BUSY channel do
  if  $T_{ac} \leq (r_1^{(i)} + r_2^{(i)})$  then
    if  $T_{ac} - E(T_{fw\_BU}^{(i)}) \leq 0$  then
      5:    $T_{ex}^{(i)} = 0$ ;
    else
       $T_{ex}^{(i)} = E(T_{ex\_BU}^{(i)}) = E(T_{fw\_BU}^{(i)}) + E(T_{FR}^{(i)}) - T_{ac}$ ;
    end if;
    else
      10:   $\widehat{T}_{ac} = (T_{ac} - E(T_{fw\_BU}^{(i)})) \bmod (r_1^{(i)} + r_2^{(i)})$ ;
        if  $\widehat{T}_{ac} - E(T_{fw\_FR}^{(i)}) \geq 0$  then
           $T_{ex}^{(i)} = 0$ ;
        else
           $T_{ex}^{(i)} = E(T_{ex\_BU}^{(i)}) = E(T_{fw\_FR}^{(i)}) - \widehat{T}_{ac}$ ;
        end if;
      end if
    end for
for previous FREE channel do
  if  $T_{ac} \leq (r_1^{(i)} + r_2^{(i)})$  then
    20:   if  $T_{ac} - E(T_{fw\_FR}^{(i)}) \geq 0$  then
       $T_{ex}^{(i)} = 0$ ;
    else
       $T_{ex}^{(i)} = E(T_{ex\_FR}^{(i)}) = E(T_{fw\_FR}^{(i)}) - T_{ac}$ ;
    end if;
    else
      25:    $\widehat{T}_{ac} = (T_{ac} - E(T_{fw\_FR}^{(i)})) \bmod (r_1^{(i)} + r_2^{(i)})$ ;
        if  $\widehat{T}_{ac} - E(T_{fw\_BU}^{(i)}) \leq 0$  then
           $T_{ex}^{(i)} = 0$ ;
        else
           $T_{ex}^{(i)} = E(T_{ex\_BU}^{(i)}) = E(T_{fw\_BU}^{(i)}) + E(T_{FR}^{(i)}) - \widehat{T}_{ac}$ ;
        end if;
      end if
    end for

```

channels according to the sequence from maximum to minimum in $\overrightarrow{T_{ex}}$. Based on previous search results and already access time T_{ac} , we also design an algorithm to construct this vector as showed below. In the algorithm, \widehat{T}_{ac} is defined as “residual already access time”, which is derived from the fact that T_{ac} may contain several BUSY/FREE periods. It should be emphasized that after several vacating, the previous information may be outdated. Therefore, SU should periodically search all channels with optimized search strategy discussed in Sect. 5.1.2 to update this “previous” information.

5.1.4 Estimation of Channel IPP Parameters

5.1.4.1 Moment Matching Estimator

Stochastically, the arrival intervals of an IPP obey 2-phase hyper-exponential distribution (H_2) [10]. The probability density function of an H_2 is:

$$f_{H_2}(t) = p\mu_1 e^{-\mu_1 t} + (1-p)\mu_2 e^{-\mu_2 t} \quad (5.11)$$

There are also three parameters (p, μ_1, μ_2) in a H_2 , which can be transformed to the three parameters of an IPP (λ, r_1, r_2) by Eqs. (5.12)–(5.14) below. Therefore, the problem of estimating IPP parameters turns into estimation of H_2 parameters.

$$\lambda = \frac{1}{p\mu_1 + (1-p)\mu_2} \quad (5.12)$$

$$r_1 = \frac{1}{\lambda\mu_1\mu_2} \quad (5.13)$$

$$r_2 = \frac{1}{\lambda p(1-p)(\mu_1 - \mu_2)^2} \quad (5.14)$$

where the headnote “(i)” is omitted.

Through adopting energy detection method [12] in physical layer, SU can obtain a vector of L samples from channel i : $\vec{\Omega}^{(i)} = (\omega_1^{(i)}, \omega_2^{(i)}, \dots, \omega_L^{(i)})$, where

$$\omega_{\kappa(1 \leq \kappa \leq L)}^{(i)} = \begin{cases} 0, & \text{if channel } i \text{ is not occupied} \\ 1, & \text{if channel } i \text{ is occupied} \end{cases} \quad (5.15)$$

Firstly, SU should accumulate the numbers of “0”: $S_0^{(i)}$ between two “1” in vector $\vec{\Omega}^{(i)}$. Then through multiplying each number and average time costed by per detection expressed by ζ , the samples set of arrival intervals $\tilde{t}^{(i)} = (\tilde{t}_1^{(i)}, \tilde{t}_2^{(i)}, \dots, \tilde{t}_M^{(i)})$ can be obtained.

Example

Supposing that:

$$\vec{\Omega}^{(i)} = (\underbrace{000}_3, 11, \underbrace{0000}_4, 11, \underbrace{000}_3, 11, \underbrace{000000}_6, 11, \underbrace{00000}_5);$$

$$\Rightarrow \begin{cases} S_0^{(i)} = (3, 4, 3, 6, 5); \\ \tilde{t}^{(i)} = (3\zeta, 4\zeta, 3\zeta, 6\zeta, 5\zeta). \end{cases}$$

■

After SU has the samples set of arrival intervals, it can use these samples to estimate corresponding parameters via matching origin moment of order 1, 2, 3. Eqs. (5.16)–(5.18) (where the headnote “(i)” is omitted) list the equation set to calculate the three parameters of H_2 , in turn the IPP parameters.

$$E(\tilde{t}) = E(t) = \int_0^{+\infty} t f_{H_2}(t) dt = \frac{p}{\mu_1} + \frac{1-p}{\mu_2} \quad (5.16)$$

$$E(\tilde{t}^2) = E(t^2) = \int_0^{+\infty} t^2 f_{H_2}(t) dt = 2\left(\frac{p}{\mu_1^2} + \frac{1-p}{\mu_2^2}\right) \quad (5.17)$$

$$E(\tilde{t}^3) = E(t^3) = \int_0^{+\infty} t^3 f_{H_2}(t) dt = 3\left(\frac{p}{\mu_1^3} + \frac{1-p}{\mu_2^3}\right) \quad (5.18)$$

5.1.4.2 Imperfect Channel Estimation

From Eqs. (5.8) and (5.9), it is obvious that the optimized search strategy depends on estimation of the instantaneous channel IPP parameters. The analysis and results in Sect. 5.1.2 are all given under the assumption of accurate estimation of these parameters. However, the moment matching estimator discussed above is imperfect, which will inevitably bring errors of P_{inf} , in turn the errors of optimized allocation results of total search time. In this section, we analyze the impact of such imperfect estimations on P_{inf} . In particular, we give the relationship between the errors $\Delta P_{inf}^{(i)}$ and $\Delta \lambda^{(i)}$, $\Delta r_1^{(i)}$, $\Delta r_2^{(i)}$ as showed in Eqs. (5.19) and (5.20), which can also be served as a metric of robustness for our method upon searching available channel.

$$\begin{aligned} \Delta P_{inf}^{(i)} &= \frac{\partial P_{inf}^{(i)}}{\partial \lambda^{(i)}} \Delta \lambda^{(i)} + \frac{\partial P_{inf}^{(i)}}{\partial r_1^{(i)}} \Delta r_1^{(i)} + \frac{\partial P_{inf}^{(i)}}{\partial r_2^{(i)}} \Delta r_2^{(i)} \quad (5.19) \\ &= \left(\frac{\partial \epsilon^{(i)}}{\partial \lambda^{(i)}} e^{-\theta^{(i)}/\lambda^{(i)}} - \frac{\theta^{(i)} SEER^{(i)}}{(\lambda^{(i)})^2} \right) \Delta \lambda^{(i)} + \left(\frac{\partial \epsilon^{(i)}}{\partial r_2^{(i)}} e^{-\theta^{(i)}/r_2^{(i)}} + \frac{\partial \eta^{(i)}}{\partial r_2^{(i)}} \frac{SEES^{(i)}}{\eta^{(i)}} \right) \Delta r_2^{(i)} \\ &\quad + \left(\frac{\partial \epsilon^{(i)}}{\partial r_1^{(i)}} e^{-\theta^{(i)}/r_1^{(i)}} + \frac{\partial \eta^{(i)}}{\partial r_1^{(i)}} \frac{SEES^{(i)}}{\eta^{(i)}} + \frac{\eta^{(i)}}{(r_1^{(i)})^2} \left(\theta^{(i)} e^{-\theta^{(i)}/r_1^{(i)}} - \sum_{j=i}^N \theta^{(j)} e^{-\sum_{i=j}^N \theta^{(j)}/r_1^{(i)}} \right) \right) \Delta r_1^{(i)} \end{aligned}$$

$$\begin{aligned} \text{where: } \frac{\partial \eta^{(i)}}{\partial r_1^{(i)}} &= \frac{r_2^{(i)}}{(r_1^{(i)} + r_2^{(i)})^2}; & \frac{\partial \eta^{(i)}}{\partial r_2^{(i)}} &= \frac{-r_1^{(i)}}{(r_1^{(i)} + r_2^{(i)})^2}; \\ \frac{\partial \epsilon^{(i)}}{\partial \lambda^{(i)}} &= \frac{r_2^{(i)}}{r_1^{(i)} + r_2^{(i)}} \frac{\tau}{(\tau + \lambda^{(i)})^2}; & \frac{\partial \epsilon^{(i)}}{\partial r_1^{(i)}} &= \frac{\lambda^{(i)}}{\tau + \lambda^{(i)}} \frac{-r_2^{(i)}}{(r_1^{(i)} + r_2^{(i)})^2}; \quad (5.20) \\ \frac{\partial \epsilon^{(i)}}{\partial r_2^{(i)}} &= \frac{\lambda^{(i)}}{\tau + \lambda^{(i)}} \frac{r_1^{(i)}}{(r_1^{(i)} + r_2^{(i)})^2}. \end{aligned}$$

5.1.5 Impact on PU's Achievable Rate

5.1.5.1 Propagation Model

In our model, the channel fading is considered as the combination of large scale path loss and small scale Rayleigh flat fading [13]. Power attenuation in channel is principally caused by these two kinds of fading and we model the power loss from transmitter T to receiver R by $\beta_{(t,r)} = \phi^2 / d_{(t,r)}^\alpha$, where $d_{(t,r)}$ is the distance from T to R , and α is attenuation exponent, ϕ is Rayleigh random variable with parameter $\bar{\phi}$.

Additionally, it is also assumed that there exists additive white Gaussian noise (AWGN) in the channel. Therefore, the power of received signals at PR and SR in Fig. 5.1 are:

$$\Psi_{pr} = \lambda_{(pt,pr)} \Psi_{pt} + \sum_{i=1}^{G_{su}} \lambda_{(st_i,pr)} \Psi_{st_i} + \sigma_N^2 \quad (5.21)$$

$$\Psi_{sr} = \lambda_{(pt,sr)} \Psi_{pt} + \lambda_{(st,sr)} \Psi_{st} + \sigma_N^2 \quad (5.22)$$

where G_{su} represents the number of SUs that may cause interference around one PR, σ_N is the variance of AWGN, and Ψ_X represents transmitted/received power at X .

5.1.5.2 PU's Achievable Rate

In Rayleigh fading channel, the Signal-to-Noise Ratio (SNR) will no longer be a constant, but a variable following the Rayleigh fading statistics [14]. The average achievable rate R_{av} in Rayleigh channel is:

$$R_{av} = \int_0^\infty \log_2(1 + \gamma) \frac{1}{\Gamma} e^{-\gamma/\Gamma} d\gamma \quad (5.23)$$

where γ is the SNR of the channel; Γ is the average power of γ , $\Gamma = E(\gamma)$.

Therefore, in order to obtain PU's achievable rate under interference of SUs, the SNR at PR should be calculated first. Firstly, in ideal AWGN channel, there is no interference caused by SUs. Under such circumstance, the ideal SNR γ_{ideal} at PR is:

$$\gamma_{ideal} = \frac{SIG}{NOI} = \frac{\beta_{(pt,pr)} \Psi_{st}}{\sigma_N^2} \quad (5.24)$$

However, in real channel, SU's dynamic access may generate interference with probability of P_{inf} as discussed in Sect. 5.1.2. Such interference should be considered as noise for PR, which is so-called Signal-to-Interference plus Noise Ratio: SINR. Eqs. (5.25) and (5.26) show the real SINR at PR γ_{pr} and corresponding achievable rate.

$$\begin{aligned}\gamma_{pr} &= \frac{SIG}{P_{inf} \cdot INF + NOI} \\ &= \frac{\beta_{(pt,pr)} \Psi_{pt}}{P_{inf} \left(\sum_{i=1}^{G_{su}} \beta_{(st_i,pr)} \Psi_{st_i} \right) + \sigma_N^2}\end{aligned}\quad (5.25)$$

$$R_{pr} = \int_0^{\infty} \log_2(1 + \gamma_{pr}) \frac{1}{\Gamma_{pr}} e^{-\gamma_{pr}/\Gamma_{pr}} d\gamma_{pr}\quad (5.26)$$

In order to guarantee PU's normal communications, it is assumed that data rate at PR should at least exceed R_{\downarrow} . In other words, R_{\downarrow} is the lower limit of PU's achievable rate. Thus, the SINR at PR should satisfy Eq. (5.27) to ensure the lowest data rate.

$$\gamma_{pr} = \frac{\beta_{(pt,pr)} \Psi_{pt}}{P_{inf} \left(\sum_{i=1}^{G_{su}} \beta_{(st_i,pr)} \Psi_{st_i} \right) + \sigma_N^2} \geq 2^{R_{\downarrow}} - 1\quad (5.27)$$

Therefore, in this case P_{inf} should satisfy Eq. (5.28), which illustrates the tolerance of PU in the network:

$$P_{inf} \leq \left(\frac{\beta_{(pt,pr)} \Psi_{pt}}{2^{R_{\downarrow}} - 1} - \sigma_N^2 \right) \Bigg/ \left(\sum_{i=1}^{G_{su}} \beta_{(st_i,pr)} \Psi_{st_i} \right)\quad (5.28)$$

5.1.6 Numerical Results

A specific embodiment of the presented scenario is the Inmarsat communication system. The Inmarsat system consists of ship stations, shore stations, network coordination stations and satellites. There are four working satellites and five standby satellites waiting to be activated at any time, each satellite covering about 1/3 of the Earth's surface in the space of Inmarsat communication system. The frequency band of the ship station (i.e. the authorized terminal) is 1535–1542.5 and 1636.3–1644 MHz in the L-band. The SCPC / FDMA mode and the channel activation technology are used for data transmission.

We developed all the simulations using Matlab. It is assumed that there are totally five independent channels ($N = 5$) in the primary network. It should be emphasized that results of our proposed searching strategy are totally independent with number of primary channels. It is true that the complexity of computing the optimized search time of each channel will increase when there are so many primary channels for SU to search. However, under such circumstance, SUs can choose a group of channels from all primary channels to search according to the channel utilization ratio: u_{on} . $u_{on}^{(i)}$ is defined as the proportion of when channel i is in FREE period,

Table 5.1 Parameters of channels

Channel/ i	1	2	3	4	5
$r_1^{(i)}/s$	0.65	1.08	1.75	2.20	2.60
$r_2^{(i)}/s$	1.80	2.10	1.75	1.60	1.60
$\lambda^{(i)}/s$	0.32	0.25	0.15	0.13	0.12

Table 5.2 The optimal allocation result

Channel	1	2	3	4	5
Search period/s	0.9048	0.6318	0.2885	0.1600	0.0940

$u_{on}^{(i)} = r_1^{(i)} / (r_1^{(i)} + r_2^{(i)})$. Therefore, SU might as well choose five channels with highest u_{on} to search first in order to achieve high success rate of sense result.

PU's each data packet averagely occupies channel by 0.1 s ($\tau = 0.1$). In order to develop the relevant simulation, parameters of these five IPP-based channels should be assumed in advance, as Table 5.1 shows below. $r_1^{(i)}/r_2^{(i)}$ are the average length of FREE/BUSY period respectively, representing the traffic density of channel i . $\lambda^{(i)}$ illustrates the arrival rate of PU's data packets in BUSY period. These three parameters are sufficient to illustrate an IPP-based channel.

5.1.6.1 Channel Parameter Estimation

First, we use the parameters of channel 1 in Table 5.1 to build an IPP channel. Then through the estimation method discussed in Sect. 5.1.4, all three parameters $(\lambda^{(1)}, r_1^{(1)}, r_2^{(1)})$ are respectively estimated. Figure 5.8 shows the result, where we adjust the original values of three parameters randomly between -10% and $+10\%$. It can be seen that the estimation results can well trace the random variation of original data, which means it can well adapt the channels with time-varying parameters. Moreover, we also simulate the error of $P_{inf}^{(1)}$ caused by inaccurate estimation, which shows that the confidence interval of $P_{inf}^{(1)}$ is around [95%, 105%].

5.1.6.2 Search Strategy

Putting the assumed parameters in Table 5.1 into Eq. (5.9) and replacing the total search time C_s by 2.0 s, the optimal allocation result can be obtained via some nonlinear programming method, such as penalty function method [15]. Table 5.2 shows the optimal allocation result, where “optimal” refers to the optimal values calculated from our optimization equation. The busy channels, which have shorter FREE period, are assigned longer search period.

In practical cognitive radio network [29, 30], the conditions of channels are changing with time. Therefore, in order to illustrate that our search strategy is also competent in time-varying channels; we adjust the values of parameter $\lambda^{(i)}$, $r_1^{(i)}$ and

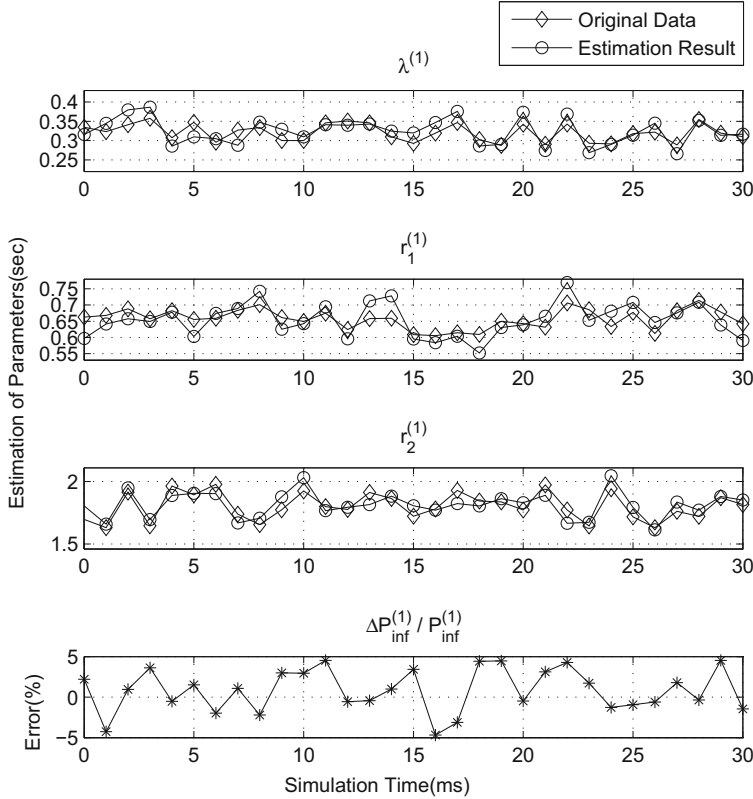


Fig. 5.8 Estimation result of Channel 1 and error of $P_{inf}^{(1)}$

$r_2^{(i)}$ randomly between -10% and $+10\%$ like in Sect. 5.1.6.1. Figure 5.9 shows the simulation result, in which total search time $C_s = 2.0$ s. It can be seen that the proposed strategy can immediately alter the allocation of total search time according to the continuously changing conditions, well adapting the time-varying channels.

Based on the parameters in Table 5.2, the optimized minimum probability of interference to PU P_{inf_opt} can be obtained through calculating Eq. (5.8). We depict the variation of P_{inf_opt} along with the increase of total search time in Fig. 5.10. The interference rapidly decreases when total search time increases from 0 to 5 s, and then gradually tends to zero. Here a comparison is conducted: optimized allocation and equal allocation. The latter means equal allocation of total search time C_s to each channel. Figure 5.10 also shows the comparison result. The interference caused by optimized allocation is nearly 50% less than that of equal allocation. Moreover, P_{inf_opt} goes to zero at 25 s. If SU searches 25 s in advance, they will not interfere PU. However, P_{inf_avr} will not tend to zero until 45 s.

In practical cognitive radio network, according to the underlay mechanism [16], a secondary transmission is allowed only if its power level is so low that the

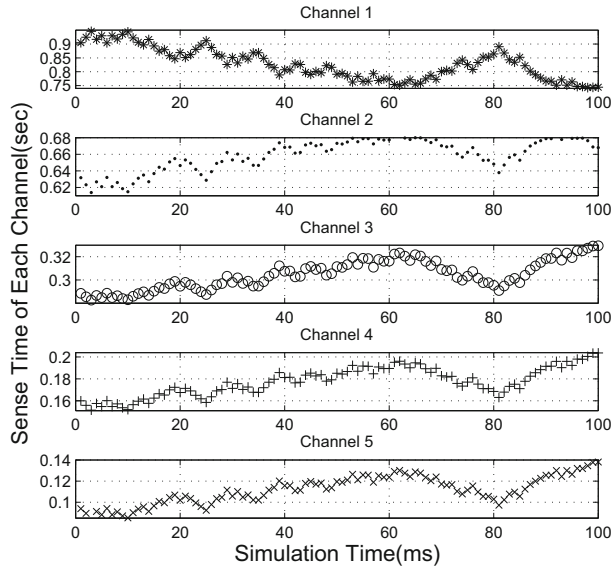


Fig. 5.9 Sense time of each time-varying channel

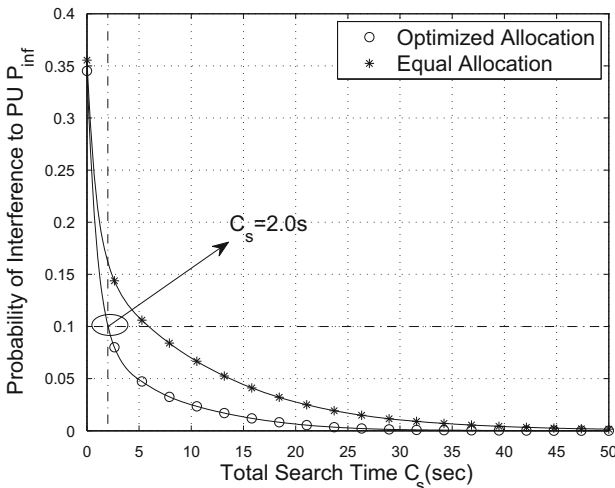


Fig. 5.10 Comparison of interference to PU

interference is not harmful to the primary data rate. Therefore, it need not blindly increase total search time to achieve zero P_{inf} . When the primary link is in a favorable condition ($\beta_{(pt,pr)}$ in Eq. (5.28) is quite large), PU can tolerate more interference from SUs. For instance, $P_{inf} = 0.1$ ($C_s = 2.0$ s) may already be able to assure PU's lowest data rate R_{\downarrow} as showed in Fig. 5.10. Thus, C_s can be

reduced in order to obtain more transmission time for SU. While when insufficient gain or severe background noise exists in primary link ($\beta_{(pt,pr)}$ is relatively small), interference from SUs should be strictly controlled, as well as C_s . Therefore, C_s depends on the tolerance of PU in the network, which was given by Eq. (5.28).

5.1.6.3 Access Time

In order to evaluate the performance of proposed search strategy and vacating strategy, we here adopt SU's "access time" as a criterion. "Access time" means the duration when SU is successfully occupying some primary channels. In this simulation, we assume that SU intends to acquire as long access time as it can: *ACT*. Based on the analysis in Sect. 5.1.2, we know that the expectation of each channel's access time is determined by the *forward recurrence time* of FREE period, as Eq. (5.29) shows:

$$\begin{aligned} i^* &= \operatorname{Arg} \max_{1 \leq i \leq N} \{E(\text{ACT}^{(i)})\} \\ &= \operatorname{Arg} \max_{1 \leq i \leq N} \{E(T_{fw-FR}^{(i)}) - C_s\} \end{aligned} \quad (5.29)$$

Another comparison is developed about the overall access time among three different access schemes:

- *Scheme 1*: SU randomly accesses one channel without sensing any channel at all;
- *Scheme 2*: SU first searches all channels with optimized search scheme, then chooses the final access channel according to Eq. (5.29) from all FREE channels;
- *Scheme 3*: Besides *Scheme 2* above, vacating strategy is also utilized in this scheme as discussed in Sect. 5.1.3.

Obviously, *Scheme 3* contains all our strategies in this section; while *Scheme 2* only includes the optimized search strategy, without vacating strategy. Figure 5.11 shows the growth of overall access time as simulation time goes by. When it is before 1.2 s, the simulation result of *Scheme 3* is nearly same as *Scheme 2*. That is because SU's first vacating appears at 1.2 s and the vacating strategy has not begun working before that time. It can be clearly seen that after that point, the third scheme can help SU attain longest access time. The turning point in *Scheme 3* is not a fixed value like 1.2s, which is a random value instead and depends on the FREE period of SU's first occupied channel in the simulation. The scheme of random access after sense comes next with about 20% access time less than *Scheme 3*. Access without search at all obtains least access time, only 50% of *Scheme 3*.

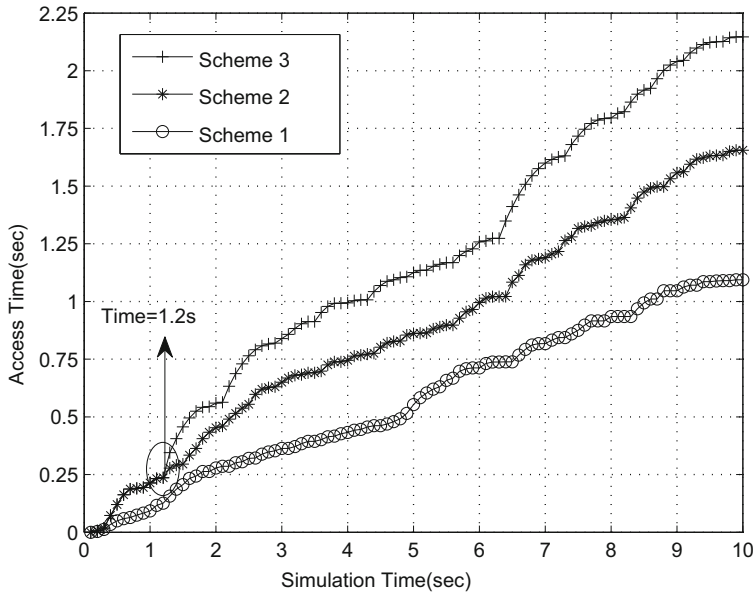


Fig. 5.11 Comparison of overall access time

Table 5.3 Parameters of the system

Parameter	Ψ_{pt}	Ψ_{st}	σ_N^2	$\bar{\phi}$	α
Value	400 W	1 W	0.05 mW	$1/\sqrt{2}$	2

5.1.6.4 PU's Achievable Rate

In order to calculate PU's achievable rate, the simulation has been run for 10,000 instantiations of the Rayleigh fading coefficients ϕ with Eqs. (5.25) and (5.26). As for calculation of link propagation, the following Table 5.3 lists values of some system parameters assumed for both PUs and SUs.

The improvement of PU's rate with variation of total search time C_s are plotted in Fig. 5.12. The increase in the search time results in the decrease in the interference probability P_{inf} , in turn an improvement in PU's rate. In the presence of one interfering SU in the system, the rate of PU rapidly rises when total search time increases from 0 to 3 s while it improves slowly in the presence of 5 and 20 s interfering nodes. After C_s achieves 30 which means a sufficient search, the rate of each scenario with interference converges to the upper limit, and does not vary significantly with C_s and the number of interfering SUs in the system.

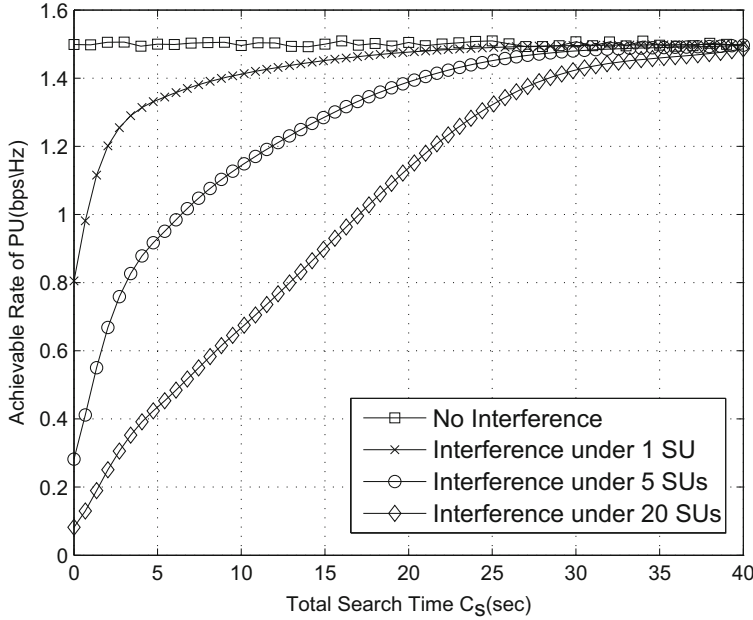


Fig. 5.12 Achievable rate of PU under the interference of SUs with parameters in Table 5.3 and $d_{(pt,pr)} = 1 \text{ km}$, $d_{(st,pr)} = 50 \text{ m}$

5.2 Asynchronous Cooperative Spectrum Sensing

In order to improve the success rate to discover free channels, collaborative spectrum sensing has been paid more and more attention in recent years. This technology uses the co-controller to complete the concentration of perceived results of the SUs, and coordinate the channel access of each terminal. This section is to optimize the sensing parameters when the SUs adopt the cooperative spectrum sensing method to access the mobile satellite communication system [17, 34–38], so that the time and throughput of data transmission can be maximized.

5.2.1 System Model

5.2.1.1 Network Entity

In our system, it is assumed that there is one primary channel shared by PUs and SUs. PUs' mutual communications are based on their own protocols, not known to the SUs. In the secondary network, a coordinator among M cooperative SUs is employed to collect sensing results from other active SUs [18], decide the availability of the primary channel and coordinate SUs' channel access. There is a narrow-band control channel for information exchange in the secondary network.

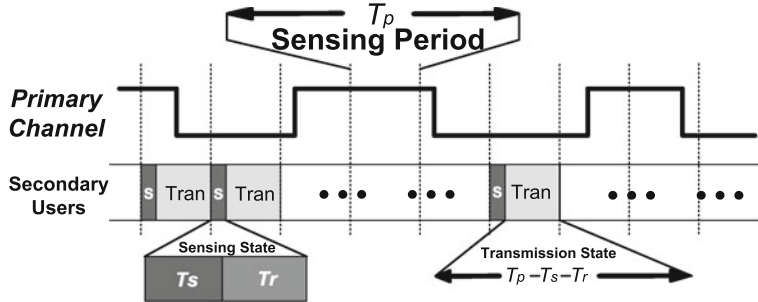


Fig. 5.13 Asynchronous cooperative spectrum sensing

5.2.1.2 ON/OFF Channel State Model

In the eyes of SUs, the primary channel alternatively switches between *busy* state and *free* state, which can be regarded as an ON/OFF process. The ON state means *busy* (PUs are present), while OFF state means *free* (PUs are absent). The lengths of the ON/OFF states T_{on}/T_{off} obey negative exponential distributions with parameters r_1/r_0 , where r_1 and r_0 denote the average lengths of the ON state and OFF state, respectively. Reference [19] provided an effective maximum likelihood estimator for the estimation of r_1 and r_0 . The ultimate goal of [19] is to maximize discovery opportunities of available spectrums from the respect of SUs, which is totally different from our work which adjust SUs' channel sensing parameters based on analyzing the detection probability and false alarm probability from the respect of PUs.

5.2.1.3 Asynchronous Cooperative Spectrum Sensing

The so-called “asynchronous” here dose not refer to the communication scheme in secondary network. Instead, it means that the system clock of SUs is asynchronous with that of PUs. In our scheme, the secondary network is still a synchronous system with time slots. Each slot is separated into two states: *sensing state* and *transmission state*, as Fig. 5.13 shows. At the beginning of each slot, SUs sense the primary channel with time T_s and sampling rate λ based on energy detection method. After sensing, SUs report their sensing results to the coordinator and then wait for the final decision within time T_r . We define one time slot of SUs as one *sensing period* expressed by T_p , which is less than the average length of ON/OFF channel state r_1 and r_0 .

5.2.2 Detection and False Alarm Probability

The performance of spectrum sensing is usually evaluated by detection probability and false alarm probability. The former, expressed by P^d is the probability that if there are primary activities, SUs can detect them successfully. And the latter, expressed by P^f is the probability that if there is no primary activity, SUs falsely decide that PUs are active. Here, we use \mathcal{H}_0 and \mathcal{H}_1 to express OFF and ON state of the primary channel, respectively. The coordinator compares the overall statistic energy from M SUs $Y = \sum_{i=1}^M y_i$ with threshold Y_{th} to decide whether primary activities exist. Once the coordinator makes the decision, it will broadcast the decision results to the SUs. Since SUs report their full sensing results, i.e., the received signal power y_i , to the coordinator, our sensing scheme is based on the “soft decision” method [20]. For simplicity, we express the coordinator’s decision results by \mathcal{D}_0 and \mathcal{D}_1 :

$$\begin{aligned}\mathcal{D}_0 : Y < Y_{th}, & \quad \text{Deciding no primary activity exists;} \\ \mathcal{D}_1 : Y \geq Y_{th}, & \quad \text{Deciding primary activities exist.}\end{aligned}$$

In our proposed sensing scheme, since the asynchronism between SUs and PUs, there are four different cases: S_{00} , S_{01} , S_{10} and S_{11} according to different beginnings and endings of SUs’ one sensing period, as shown in Fig. 5.14. Since T_p is relatively small compared with the average lengths of ON and OFF states, r_1 and r_2 as discussed in Sect. 5.2.1.3, the situation that SUs’ one sensing period contains two or more ON/OFF states rarely happens, which is not considered in the following analysis. In the simulation, we will verify this assumption through comparison of theoretical and simulation results. We will separately derive the closed-form expressions for P^d and P^f of each case.

5.2.2.1 Case $S_{00} : P_{00}^f$ and P_{00}^d

In this case, SUs’ one sensing period wholly falls into the OFF channel state, as shown in Fig. 5.14a. P_{00}^f can be calculated by Eq. (5.30):

$$\begin{aligned}P_{00}^f &= \Pr[S_{00} \& (\mathcal{D}_1 | \mathcal{H}_0)] \\ &= \Pr[S_{00}] \cdot \Pr[(\mathcal{D}_1 | \mathcal{H}_0) | S_{00}].\end{aligned}\tag{5.30}$$

$\Pr[S_{00}]$ denotes the occurrence probability of S_{00} . S_{00} happens when SUs’ sensing period begins in OFF state and the period T_p is shorter than SUs’ *forward recurrence time* of OFF state F_{of} . SUs’ *forward recurrence time* of OFF state refers to the duration from SUs’ sensing point (the time point when SUs begin to sense the channel) to the end of OFF state. According to the renewal theory [11], F_{of} still obeys the negative exponential distribution with parameter r_0 like OFF state.

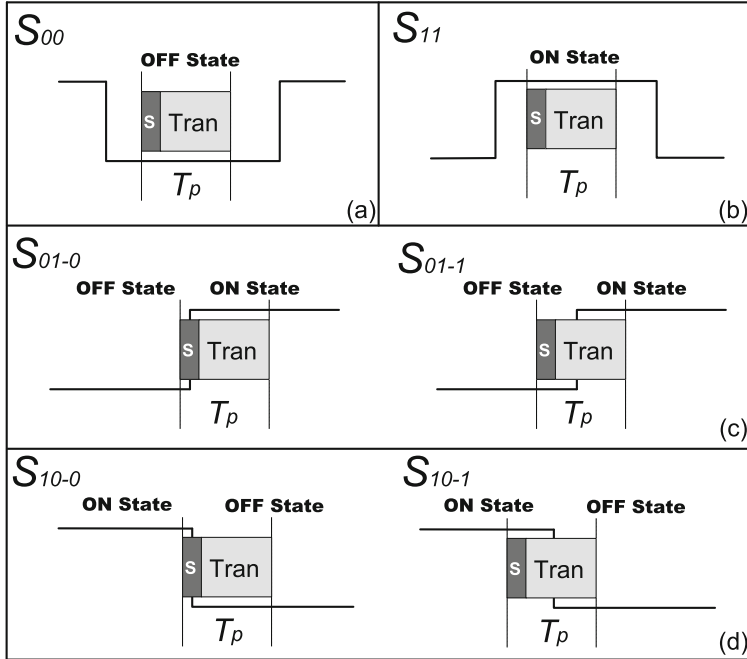


Fig. 5.14 Four different cases of detection and false alarm probability

Therefore, the first item of Eq. (5.30) is:

$$\begin{aligned} \Pr[S_{00}] &= \mu_0 \Pr(F_{of} \geq T_p) \\ &= \mu_0 \int_{T_p}^{+\infty} \frac{1}{r_0} e^{-\frac{f_{of}}{r_0}} df_{of} = \mu_0 e^{-\frac{T_p}{r_0}}, \end{aligned} \quad (5.31)$$

where $\mu_0 = \frac{r_0}{r_0 + r_1}$ is the occurrence probability of OFF state.

As to the second item of Eq. (5.30), since \mathcal{H}_0 always accompanies Case S_{00} , $\Pr[(\mathcal{D}_1 | \mathcal{H}_0) | S_{00}] = \Pr[\mathcal{D}_1 | \mathcal{H}_0]$. Therefore, according to [21], we have:

$$\begin{aligned} \Pr[(\mathcal{D}_1 | \mathcal{H}_0) | S_{00}] &= \Pr[\mathcal{D}_1 | \mathcal{H}_0] \\ &= \Pr[Y \geq Y_{th} | H_0] \\ &= Q\left(\left(\frac{Y_{th}}{\sigma^2} - 1\right) \sqrt{\lambda M T_s}\right) = Q_I, \end{aligned} \quad (5.32)$$

where $Q(x) = \frac{1}{\sqrt{2\pi}} \int_x^{+\infty} \exp\left(-\frac{x^2}{2}\right) dx$, σ^2 is the variance of background noise and Q_I is the simplified expression. Thus, combining Eqs. (5.31) and (5.32), we have:

$$P_{00}^f = \mu_0 e^{-\frac{T_p}{r_0}} Q_I. \quad (5.33)$$

Because it is impossible that \mathcal{H}_1 and Case S_{00} happen together, $P_{00}^d = \Pr[S_{00} \& (\mathcal{D}_1 | \mathcal{H}_1)] = 0$.

5.2.2.2 Case S_{11} : P_{11}^f and P_{11}^d

As shown in Fig. 5.14b, $P_{11}^f = \Pr[S_{11} \& (\mathcal{D}_1 | \mathcal{H}_0)] = 0$ since Case S_{11} and \mathcal{H}_0 can not happen simultaneously. And P_{11}^d is given by:

$$\begin{aligned} P_{11}^d &= \Pr[S_{11} \& (\mathcal{D}_1 | \mathcal{H}_1)] \\ &= \mu_1 \Pr(F_{on} \geq T_p) \cdot \Pr[Y \geq Y_{th} | \mathcal{H}_1] \\ &= \mu_1 \int_{T_p}^{+\infty} \frac{1}{r_1} e^{-\frac{f_{on}}{r_1}} df_{on} \cdot Q\left(\left(\frac{Y_{th}}{\sigma^2} - \gamma - 1\right) \sqrt{\frac{\lambda M T_s}{2\gamma + 1}}\right) \\ &= \mu_1 e^{-\frac{T_p}{r_1}} Q_{\text{II}}, \end{aligned} \quad (5.34)$$

where $\mu_1 = \frac{r_1}{r_0 + r_1}$ is the occurrence probability of ON state; F_{on} is SUs' *forward recurrence time* of ON state which obeys the negative exponential distribution with parameter r_1 ; the expression of $\Pr[Y \geq Y_{th} | \mathcal{H}_1]$ is according to [21]; γ is the average SNR of the primary signal received by SUs; Q_{II} is the simplified expression.

5.2.2.3 Case S_{01} : P_{01}^f and P_{01}^d

This case means that SUs' sensing period begins in OFF state of channel and ends in ON state. There are two subcases as shown in Fig. 5.14c, one is the ON/OFF switches in the *sensing state*, while the other is the ON/OFF switches in the *transmission state*. For the first subcase, denoted as S_{01-0} , although when the coordinator may make a wrong sensing decision, i.e., \mathcal{D}_1 , it is a correct detection for the latter *transmission state*. Therefore, P_{01-0}^d should not be simply considered as zero like P_{00}^d . In such a case, we have:

$$\begin{aligned} P_{01-0}^d &= \Pr[S_{01-0}] \cdot \Pr[(\mathcal{D}_1 | \mathcal{H}_0) | S_{01-0}] \\ &= \mu_0 \Pr(F_{of} \leq T_s + T_r) \cdot \Pr[\mathcal{D}_1 | \mathcal{H}_0] \\ &= \mu_0 \left(1 - e^{-\frac{T_s + T_r}{r_0}}\right) Q_{\text{I}}. \end{aligned} \quad (5.35)$$

For P_{01-0}^f , we have $P_{01-0}^f = 0$ since the latter *transmission state* is always in the ON state in Case S_{01-0} .

For the second subcase denoted as S_{01-1} , similar with Case S_{01-0} , although the coordinator may falsely alarm channel is in ON state at the beginning, this "mistake" is correct for the latter period after the channel turns into ON state. We define P_{01-1}^d

as Eq. (5.36) below, where the weight $\frac{T_p - F_{of}}{T_p}$ is because the coordinator's false alarm is a successful detection for the latter period $T_p - F_{of}$ as Fig. 5.14c shows.

$$P_{01-1}^d = \frac{T_p - F_{of}}{T_p} \Pr[S_{01-1} \& (\mathcal{D}_1 | \mathcal{H}_0)], \quad (5.36)$$

where $T_s + T_r \leq F_{of} \leq T_p$. The expectancy of P_{01-1}^d is

$$\mathbb{E}(P_{01-1}^d) = \frac{\Pr[S_{01-1} \& (\mathcal{D}_1 | \mathcal{H}_0)]}{T_p} \mathbb{E}_{[T_s + T_r \leq F_{of} \leq T_p]}(T_p - F_{of}), \quad (5.37)$$

where for $\Pr[S_{01-1} \& (\mathcal{D}_1 | \mathcal{H}_0)]$, we have

$$\begin{aligned} \Pr[S_{01-1} \& (\mathcal{D}_1 | \mathcal{H}_0)] &= \Pr[S_{01-1}] \cdot \Pr[(\mathcal{D}_1 | \mathcal{H}_0) | S_{01-1}] \\ &= \mu_0 \Pr(T_s + T_r \leq F_{of} \leq T_p) \cdot \Pr[\mathcal{D}_1 | \mathcal{H}_0] \\ &= \mu_0 (e^{-\frac{T_s + T_r}{r_0}} - e^{-\frac{T_p}{r_0}}) Q_I. \end{aligned} \quad (5.38)$$

$\mathbb{E}_{[0 \leq F_{of} \leq T_p]}(T_p - F_{of})$ is the expectancy of $T_p - F_{of}$ over interval $[T_s + T_r \leq F_{of} \leq T_p]$. The *p.d.f* (probability density function) of $T_p - F_{of}$ over interval $[T_s + T_r \leq F_{of} \leq T_p]$ is:

$$\begin{aligned} F_{of} &\sim \frac{1}{r_0} e^{-\frac{f_{of}}{r_0}} \quad (0 \leq f_{of} \leq +\infty) \\ &\downarrow \text{Substitution} \\ T_p - F_{of} = U_1 &\sim \frac{1}{r_0} e^{-\frac{T_p - u_1}{r_0}} \quad (-\infty \leq u_1 \leq T_p) \\ &\downarrow \text{Normalization over} \\ &\quad [T_s + T_r \leq F_{of} \leq T_p] \\ U_{1[T_s + T_r \leq F_{of} \leq T_p]} = U_2 &\sim \frac{\frac{1}{r_0} e^{-\frac{T_p - u_2}{r_0}}}{\int_{T_s + T_r}^{T_p} \frac{1}{r_0} e^{-\frac{T_p - u_1}{r_0}} du_1} \\ &= \frac{e^{\frac{u_2 - T_p}{r_0}}}{r_0 (1 - e^{\frac{T_s + T_r - T_p}{r_0}})} \quad (5.39) \\ &\quad (T_s + T_r \leq u_2 \leq T_p). \end{aligned}$$

Through substitution and normalization, we obtain the *p.d.f* of $T_p - F_{of}$ over $[T_s + T_r \leq F_{of} \leq T_p]$. Then, we have:

$$\begin{aligned}
\mathbb{E}(P_{01-1}^d) &= \frac{\mu_0 \left(e^{-\frac{T_s+T_r}{r_0}} - e^{-\frac{T_p}{r_0}} \right) Q_I}{T_p} \int_{T_s+T_r}^{T_p} \frac{u_2 e^{\frac{u_2-T_p}{r_0}}}{r_0 \left(1 - e^{\frac{T_s+T_r-T_p}{r_0}} \right)} du_2 \\
&= \frac{\mu_0 Q_I \left(e^{-\frac{T_s+T_r}{r_0}} - e^{-\frac{T_p}{r_0}} \right) \left(T_p - r_0 + (r_0 - T_s - T_r) e^{\frac{T_s+T_r-T_p}{r_0}} \right)}{T_p \left(1 - e^{\frac{T_s+T_r-T_p}{r_0}} \right)}. \tag{5.40}
\end{aligned}$$

Similarly, for P_{01-1}^f the decision \mathcal{D}_1 is a false alarm for the period F_{of} , which can be calculated by

$$P_{01-1}^f = \frac{F_{of}}{T_p} \Pr[S_{01-1} \& (\mathcal{D}_1 | \mathcal{H}_0)], \quad [T_s + T_r \leq F_{of} \leq T_p]. \tag{5.41}$$

And the expectancy of P_{01-1}^f is:

$$\begin{aligned}
\mathbb{E}(P_{01-1}^f) &= \frac{\Pr[S_{01-1} \& (\mathcal{D}_1 | \mathcal{H}_0)]}{T_p} \mathbb{E}_{[T_s+T_r \leq F_{of} \leq T_p]}(F_{of}) \\
&= \frac{\mu_0 Q_I \left(e^{-\frac{T_s+T_r}{r_0}} - e^{-\frac{T_p}{r_0}} \right) \left(r_0 - (T_p + r_0 - T_s - T_r) e^{\frac{T_s+T_r-T_p}{r_0}} \right)}{T_p \left(1 - e^{\frac{T_s+T_r-T_p}{r_0}} \right)}. \tag{5.42}
\end{aligned}$$

To summarize, according to Eqs. (5.35), (5.40) and (5.42), we can have detection and false-alarm probabilities in Case S_{01} as

$$\mathbb{E}(P_{01}^d) = \mathbb{E}(P_{01-0}^d) + \mathbb{E}(P_{01-1}^d), \tag{5.43}$$

$$\mathbb{E}(P_{01}^f) = \mathbb{E}(P_{01-0}^f) + \mathbb{E}(P_{01-1}^f) = \mathbb{E}(P_{01-1}^f). \tag{5.44}$$

5.2.2.4 Case S_{10} : P_{10}^f and P_{10}^d

Like analysis of Case S_{01} , there are also two subcases in Case S_{10} according to whether ON/OFF switches in the *sensing state*, as shown in Fig. 5.14d. For the first subcase, denoted as S_{10-0} , the coordinator's successful detection becomes a false alarm for the latter *transmission state*. In such a case, P_{10-0}^f can be derived as below:

$$\begin{aligned}
P_{10-0}^f &= \Pr[S_{10-0}] \cdot \Pr[(\mathcal{D}_1 | \mathcal{H}_1)] \\
&= \mu_1 \Pr(F_{on} \leq T_s + T_r) \cdot \Pr[Y \geq Y_{th} | \mathcal{H}_1] \\
&= \mu_1 \left(1 - e^{-\frac{T_s+T_r}{r_1}} \right) Q_{II}. \tag{5.45}
\end{aligned}$$

Beside, we have $P_{10-0}^d = 0$ since the *transmission state* is always in the OFF state, i.e., there is no PU.

For the second case denoted as S_{10-1} , The derivations of $\mathbb{E}(P_{10-1}^d)$ and $\mathbb{E}(P_{10-1}^f)$ are similar as analysis of $\mathbb{E}(P_{01-1}^d)$ and $\mathbb{E}(P_{01-1}^f)$, hence the detailed process is omitted.

$$\begin{aligned}\mathbb{E}(P_{10-1}^d) &= \frac{\Pr[S_{10-1} \& (\mathcal{D}_1 | \mathcal{H}_1)]}{T_p} \mathbb{E}_{[T_s + T_r \leq F_{on} \leq T_p]}(F_{on}) \\ &= \frac{\mu_1 Q_{II} \left(e^{-\frac{T_s + T_r}{r_1}} - e^{-\frac{T_p}{r_1}} \right) \left(r_1 - (T_p + r_1 - T_s - T_r) e^{\frac{T_s + T_r - T_p}{r_1}} \right)}{T_p \left(1 - e^{\frac{T_s + T_r - T_p}{r_1}} \right)}.\end{aligned}\quad (5.46)$$

$$\begin{aligned}\mathbb{E}(P_{10-1}^f) &= \frac{\Pr[S_{10-1} \& (\mathcal{D}_1 | \mathcal{H}_1)]}{T_p} \mathbb{E}_{[T_s + T_r \leq F_{on} \leq T_p]}(T_p - F_{on}) \\ &= \frac{\mu_1 Q_{II} \left(e^{-\frac{T_s + T_r}{r_1}} - e^{-\frac{T_p}{r_1}} \right) \left(T_p - r_1 + (r_1 - T_s - T_r) e^{\frac{T_s + T_r - T_p}{r_1}} \right)}{T_p \left(1 - e^{\frac{T_s + T_r - T_p}{r_1}} \right)}.\end{aligned}\quad (5.47)$$

To summarize, according to Eqs. (5.45)–(5.47), we can have detection and false-alarm probabilities in Case S_{10} as

$$\mathbb{E}(P_{10}^d) = \mathbb{E}(P_{10-0}^d) + \mathbb{E}(P_{10-1}^d) = \mathbb{E}(P_{10-1}^d), \quad (5.48)$$

$$\mathbb{E}(P_{10}^f) = \mathbb{E}(P_{10-0}^f) + \mathbb{E}(P_{10-1}^f). \quad (5.49)$$

In the practical systems, the length of *sensing state* is relatively short compared with that of *transmission state*, i.e., $T_s + T_r \ll T_p$. In such a case, we can assume that there is no ON/OFF switching during the *sensing state* in Case S_{01} and S_{10} . With this assumption, the term of $T_s + T_r$ in the expressions of $\mathbb{E}(P^d)$ and $\mathbb{E}(P^f)$ can be approximated by 0, which simplified the expressions a lot. In the simulation, we will verify this assumption through comparing the case where ON/OFF switching during $T_s + T_r$ is considered and the case where ON/OFF switching is not considered.

5.2.3 Optimal Sensing Parameters

In our scheme, there are two sensing parameters: channel sensing time T_s and sensing period T_p . On one hand, a longer sensing period T_p can help SUs obtain more transmission time and higher throughput, but decreasing the channel sensing frequency and the detection probability P^d . On the other hand, a shorter sensing time T_s can also help SUs obtain more transmission time, but decreasing P^d as well.

Table 5.4 Numerical parameters for performance evaluation

Parameter	Value	Description
M	10	Number of Cooperative SUs
λ	5 kHz	Sampling rate
T_r	60 ms	Reporting time of each sensing period
$\frac{Y_{th}}{\sigma^2}$	-10 dB	Decision threshold to the variance of noise

In order to ensure PUs' communication quality of service (QoS), here we get the optimal T_s^* and T_p^* under the constraint that the detection probability P^d should at least exceed a predetermined threshold P_{th}^d .

$$\max T_p - (T_s + T_r), \quad (5.50)$$

$$\text{s.t. } \begin{cases} P^d = \sum_{j=00}^{11} \mathbb{E}(P_j^d) \geq P_{th}^d, \\ T_s + T_r < T_p < \min(r_0, r_1). \end{cases} \quad (5.51)$$

5.2.4 Simulation and Numerical Results

Simulation results are introduced in this section. The relevant parameters used in the evaluation are listed in Table 5.4. The parameters of primary ON-OFF channel are set to be $r_0 = 3.0$ s and $r_1 = 4.0$ s.

5.2.4.1 Detection and False Alarm Probability

Figure 5.15 shows the simulation and theoretical results of detection and false alarm probability versus the SNR of primary signals at SUs γ , with $T_p = 1400$ ms and $T_s = 40$ ms, where $T_s = 40$ ms means each SU has 200 samples since the sample rate $\lambda = 5$ kHz. Generally, we can see that the larger γ , the larger detection probability P_d and the less false-alarm probability P_f . The theoretical results are from the analysis in Sect. 5.2.2, where there are two theoretical results. One is with the assumption that no ON/OFF switches during *sensing state* denoted by “with assumption”, and the other is without this assumption denoted by “without assumption”.

In the simulation, we first generate a primary ON/OFF channel with parameters $r_0 = 3.0$ s and $r_1 = 4.0$ s using Matlab. Then, a secondary network is established with $M = 10$ nodes (half transmitters and half receives), the MAC protocol of which was based on asynchronous cooperative sensing and CSMA/CD of IEEE 802.11. Through periodically counting the detection and false alarm probability, we have the simulation results denoted by black lines in Fig. 5.15. It can be seen

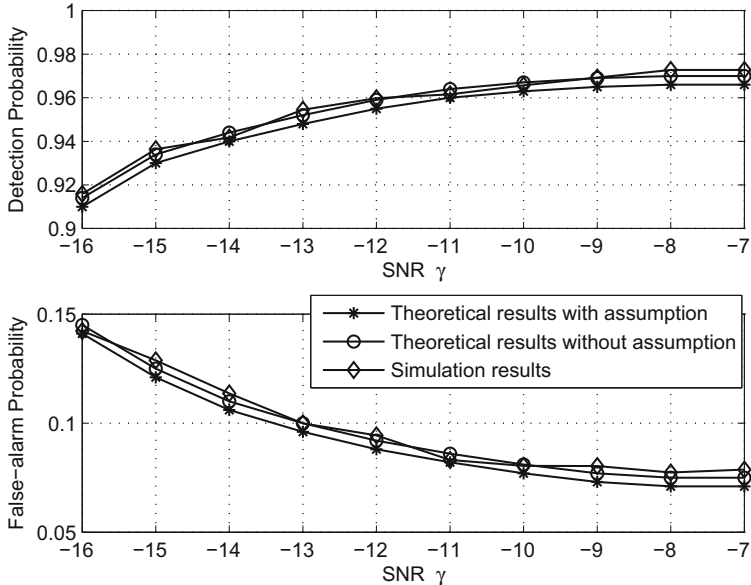


Fig. 5.15 Detection and false-alarm probabilities: P^d and P^f

that the simulation results finally match well with the theoretical values. Moreover, we can see that the assumption that no ON/OFF switches during *sensing state* has little effect to the results and can be adopted. Through performing ten thousand times independent simulations, we find the expected rate of the case that ON/OFF switches during *sensing state* is about 0.5%. Therefore, our analysis in Sect. 5.2.2 are correct and can be used to calculate the detection and false-alarm probabilities in the practical cognitive radio system.

5.2.4.2 Optimal Sensing Parameters

Putting the parameters in Table 5.4 into Eqs. (5.50), (5.51), the optimal sensing period T_p^* and channel sensing time T_s^* can be obtained. Figure 5.16 plots T_p^* and T_s^* versus the SNR of primary signals at SUs γ . We also use Mote Carlo simulation to find the optimal parameters that satisfy the constraints, which are in accord with our theoretical results as shown by dotted lines in Fig. 5.16. It can be seen that T_p^* keeps ascending and T_s^* keeps descending with the increasing SNR γ . This is because a higher γ means SUs can discover PUs more easily with a shorter T_s^* , and also enhance the detection probability. Thus, the same threshold P_{th}^d can be satisfied by a longer sensing period T_p^* . Additionally, we also compare the optimal T_p^* and T_s^* under different thresholds P_{th}^d in Fig. 5.16. It can be seen that T_p^* can be extended and T_s^* can be shorten when the threshold P_{th}^d is relaxed from 0.98 to 0.9.

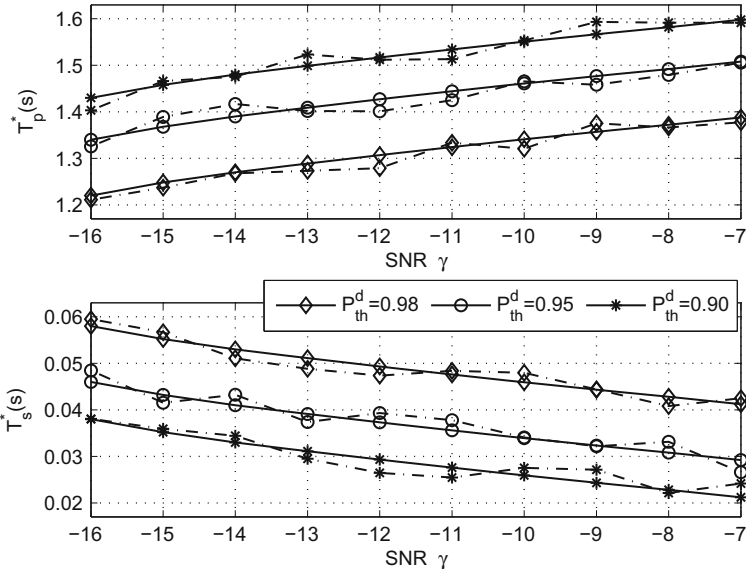


Fig. 5.16 Optimal T_p^* and T_s^* under different SNR γ and P_{th}^d

5.3 Effective Management of Terrestrial User's Density

How to manage the scale of the terrestrial SUs around the ground station of the satellite has become a major difficulty. This section puts forward a reasonable configuration of SUs' deployment area [22], through scientifically controlling the number (density) of unauthorized terminal deployment in order to achieve maximum utilization of idle spectrum resources and meet the communication needs of the satellite networks.

5.3.1 System Model

5.3.1.1 Network Entity

The scenario we will discuss is shown in Fig. 5.17. The primary transmitter (i.e. the satellite) is at the top of the center of the region. The supposed receiver (PR) is d meters away from the satellite. Terrestrial SUs build a half-duplex multi-hop network and seek for available time slots to access primary channels [23, 24]. In secondary network, IEEE 802.11 RTS/CTS mechanism is employed to avoid collision and interference. Once a pair of SUs discover that some channel is occupied, they will not try to access this channel. Therefore, it is reasonable to assume that within the interference range of secondary transmitter, only one pair of

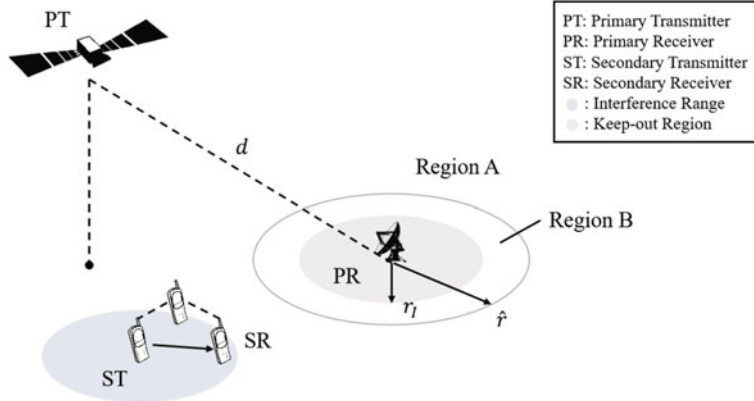


Fig. 5.17 Topology of the network

SUs communicate with each other at any one moment, as ST and SR in Fig. 5.17. Although users' locations are used in the below derivation of SUs' density, the implementation of this method does not require such information. Because when deploying the secondary network, as long as the density and channel condition (SNR) of primary network are known, we can obtain the allowed density of SU and provide a deployment standard according to the analysis results in this letter. Meanwhile, it should be mentioned here that our method is more appropriate for primary networks with relatively sparse PUs. Actually, primary works with high density are not available for SUs to dynamically access.

5.3.1.2 Channel Model

In our model, channel fading is modeled as the combination of large scale path loss and small scale Rayleigh flat fading [13]. The power loss from transmitter T to receiver R is expressed by $\lambda_{(t,r)} = \phi^2 / d_{(t,r)}^\alpha$, where $d_{(t,r)}$ is the distance from T to R , α is the attenuation exponent, and ϕ is a Rayleigh random variable with parameter $\bar{\phi}$. Additionally, it is also assumed that there exists additive white Gaussian noise (AWGN) in channels. Therefore, the received power at PR and SR in Fig. 5.17 are respectively:

$$P_{pr} = \lambda_{(p,p)} P_{pt} + \sum_{i=1}^{\mathcal{E}_s} \lambda_{(s_i,p)} P_{st_i} + \sigma_N^2 \quad (5.52)$$

$$P_{sr} = \lambda_{(p,s)} P_{pt} + \lambda_{(s,s)} P_{st} + \sigma_N^2 \quad (5.53)$$

where \mathcal{E}_s represents the number of SUs that may generate interference, σ_N is the variance of AWGN in channel, and P_X represents transmitted/received power at X .

5.3.1.3 Keep-out Region of Secondary Users

In broadcasting networks, PRs are principally passive devices and it is difficult for SU to detect them. Therefore, to setup a certain distance from ST to PR, within which secondary communications are not permitted, is an effective way to allay inference caused by SUs [25]. According the definition of protocol interference model [26], successful communication requires PR to lie in the transmission range of PT, while out of the interference range of surrounding ST. Therefore, we define the radius of that keep-out region as the interference ranges of ST. In our model, an interference power from node I is considered non-negligible only if it exceeds $1/\xi_I$ times of the power of AWGN at receiver R . Thus, the interference radius r_I can be illustrate as:

$$\frac{\bar{\phi}^2 P_I}{d_{(i,r)}^\alpha} \geq \frac{\sigma_N^2}{\xi_I} \Rightarrow r_I = \left(\frac{\xi_I \bar{\phi}^2 P_I}{\sigma_N^2} \right)^{1/\alpha} \quad (\xi_I \geq 1) \quad (5.54)$$

The grid area in Fig. 5.17 shows keep-out region of the ST. Although the exclusive region is definitely illustrated, it does not mean that STs will not bring any interference to PR at anywhere out of this region. From the view of physical interference model [31–33, 44], secondary communications outside this keep-out region should also be considered as noise to PR. Thus, ST's acceptable region is divided into two sub-regions: Region A and Region B, as shown in Fig. 5.17. Region B is the area where SUs' communications are still considered as noise to PR. In next section, we will explicitly discuss the achievable density of STs in this Region B.

5.3.2 Density Control Mechanism

According to the underlay mechanism [27], a secondary transmission is allowed only if its power level is so low that the interference is not harmful to the primary data rate. Therefore, it is important to control the density of STs in order to effectively adjust the overall interference power from Region B. Here we use ρ , which is defined as the number of STs in Region B, to illustrate the density of SUs. ρ represents how many STs can exist at most around one PR without degrading the primary specified data rate. On one hand, the value of ρ is restricted by PU's tolerance to interference caused by STs. On the other hand, ρ is also related with SUs themselves in the sense that crowded SUs will make the average network capacity dramatically decline. The following sections will explicitly discuss difference cases of ρ .

5.3.2.1 Restricted by Primary User

Firstly of all, we define the signal-to-interference-and-noise ratio (SINR) at PR γ_p according to Eq. (5.52).

$$\gamma_p = \frac{\lambda_{(p,p)}P_{pt}}{\sum_{i=1}^{\rho} \lambda_{(s_i,p)}P_{st_i} + \sigma_N^2} = \frac{SNR_p}{INR_p + 1} \quad (5.55)$$

where $SNR_p = \lambda_{(p,p)}P_{pt}/\sigma_N^2$ is SNR at PR without SU, $INR_p = \sum_{i=1}^{\rho} \lambda_{(s_i,p)}P_{st_i}/\sigma_N^2$ represents interference-to-noise ratio (INR). In order to guarantee PU's normal communications, it is assumed that data rate of PU should at least exceed R_p . In other words, R_p is the lower limit of PU's achievable rate. Thus, the SINR at PR should satisfy $\gamma_p \geq 2^{R_p} - 1$ to ensure the lowest data rate. As referred in Sect. 5.3.1.2, $\lambda_{(s_i,p)}$ is inversely proportional to the distance between ST and PR. For a conservative estimation, we assume that all interference transmitters are located at the nearest position to PR. Supposing $\tilde{\lambda}_{(s,p)} = \max_{1 \leq i \leq \rho} \{\lambda_{(s_i,p)}\}$, we can obtain Eq. (5.56).

$$\gamma_p \geq \frac{\lambda_{(p,p)}P_{pt}}{\rho \tilde{\lambda}_{(s,p)}P_{st} + \sigma_N^2} \geq 2^{R_p} - 1 \quad (5.56)$$

Therefore, ρ should satisfy Eq. (5.57) below, where $\widetilde{SNR}_p = 2^{R_p} - 1$ represents minimum SINR at PR, while $\widetilde{INR}_p = \tilde{\lambda}_{(s,p)}P_{st}/\sigma_N^2$ represents maximum INR at PR.

$$\rho \leq \left(\frac{\lambda_{(p,p)}P_{pt}}{2^{R_p} - 1} - \sigma_N^2 \right) / \left(\tilde{\lambda}_{(s,p)}P_{st} \right) = \frac{1}{\widetilde{INR}_p} \left(\frac{\widetilde{SNR}_p}{\widetilde{INR}_p} - 1 \right) \quad (5.57)$$

5.3.2.2 Restricted by Secondary Users Themselves

In secondary network, IEEE 802.11 RTS/CTS mechanism is used to avoid collision and interference. When some ST is sending data packets, other transmitters within its interference range will not try to access. Thus, it is estimated that transmitters in Region B is less than $S_B/\pi r_I^2$ at one moment, where S_B is the area of Region B. Therefore, ρ is also restricted by Eq. (5.58), where \hat{r} is the radius of Region B and $\hat{\rho}$ represents the theoretical maximum value of ρ .

$$\rho \leq \frac{\pi \hat{r}^2 - \pi r_I^2}{\pi r_I^2} = \left(\frac{\hat{r}}{r_I} \right)^2 - 1 = \hat{\rho} \quad (\hat{r} \geq r_I \Rightarrow \hat{\rho} \geq 0) \quad (5.58)$$

5.3.2.3 Overall Analysis

Considering above two restrictions together, the density of SUs ρ should satisfy Eq. (5.59) below:

$$\rho = \min \left\{ \widehat{\rho}, \frac{1}{\widetilde{INR}_p} \left(\frac{SNR_p}{\widetilde{SINR}_p} - 1 \right) \right\} \quad (5.59)$$

There are three cases about ρ :

- Case 1: $SNR_p \leq \widetilde{SINR}_p$

In this case, SNR at PR already falls below the lower limit $2^{R_p} - 1$, which may due to the insufficient gain ϵ_p of primary channel or severe white noise in channel. PR is unable to correctly decode data packets from corresponding transmitter. Thus, the secondary communication will not have negative influence on PU. Therefore, the number of SUs is only confined by their own network: $\rho = \widehat{\rho}$.

- Case 2: $\widetilde{SINR}_p \leq SNR_p \leq \widetilde{SINR}_p(1 + \widehat{\rho}\widetilde{INR}_p)$

According to this case condition and Eq. (5.59):

$$\begin{aligned} \widehat{\rho} &\geq \frac{1}{\widetilde{INR}_p} \left(\frac{SNR_p}{\widetilde{SINR}_p} - 1 \right) \geq 0 \\ \Rightarrow \rho &= \frac{1}{\widetilde{INR}_p} \left(\frac{SNR_p}{\widetilde{SINR}_p} - 1 \right) \end{aligned} \quad (5.60)$$

$SNR_p \geq \widetilde{SINR}_p = 2^{R_p} - 1$ means that the primary link is in a favorable condition. Therefore, ρ should be well adjusted by Eq. (5.60) to ensure PU's normal communications.

- Case 3: $SNR_p \geq \widetilde{SINR}_p(1 + \widehat{\rho}\widetilde{INR}_p)$

This case is another extreme condition in contrast to Case 1: the primary channel gain ϵ_p is so high that PR can tolerate nearly all interference from that Region B. Therefore, like Case 1, the density of SUs $\rho = \widehat{\rho}$.

At last, we can summarize mechanism for controlling the density of STs in Region B as Eq. (5.61) shows below, where Γ_p is used for expressing SNR_p for simplicity. It can be seen that ρ is a discontinuous function of SNR at PR.

$$\rho(\Gamma_p) = \begin{cases} A\Gamma_p - B, & \frac{B}{A} \leq \Gamma_p \leq \frac{B+\widehat{\rho}}{A}; \\ \widehat{\rho}, & \text{Else.} \end{cases} \quad (5.61)$$

$$\text{where: } \begin{cases} A = 1/(\widetilde{INR}_p \cdot \widetilde{SINR}_p) \\ B = 1/\widetilde{INR}_p \end{cases}$$

5.3.3 Achievable Rate of Secondary Users

This section will discuss the achievable rate of SU under density control mechanism. Firstly, it is assumed that there are totally Θ intended STs in Region B. Since only ρ of them are allowed to communicate with each other as discussed in Sect. 5.3.2.2, the instantaneous rate of SU can be illustrated by Eq. (5.62) below, where $\gamma_s = |\epsilon_s|^2 P_{st} / \sigma_N^2$ is SNR at SR.

$$R_{inst} = \frac{\rho}{\Theta} \log(1 + \gamma_s) \quad (5.62)$$

It is obvious that R_{inst} is also a function of Γ_p in respect that R_{inst} is proportional to ρ and ρ is a function of Γ_p . Thus, according to [28], we can obtain the average achievable rate R_{av} of SU by averaging R_{inst} over Γ_p . Due to the discontinuity of ρ , the integration in Eq. (5.63) should be separated into three parts like analysis in Sect. 5.3.2. For simplicity, we will use simplified expressions in Eq. (5.61).

$$R_{av} = \int_0^{+\infty} R_{inst} \frac{1}{\bar{\Gamma}_p} \exp \left\{ -\frac{\Gamma_p}{\bar{\Gamma}_p} \right\} d\Gamma_p \quad (5.63)$$

- Case 1 or 3: $0 \leq \Gamma_p \leq B/A$ or $\Gamma_p \geq (B + \hat{\rho})/A$;

In these two cases, the density of STs $\rho = \hat{\rho}$. Therefore, the instantaneous rate $R_{inst13} = \frac{\hat{\rho}}{\Theta} \log(1 + \gamma_s)$. Thus, the average rate of SU in Case 1 and 3 is:

$$\begin{aligned} R_{av13} &= \left(\int_0^{\frac{B}{A}} + \int_{\frac{B+\hat{\rho}}{A}}^{+\infty} \right) \frac{R_{inst13}}{\bar{\Gamma}_p} \exp \left\{ -\frac{\Gamma_p}{\bar{\Gamma}_p} \right\} d\Gamma_p \\ &= \frac{\hat{\rho} \log(1 + \gamma_s)}{\Theta \bar{\Gamma}_p} \left(\int_0^{\frac{B}{A}} + \int_{\frac{B+\hat{\rho}}{A}}^{+\infty} \right) \exp \left\{ -\frac{\Gamma_p}{\bar{\Gamma}_p} \right\} d\Gamma_p \\ &= \frac{\hat{\rho}}{\Theta} \log(1 + \gamma_s) \cdot \left(1 - \exp \left\{ -\frac{B}{A \bar{\Gamma}_p} \right\} \right. \\ &\quad \left. + \exp \left\{ -\frac{B + \hat{\rho}}{A \bar{\Gamma}_p} \right\} \right) \end{aligned} \quad (5.64)$$

- Case 2: $B/A \leq \Gamma_p \leq (B + \hat{\rho})/A$;

In this case, SUs' communications bring non-ignorable interference to PR and the density $\rho = A\Gamma_p - B$. Therefore, the instantaneous rate in Case 2 $R_{inst2} = \frac{A\Gamma_p - B}{\Theta} \log(1 + \gamma_s)$. Thus, the average achievable rate of SU R_{av2} is:

Table 5.5 Parameters of the system

Parameter	P_{pt}	P_{st}	σ_N^2	R_p	$\bar{\phi}$	α
Value	400 W	1 W	$50 \mu\text{W}$	1 bps/Hz	$1/\sqrt{2}$	2

$$\begin{aligned}
R_{av2} &= \int_{\frac{B}{A}}^{\frac{B+\hat{\rho}}{A}} \frac{R_{inst2}}{\bar{\Gamma}_p} \exp \left\{ -\frac{\Gamma_p}{\bar{\Gamma}_p} \right\} d\Gamma_p \\
&= \frac{\log(1 + \gamma_s)}{\Theta \bar{\Gamma}_p} \int_{\frac{B}{A}}^{\frac{B+\hat{\rho}}{A}} (A\Gamma_p - B) \exp \left\{ -\frac{\Gamma_p}{\bar{\Gamma}_p} \right\} d\Gamma_p \\
&= \frac{1}{\Theta} \log(1 + \gamma_s) \cdot \left\{ A\bar{\Gamma}_p \exp \left\{ -\frac{B}{A\bar{\Gamma}_p} \right\} \right. \\
&\quad \left. - \left(\hat{\rho} + A\bar{\Gamma}_p \right) \exp \left\{ -\frac{B + \hat{\rho}}{A\bar{\Gamma}_p} \right\} \right\} \tag{5.65}
\end{aligned}$$

At last, we can obtain the average rate of SU R_{av} below:

$$\begin{aligned}
R_{av} &= R_{av13} + R_{av2} \\
&= \frac{1}{\Theta} \log(1 + \gamma_s) \cdot \left\{ \left(A\bar{\Gamma}_p - \hat{\rho} \right) \exp \left\{ -\frac{B}{A\bar{\Gamma}_p} \right\} \right. \\
&\quad \left. - A\bar{\Gamma}_p \exp \left\{ -\frac{B + \hat{\rho}}{A\bar{\Gamma}_p} \right\} + \hat{\rho} \right\} \tag{5.66}
\end{aligned}$$

5.3.4 Simulation

We developed all the simulations using Matlab. Terrestrial SUs are located uniformly in Region A and B. While satellite PT and PR lie in positions as Fig. 5.17 shows. As for calculation of link propagation, the following Table 5.5 lists values of some system parameters assumed for both PUs and SUs.

5.3.4.1 Achievable Density

According to Eq. (5.61), we can illustrate the theoretical density ρ varying with SNR of PU. As for $\hat{\rho}$, it is assumed that the radius of Region B \hat{r} is 5 times of keep-out region r_l . Thus, $\hat{\rho} = 24$ is the upper limit of ρ . In Case 1 and 3, $\rho = \hat{\rho} = 24$; while ρ is linearly increasing with Γ_p in Case 2. In the simulation part, SUs are uniformly distributed in Region B and the centered PR's lowest rate R_p is configured

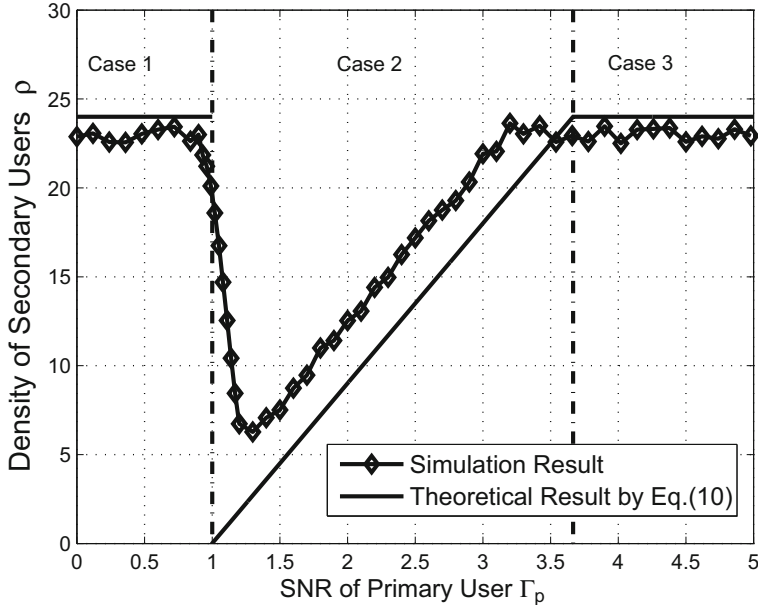


Fig. 5.18 Density of SUs with parameters in Table 5.5 and $\hat{\rho} = 24$

as 1bps/Hz. Through setting different distances between PT and PR z , we can get different SNR Γ_p . Then under these different Γ_p , the simulation adjusts the number of STs ρ in Region B to ensure PU's lowest rate and plot all ρ by black diamond line in Fig. 5.18. It can be seen that in Case 2, the theoretical line is always above the simulation values. This is due to the conservative estimation in Eq. (5.56) which assumed all STs are located at the nearest position to PR. While in the simulation, STs are uniformly distributed in Region B.

5.3.4.2 Average Achievable Rate

Figure 5.19 below plots the average rate of SUs R_{av} versus PU's data rate R_p under different SNR at SR γ_s . The curves show that SU's average achievable rate keeps descending with increase of PU's rate R_p when R_p is low, while ascending with R_p when R_p is higher than some certain value. As we defined above, R_p is the lower limit of PU's data rate. When R_p is small, the primary link is easily guaranteed and can tolerate more noise from STs. Thus, the probability that Γ_p lies in Case 3 is high which means that the density of SUs has a big chance to achieve $\hat{\rho}$, in turn achieving a high average data rate. When R_p is so large that primary link has no access to satisfy this lowest rate, the probability that Γ_p lies in Case 1 is high which results in a big chance for ρ achieving $\hat{\rho}$ again. Therefore, R_{av} shows the process of descending first and ascending last. Additionally, it also can be seen from the

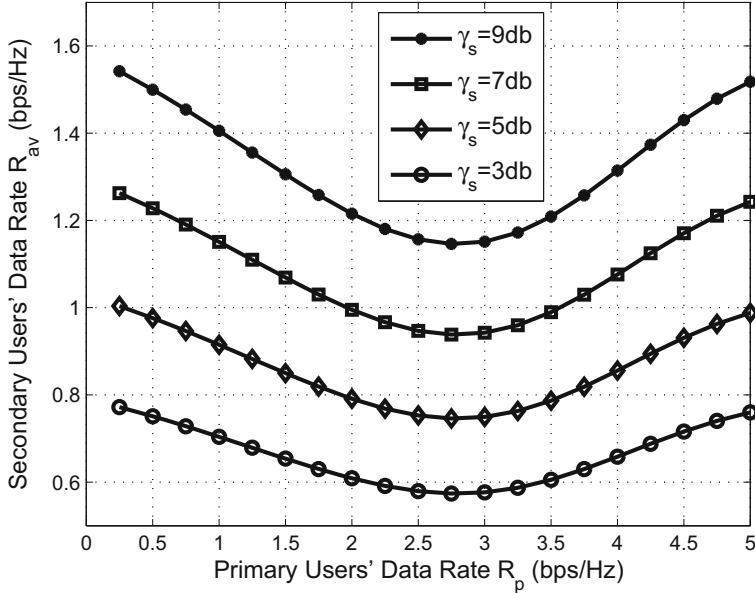


Fig. 5.19 SU's achievable data rate with parameters in Table 5.5 and $\Theta = 2\hat{\rho}$

figure that γ_s plays a positive role in enhancing SU's rate. This is because higher γ_s means better condition of secondary link or shorter distance between transmitter and receiver, all of which can bring SUs higher data rate R_{av} .

5.4 Summary

In this chapter, we consider the terrestrial system as secondary user (SU) and the satellite system as primary user (PU), where the SUs attempt to sense and access the PUs' channels. We first advance a strategy for SUs to search available spectrums with asynchronous MAC-layer sensing. Then, we discuss the asynchronous cooperative sensing situation, and derive the optimal sensing parameters under such asynchronous scenario. Finally, we propose a density control mechanism for managing number of terrestrial secondary transmitters around one satellite ground station in order to guarantee that the primary communications are not interfered.

References

- Q. Zhao, S. Geirhofer, L. Tong, B.M. Sadler, Optimal dynamic spectrum access via periodic channel sensing, in *IEEE WCNC*, 2007, pp. 33–37
- S. Sankaranarayanan, P. Papadimitratos, A. Mishra, S. Hershey, A bandwidth sharing approach to improve licensed spectrum utilization, in *IEEE DySPAN*, 2005, pp. 279–288
- H. Su, X. Zhang, Cross-layer based opportunistic MAC protocols for QoS provisionings over cognitive radio wireless networks. *IEEE J. Sel. Areas Commun.* **26**, 118–129 (2008)
- Q. Zhao, L. Tong, A. Swami, Decentralized cognitive MAC for dynamic spectrum access, in *IEEE DySPAN*, 2005, pp. 224–232
- H. Kim, K.G. Shin, Efficient discovery of spectrum opportunities with MAC-Layer sensing in cognitive radio networks. *IEEE Trans. Mob. Comput.* **7**, 533–545 (2008)
- C. Jiang, N. Beaulieu, L. Zhang, Y. Ren, M. Peng, H. Chen, Cognitive radio networks with asynchronous spectrum sensing and access. *IEEE Netw.* **29**(3), 88–95 (2015)
- H. Kim, K.G. Shin, Fast discovery of spectrum opportunities in cognitive radio networks, in *IEEE DySPAN*, 2008, pp. 1–12
- Z. Ma, Z. Cao, W. Chen, A fair opportunistic spectrum access (FOSA) scheme in distributed cognitive radio networks, in *IEEE ICC'08*, 2008, pp. 4054–4058
- Z. Ma et al., Secondary user cooperation access scheme in opportunistic cognitive radio networks, in *IEEE MILCOM'07*, 2007, pp. 1–5
- A. Papoulis, S. Pillai, *Probability, Random Variables and Stochastic Processes*, 4th edn. (McGraw-Hill College, New York, 2002)
- D.R. Cox, *Renewal Theory* (Butler and Tanner, Frome, 1967)
- K. Jong-Ho, H. Seung-Hoon, H. Deok-Kyu, Energy detector using a hybrid threshold in cognitive radio systems. *IEICE Trans. Commun.* **E92-B**(10), 3079–3083 (2009)
- S. Bernard, Rayleigh fading channels in mobile digital communication systems, part I: characterization. *IEEE Commun. Mag.* **35**(7), 90–100 (1997)
- W.C.Y. Lee, Estimate of channel capacity in Rayleigh fading environment. *IEEE Trans. Veh. Technol.* **39**(3), 187–189 (1990)
- D.P. Bertsekas, *Nonlinear Programming*. (Athena Scientific, Belmont, 1999)
- D. Cabric, I.D. O'Donnell, M.S. Chen, R.W. Brodersen, Spectrum sharing radios. *IEEE Circuits Syst. Mag.* **6**(2), 30–45 (2006)
- C. Jiang, H. Chen, P. Zhao, N. He, C. Chen, Y. Ren, Adaptive channel sensing for asynchronous cooperative spectrum sensing scheme. *IEICE Trans. Commun.* **96-B**(3), 918–922 (2013)
- Y. Gan, C. Jiang, N. Beaulieu, J. Wang, Y. Ren, Secure collaborative spectrum sensing: a peer-prediction method. *IEEE Trans. Commun.* **64**(10), 4283–4294 (2016)
- H. Kim, K.G. Shin, Efficient discovery of spectrum opportunities with MAC-Layer sensing in cognitive radio networks. *IEEE Trans. Mob. Comput.* **7**(5), 533–545 (2008)
- H. Uchiyama, K. Umebayashi, T. Fujii, F. Ono, K. Sakaguchi, Y. Kamiya, Y. Suzuki, Study on soft decision based cooperative sensing for cognitive radio networks. *IEICE Trans. Commun.* **E91-B**(1), 95–101 (2008)
- Y. Liang, Y. Zeng, E.C. Peh, A.T. Hoang, Sensing-throughput tradeoff for cognitive radio networks. *IEEE Trans. Wirel. Commun.* **7**(4), 1326–1337 (2008)
- C. Jiang, S. Fan, C. Chen, J. Ma, Y. Ren, Effective management of secondary user's density in cognitive radio networks. *IEICE Trans. Commun.*, **93-B**(9), 2443–2447 (2010)
- C. Jiang, Y. Chen, Y. Gao, K.J.R. Liu, Indian buffet game with negative network externality and non-bayesian social learning. *IEEE Trans. Syst. Man Cybern. Syst.* **45**(4), 609–623 (2015)
- H. Zhang, C. Jiang, X. Mao, H. Chen, Interference-limited resource optimization in cognitive femtocells with fairness and imperfect spectrum sensing. *IEEE Trans. Veh. Technol.* **65**(3), 1761–1771 (2016)
- M. Vu, N. Devroye, V. Tarokh, The primary exclusive regions in cognitive networks. *IEEE Trans. Wirel. Commun.* **8**, 3380–3385 (2008)

26. P. Gupta, P. Kumar, The capacity of wireless networks. *IEEE Trans. Inf. Theory* **46**, 388–404 (2000)
27. D. Cabric et al., Spectrum sharing radios. *IEEE Circuits Syst. Mag.* **6**(2), 30–45 (2006)
28. W.C.Y. Lee, Estimate of channel capacity in Rayleigh fading environment. *IEEE Trans. Veh. Technol.* **39**(3), 187–189 (1990)
29. X. Zhou, *Cognitive Radio* (National Defense Industry Press, Beijing, 2008)
30. I.F. Akyildiz, W.Y. Lee, M.C. Vuran, M. Shantidev, Next generation/dynamic spectrum access/cognitive radio wireless networks: a survey. *Comput. Netw.* **50**(13), 2127–2159 (2006)
31. F. Manavi, Y. Shayani, Implementation of OFDMmodem for the physical layer of IEEE 802.11a standard based on Xilinx Virtex-II FPGA. *IEEE VTC'04*, 2004, pp. 1768–1772
32. Wireless LAN media access control (MAC) and physical layer (PHY) specifications, Tech. Rep., IEEE 802 LAN/MAN Standards Committee (2009). <http://standards.ieee.org/getieee802/>
33. S. Buljore, M. Muck, P. Martigne, P. Houze, H. Harada, K. Ishizu, O. Holland, A. Mihailovic, K.A. Tsagkaris, O. Sallent, G. Clemo, M. Sooriyabandara, V. Ivanov, K. Nolte, M. Stametalos, Introduction to IEEE P1900.4 activities. *IEICE Trans. Commun.* **E91-B**(1), 2–9 (2008)
34. Z. Quan, S. Cui, A.H. Sayed, An optimal strategy for cooperative spectrum sensing in cognitive radio networks, in *IEEE GLOBECOM'07*, 2007, pp. 2947–2951
35. W. Zhang, R.K. Mallik, K.B. Letaief, Cooperative spectrum sensing optimization in cognitive radio networks, in *IEEE ICC'08*, 2008, pp. 3411–3415
36. J. Shen, T. Jiang, S. Liu, Z. Zhang, Maximum channel throughput via cooperative spectrum sensing in cognitive radio networks. *IEEE Trans. Wirel. Commun.* **8**(10), 5166–5175 (2009)
37. C. Sun, W. Chen, K.B. Letaief, Joint scheduling and cooperative sensing in cognitive radios: a game theoretic approach, in *IEEE WCNC'09*, 2009, pp. 1–5
38. C. Song, Q. Zhang, Achieving cooperative spectrum sensing in wireless cognitive radio networks. *ACM SIGMOBILE Mob. Comput. Commun. Rev.* **13**(2), 14–25 (2009)
39. C. Jiang, X. Ma, X. Zhang, Y. Ren, An asynchronous interference-aware dynamic spectrum access algorithm for secondary users, in *IEEE WCNC'10*, 2010, pp. 1–6
40. C. Jiang, X. Ma, C. Chen, J. Ma, Y. Ren, On searching available channels with asynchronous MAC-layer spectrum sensing. *IEICE Trans. Commun.* **E93-B**(8), 2113–2125 (2010)
41. C. Jiang, Y. Chen, K.J.R. Liu, Y. Ren, Analysis of interference in cognitive radio networks with unknown primary behavior, in *Proceedings of the IEEE ICC*, 2012, pp. 1746–1750
42. C. Jiang, Y. Chen, K.J.R. Liu, A renewal-theoretical framework for dynamic spectrum access with unknown primary behavior, in *Proceedings of the IEEE Globecom*, 2012, pp. 1–6
43. C. Jiang, Y. Chen, K.J.R. Liu, Y. Ren, Renewal-theoretical dynamic spectrum access in cognitive radio network with unknown primary behavior. *IEEE J. Sel. Areas Commun.* **31**(3), 406–416 (2013)
44. B. Soodesh et al., Introduction to IEEE P1900.4 activities. *IEICE Trans. Commun.* **E91-B**, 2–9 (2008)
45. N.S. Shankar, C. Cordeiro, Analysis of aggregated interference at DTV receivers in TV bands, in *IEEE CrownCom*, 2008, pp. 1–6
46. M. Vu, N. Devroye, V. Tarokh, Interference aggregation in spectrum-sensing cognitive wireless networks. *IEEE J. Sel. Top. Sig. Process.* **2**, 41–56 (2008)
47. M. Hanif et al., Interference and deployment issues for cognitive radio systems in shadowing environments, in *IEEE ICC'09*, 2009, pp. 1–6
48. Digital Video Broadcasting (DVB); Implementation guidelines for DVB terrestrial services; Transmission aspects, Tech. Rep., European Broadcasting Union (2008). <http://www.dvb.org/>

Chapter 6

Multiple Access Resource Allocation

The increasing traffic demand in both ground and satellite communication systems will lead to increasing spectrum demand. Spectrum sharing would become a challenging issue in future between terrestrial and satellite systems with frequency reusing, which would lead to co-channel interference. In this case, it is of great importance to allocate the system resources reasonably to optimize the system performance. Upon this, we propose two resource allocation schemes for two multiple access integrated system. First, we investigate the problem of interference controlling and power allocation in a terrestrial-satellite spectrum sharing network. In order to protect the terrestrial users, interference temperature limit is introduced for the satellite to control the interference caused to BS users. Then, under this constraint, we maximize the total capacity of the satellite system and obtain the optimal power allocation scheme. Second, we propose the concept of the Cloud Based Integrated Terrestrial-Satellite Network (CTSN), where both base stations of the cellular networks and the satellite are connected to a cloud central unit and the signal processing procedures are executed centrally at the cloud. By utilizing the channel state information (CSI), the interference from the mixed signal can be mitigated. When it comes to the case of imperfect CSI, we propose a resource allocation scheme in respect to subchannel and power to maximize the total capacity of the terrestrial system.

6.1 Power Allocation in Terrestrial-Satellite Networks

6.1.1 *Background*

Due to the increasing demand of wireless communication, wireless networks are now facing more and more challenges to provide larger communication capacity. In the next generation of wireless network, new spectrum have been proposed as

a method of improving the system capacity. At the same time, satellite networks are also in great demand of extra spectrum with the rapid growing of data traffic [1]. During the development of communication, limited spectrum resources have always been the constraint of communication capacity. With limited spectrum resources, spectrum sharing shows great potential for extra performance improvement. Coexistence of terrestrial networks and satellite networks are now been considered for comprehensive coverage of ground users [2]. It can be envisioned that spectrum sharing between the terrestrial system and the satellite system will play an important role in future networks [3, 4].

In spectrum sharing networks, interference mitigation is a important issue for the sake of system performance. In [1, 5], the technology of Cognitive Radio (CR) was considered for the satellite, which allows dynamic spectrum access for the satellite while controlling the interference caused to the terrestrial system. In [6], the technique of beamforming was utilized to mitigated the interference from the terrestrial users, and a semi-adaptive algorithm was proposed to reduce computing complexity. Furthermore, the concept of exclusive zone (EZ) was discussed in [7] to manage the interference between terrestrial and satellite networks. Within the range of EZ, the terrestrial network is not allowed to use the frequency of the satellite to protect the satellite users.

In this section, we consider a terrestrial-satellite spectrum sharing network, in which base stations (BSs) and the satellite share the entire bandwidth to provide service to ground users. In order to control the interference caused to BS users, we introduce the interference temperature limit for the satellite and formulate the power allocation problem to maximize the capacity of the satellite system. Then, by means of the successive convex approximation (SCA) approach and the Lagrangian dual method, we obtain the optimal power allocation scheme for the satellite.

6.1.2 System Model

Consider a terrestrial-satellite spectrum sharing network as illustrated in Fig. 6.1, in which BSs and one satellite serve users simultaneously while sharing the entire bandwidth. The BSs mainly provide service for the high density populations in urban areas, while the satellite can provide extra coverage for those users that have no access to BSs, such as suburban areas or mountain areas. The satellite is equipped with M antennas and thus can serve up to M users by utilizing beamforming techniques. The total number of BS users is assumed to be K , and both the satellite users and the BS users are equipped with a single antenna.

Then the transmit signal of the satellite is

$$\mathbf{x}_S = \sum_{j=1}^M \mathbf{v}_j \sqrt{P_j} s_j, \quad (6.1)$$

where \mathbf{v}_j , $\|\mathbf{v}_j\| = 1$, is the beamforming vector, P_j is the allocated power, and s_j , $E[|s_j|^2] = 1$, is the transmit signal for user j .

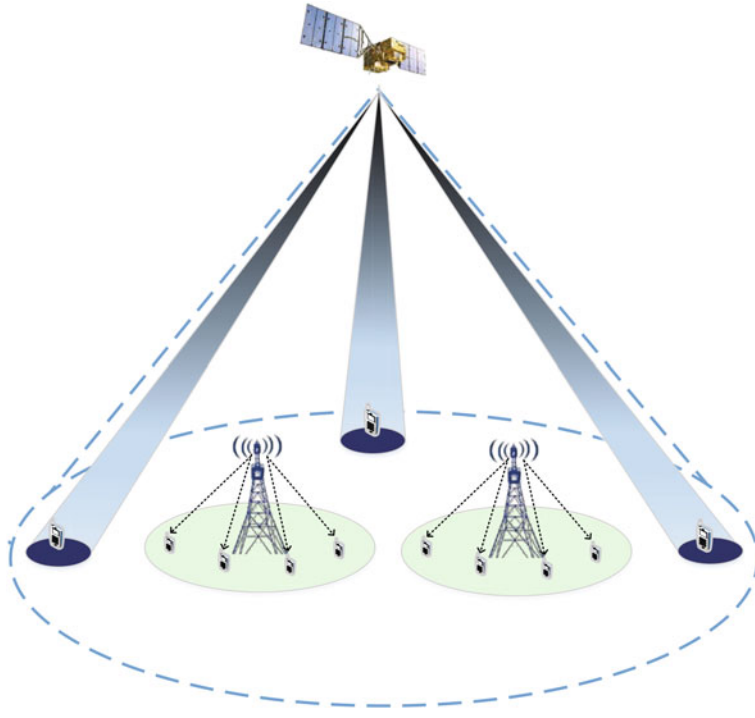


Fig. 6.1 System model of terrestrial-satellite spectrum sharing networks

Since the satellite channel generally experiences small channel fluctuations, we apply maximum ratio transmission (MRT) beamforming for the satellite, in which the beamforming vectors are designed as

$$\mathbf{v}_J = \frac{\mathbf{g}_J}{\|\mathbf{g}_J\|}, \quad (6.2)$$

where \mathbf{g}_J is the channel from the satellite to satellite user J .

As stated before, the satellite users are located in areas that have no coverage of BSs, and thus the satellite users will not receive interference from BSs. The received signal of the satellite user is

$$\begin{aligned} y_{S,J} &= \mathbf{g}_J^H \sum_{j=1}^M \mathbf{v}_j \sqrt{P_j} s_j + n \\ &= \mathbf{g}_J^H \mathbf{v}_J \sqrt{P_J} s_J + \mathbf{g}_J^H \sum_{j=1, j \neq J}^M \mathbf{v}_j \sqrt{P_j} s_j + n, \end{aligned} \quad (6.3)$$

where n is the additive white Gaussian noise (AWGN).

The SINR of the satellite users can be calculated as

$$\gamma_{S,J} = \frac{|\mathbf{g}_J^H \mathbf{v}_J|^2 P_J}{\sum_{j=1, j \neq J}^M |\mathbf{g}_J^H \mathbf{v}_j|^2 P_j + \sigma_n}. \quad (6.4)$$

Then the total capacity of the satellite is

$$C_S = \sum_{J=1}^M C_{S,J} = \sum_{J=1}^M \log_2(1 + \gamma_{S,J}). \quad (6.5)$$

Although the satellite users may not be interfered by the BSs, the satellite will cause interference to all BS users within its coverage. To protect the transmission of BS users, we introduce the interference temperature for the satellite. The transmit power of the satellite need to be controlled under the constraint that the interference received by all BS users should not be larger than the interference temperature limit P_{th} :

$$P_{B,I} = \sum_{j=1}^M |\mathbf{h}_I^H \mathbf{v}_j|^2 P_j \leq P_{th}, \quad I \in \{1, 2, \dots, K\}, \quad (6.6)$$

where \mathbf{h}_I is the channel from the satellite to the BS users.

Then, we maximize the satellite capacity under the power constraints and the interference constraints:

$$\begin{aligned} \max_{\mathbf{P}} C_S &= \sum_{J=1}^M \log_2\left(1 + \frac{|\mathbf{g}_J^H \mathbf{v}_J|^2 P_J}{\sum_{j=1, j \neq J}^M |\mathbf{g}_J^H \mathbf{v}_j|^2 P_j + \sigma_n}\right) \\ C1 : P_{B,I} &= \sum_{j=1}^M |\mathbf{h}_I^H \mathbf{v}_j|^2 P_j \leq P_{th}, \quad \forall I, \\ C2 : \sum_{J=1}^M P_J &\leq P_{S,\max}, \\ C3 : P_J &\geq 0, \quad \forall J. \end{aligned} \quad (6.7)$$

6.1.3 Optimal Power Allocation Scheme

The optimization problem in (6.7) is non-convex due to the non-convex objective function (6.5). To solve this problem, we utilized the successive convex approximation (SCA) approach in [8] to transform the original problem into a series convex subproblems that can be solved as follows:

- Set $t = 1$, and initialize the SCA approach from a feasible point $\mathbf{P}[1]$.
- In the t th iteration, approximate the non-convex function in original problem use convex function within a small range around the point $\mathbf{P}[t]$. Then, the non-convex problem can be transformed into a convex subproblem by approximation.
- By means of optimization theory, solve the approximate convex subproblem and obtain the power allocation scheme $\mathbf{P}[t + 1]$ of the subproblem.
- Update $t = t + 1$, continue the iteration to increase the accuracy of the results until $\mathbf{P}[t]$ converges.

By means of logarithmic approximation [9], the non-convex function can be approximated by

$$\ln(1 + \gamma_J) \geq \theta_J \ln \gamma_J + \beta_J, \quad (6.8)$$

which is tight at $\gamma_J = \bar{\gamma}_J$ if we select $\theta_J = \frac{\bar{\gamma}_J}{1+\bar{\gamma}_J}$ and $\beta_J = \ln(1 + \bar{\gamma}_J) - \frac{\bar{\gamma}_J}{1+\bar{\gamma}_J} \ln \bar{\gamma}_J$.

Applying the logarithmic approximation to the objective function, and changing the variables using $\widehat{\mathbf{P}} = \ln \mathbf{P}$, we can then obtain the approximate lower bound of the objective function as

$$\begin{aligned} \sum_J^M C_{S,J} &\geq \sum_{J=1}^M C_{S,J}(e^{\widehat{P}_J}, \theta_J, \beta_J) \\ &= \sum_J^M \frac{1}{\ln 2} \theta_J \ln \left(\frac{|\mathbf{g}_J^H \mathbf{v}_J|^2 e^{\widehat{P}_J}}{\sum_{j=1, j \neq J}^M |\mathbf{g}_j^H \mathbf{v}_j|^2 e^{\widehat{P}_j} + \sigma_n} \right) + \beta_J. \end{aligned} \quad (6.9)$$

Then the original problem can be transformed into the subproblem:

$$\begin{aligned} \min_{\widehat{\mathbf{P}}} & - \sum_{J=1}^M C_{S,J}(e^{\widehat{P}_J}, \theta_J, \beta_J) \\ C1 : & P_{th} - \sum_{j=1}^M |\mathbf{h}_I^H \mathbf{v}_j|^2 e^{\widehat{P}_j} \geq 0, \forall I, \\ C2 : & P_{S,\max} - \sum_{J=1}^M e^{\widehat{P}_J} \geq 0. \end{aligned} \quad (6.10)$$

Note that the problem is rewritten in the standard form. Based on the truth that the log-sumexp function is convex [10], it can be proved that the subproblem (6.10) is a standard convex problem, and we solve this subproblem by means of the Lagrangian dual method.

The Lagrangian function can be obtained as

$$\begin{aligned} L(\widehat{\mathbf{P}}, \boldsymbol{\mu}, \lambda) &= - \sum_{J=1}^M C_{S,J}(e^{\widehat{P}_J}, \theta_J, \beta_J) \\ &\quad - \sum_{I=1}^K \mu_I (P_{th} - \sum_{j=1}^M |\mathbf{h}_I^H \mathbf{v}_j|^2 e^{\widehat{P}_j}) - \lambda (P_{S,\max} - \sum_{J=1}^M e^{\widehat{P}_J}), \end{aligned} \quad (6.11)$$

where $\boldsymbol{\mu}$ and λ are the Lagrange multipliers for constraints C1 and C2.

By solving $\frac{\partial L}{\partial P_J} = 0$, we can obtain the power allocation scheme of the subproblem as

$$P_J = \left[\frac{\theta_J}{\sum_{j=1, j \neq J}^M \theta_j \frac{|\mathbf{g}_j^H \mathbf{v}_J|^2}{I_j} + \ln 2 \sum_{I=1}^K \mu_I |\mathbf{h}_I^H \mathbf{v}_J|^2 + \lambda \ln 2} \right]^+, \quad (6.12)$$

where $(x)^+ = \max(0, x)$, and I_j is calculated by

$$I_j = \sum_{m=1, m \neq j}^M |\mathbf{g}_j^H \mathbf{v}_m|^2 e^{\widehat{P}_m} + \sigma_n. \quad (6.13)$$

The Lagrange multipliers can be calculated using the subgradient method:

$$\begin{aligned} \mu_I[t_\delta + 1] &= [\mu_I[t_\delta] - \delta_I (P_{th} - \sum_{j=1}^M |\mathbf{h}_I^H \mathbf{v}_j|^2 P_j)]^+, \\ \lambda[t_\delta + 1] &= [\lambda[t_\delta] - \delta (P_{S, \max} - \sum_{J=1}^M P_J)]^+, \end{aligned} \quad (6.14)$$

in which t_δ is the subgradient iteration step and δ is the step size for updating of the Lagrange multipliers.

The subproblem (6.10) is only the lower bound of the original problem. To obtain the optimal solutions, the SCA approach, which is stated before, needs to be adopted. We summarize the entire process as Algorithm 4.

Algorithm 4 Optimal power allocation algorithm

- 1: Initialize $t = 1$, $\theta = 1$, $\beta = 0$ and $\mathbf{P}[1] = 0$
 - 2: **repeat**
 - 3: Initialize $t_\delta = 1$, $\mu > 0$, and $\lambda > 0$
 - 4: Initialize \mathbf{I} referring to (6.13)
 - 5: **repeat**
 - 6: Update \mathbf{P} referring to (6.12)
 - 7: Update μ , and λ referring to (6.14)
 - 8: Update \mathbf{I} referring to (6.13)
 - 9: Set $t_\delta = t_\delta + 1$
 - 10: **until** \mathbf{P} converge
 - 11: Set $\mathbf{P}[t] = \mathbf{P}[t + 1]$
 - 12: Update θ, β
 - 13: Set $t = t + 1$
 - 14: **until** \mathbf{P} converge
-

6.1.4 Performance Evaluation

In this section, we give the simulation results to evaluate the performance of the proposed algorithm. The carrier frequency is set as 2 GHz, and the bandwidth B is 10 MHz. Then the AWGN power is $\sigma_n = BN_0$, in which $N_0 = -174$ dBm/Hz is the AWGN power spectral density. The satellite is assumed to be a LEO on the orbit of 1000 km, and the radio frequency (RF) power of the satellite is set as 80 W, while the transmit antenna gain is 40 dBi. The satellite channel is modeled as Rician channel according to [11].

Figure 6.2 shows the convergence process of Algorithm 4, when we set the number of satellite antennas $M = 4$. We can observe that in different case of BS user numbers, the algorithm converges fast within no more than ten iteration. Also, we can see that as the number of BS users increases, the total capacity of the satellite will decrease, since the satellite need to control its transmit power to avoid interference to more BS users. When the number of BS users increases from 4 to 16, there is about 15% loss of capacity for the satellite.

Figure 6.3 shows the variation of total system capacity of different interference temperature limit, in which we set $K = 4$. We can observe that the total capacity almost increases linearly in the logarithm coordinate as the interference temperature limit increases. Due to the small channel fluctuations of satellite, the interference temperature limit actually limit the transmit power of the satellite with a relative high correlation. Thus the selection of P_{th} will significantly influence the capacity performance of the satellite. For $M = 16$, the system capacity increases from 8 to 15 bps/Hz if P_{th} increases from -80 to -60 dBm. In addition, we can see that

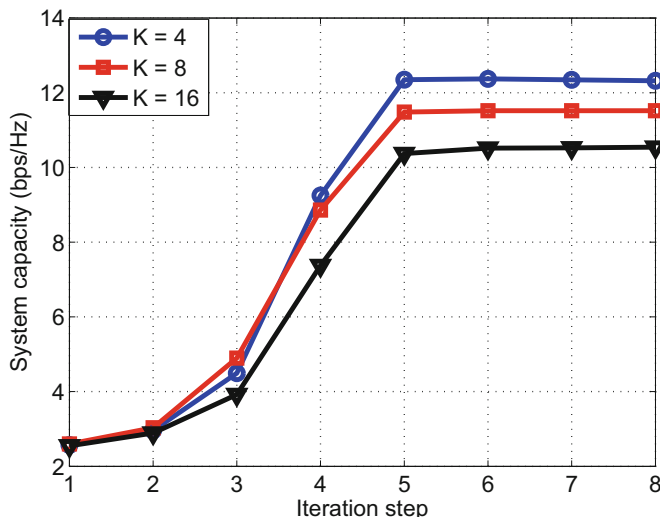


Fig. 6.2 The convergence process over iteration

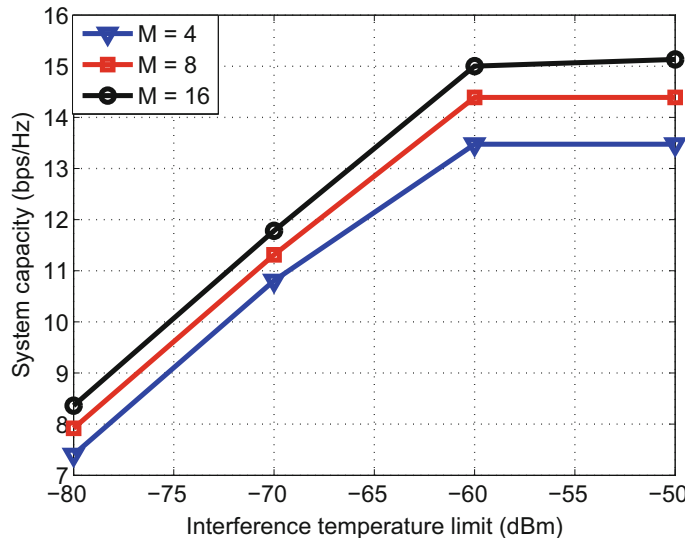


Fig. 6.3 Total System capacity of different interference temperature limit

when the transmit antennas increases from 4 to 16, the system capacity increases by about 12% when $P_{th} = -60$ dBm. Although more antennas can bring multiple user diversity gaining, it will also bring larger co-channel interference among users.

Note that the optimal power allocation scheme need the channel state information (CSI) of all BS users, which may lead to larger delay and resource occupation. For this reason, the simulation results of a distribute suboptimal algorithm is also illustrated in Fig. 6.4 for comparison. Instead of using the instant CSI of BS users, a conservative empirical value is used for estimation of the interference caused to BS users. We can observe that there will be about 15% capacity loss if we do not use the instant CSI in the suboptimal algorithm. There will be a trade-off among system delay, feedback, and the user capacity. In addition, the red line gives the results of a greedy strategy based algorithm, in which we allocated the power greedily based on the channel conditions of satellite users. Due to co-channel interference among users, the greedy algorithm cannot achieve well system performance, especially when the interference limit is large. When $P_{th} = -60$ dBm, there will be about 50% capacity loss compared with the optimal algorithm.

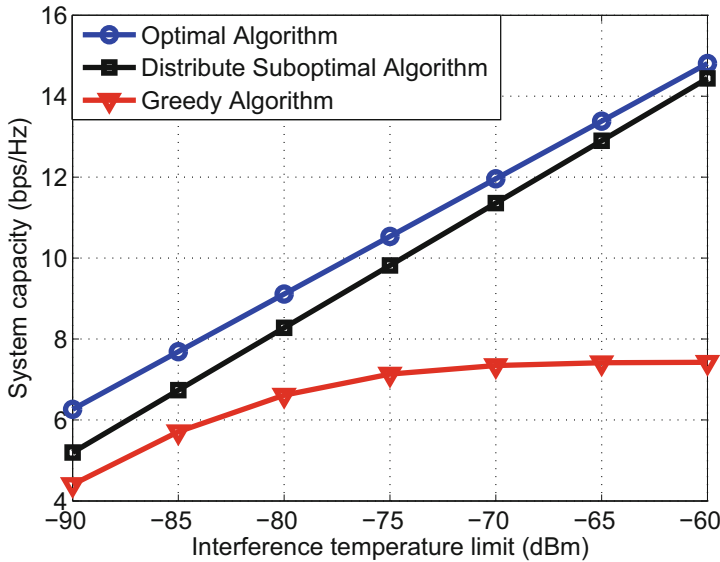


Fig. 6.4 Comparison with the distribute suboptimal algorithm

6.2 Resource Allocation in Cloud Based Terrestrial-Satellite Networks

6.2.1 Background

The rapid growing data traffic brings more and more pressure to the wireless network, which is predicted to increase by over 10,000 times in the next 20 years [12]. In addition to the continuous decrease of cell sizes and the utilization of massive MIMO, which can significantly improve the capacity is to find new available spectrum. Meanwhile, in satellite communication systems, extra spectrum is also in great need to accommodate the increasing traffic demand [1]. While the millimeter wave band has drawn much attention for the possible bandwidth, spectrum sharing has also shown great potential for improving the capacity performance. It can be envisioned that spectrum sharing would become one attracting method in future terrestrial and satellite communications systems, such as the spectrum sharing in S-band.

In this chapter, we propose the concept of the Cloud Based Integrated Terrestrial-Satellite Network (CTSN), which provides a new feasible method for interference management in spectrum-sharing systems. Cloud Radio Access Networks (C-RANs) have been proposed as one solution to the problem of interference management in recent works [13] and we expand this concept to the integrated terrestrial-satellite network. In the CTSN, both base stations (BSs) of the cellular networks and the satellite are connected to a cloud central unit via wired/wireless

backhaul links. Instead of each BS and the satellite encoding/decoding separately, the signal processing procedures of both systems are executed centrally at the cloud [14, 15]. By utilizing the channel state information (CSI), the interference from the mixed signal can be mitigated. However, in real systems, perfect CSI is generally difficult to be obtained, and thus the interference cannot be fully canceled. To avoid significant interference, power constraints have to be taken into account. When the prevailing orthogonal frequency division multiple access (OFDMA) technology is adopted, the strategy of resource allocation is of great importance to maximize the capacity of the system [16–19]. We introduce the concept interference level limit for ground BSs to constrain the interference caused to the satellite. Based on the interference model, we solve the maximizing problem of the total capacity of BSs with respect to subchannel and power allocation.

Recently, quite a few works have been developed focusing on the problem of spectrum-sharing between satellite and terrestrial networks. The technology of Cognitive Radio (CR) was discussed in [1, 5] to enable dynamic spectrum access. In [5], power and carrier allocation schemes were proposed to maximize the throughput for the cognitive spectrum utilization scenario. In [6], the authors proposed a semi-adaptive beamforming algorithm at the satellite to mitigate the interference from terrestrial users. The concept of exclusive zone (EZ) was introduced in [7, 20] to avoid co-channel interference (CCI), where terrestrial users are not allowed to use satellite frequencies. In [21, 22], the symbol error and capacity performance of the hybrid satellite terrestrial relay network (HSTRN) was studied in the presence of CCI. However, all those previous works tend to consider the satellite and terrestrial networks as two separate systems, where signal processing procedures are executed within each system. In our proposed model, both BSs of the cellular networks and the satellite are connected to a cloud central unit and are treated as one integrated system.

6.2.2 System Model

Consider a OFDMA-based CSTN, as shown in Fig. 6.5, where the satellite and terrestrial cellular systems cooperate to provide seamless service. While terrestrial networks provide high quality service for populations in urban areas, the satellite can help to coverage low-density populations in suburban or rural areas. As stated before, both the satellite and terrestrial systems are operated in the same frequency band, and spectrum-sharing is considered in the system. Due to the long-distance attenuation between the satellite and the terrestrial system, the interference from the satellite to the terrestrial system is negligible compared with the transmit power of BSs and BS users. On the other hand, the satellite user of low-density populations is generally located in areas out of the range of cellular networks. Thus, the interference between the satellite user and the terrestrial system is also negligible. The main interference in the CSTN is the interference from the terrestrial system to the uplink of the satellite, based on the fact that the transmit power of BSs or

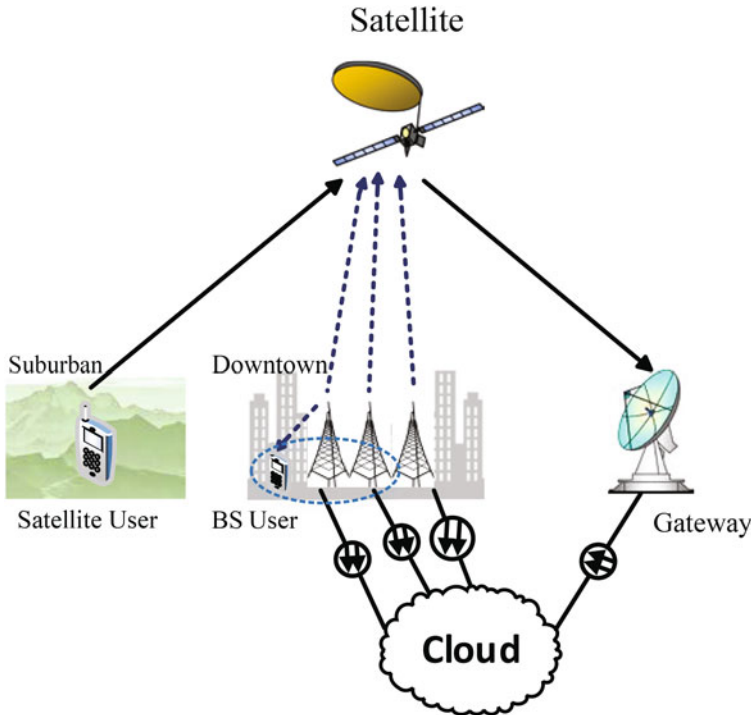


Fig. 6.5 Cloud based integrated terrestrial-satellite network

BS users is comparable to the power of mobile satellite users while the free-space attenuation are similar for the two cases. In the CTSN, all BSs are connected to the cloud central unit, and the signal processing procedures of BSs are executed at the cloud, while BSs users are generally randomly distributed and have no wired connection to the cloud. The downlink interference from BSs is of more convenience for interference management compared with the uplink interference from BS users, and thus we consider the reverse interference mode in the CTSN, i.e., the uplink of the satellite and the downlink of terrestrial systems share the same frequency band. In this case, the downlink signals of BSs would lead to interference at the satellite. The mixed signal at the satellite is first transmitted to the terrestrial gateway, and then transmitted to the cloud. By utilizing the CSI, the interference of BSs can be mitigated by subtracting the signals of BSs from the mixed signal.

We consider the scenario of one satellite user and K BSs, and let I denote the number of users of each BS. The bandwidth of the system is assumed to be B , which is divided into M subchannels. The signal of the satellite user on subchannel m is $a_{u,m}u_m$, $m \in \{1, 2, \dots, M\}$, where $a_{u,m} \in \{0, 1\}$ means whether subchannel m is assigned to the satellite user. Also, the signal from BS k to user i on subchannel m is $a_{k,i,m}z_{k,i,m}$, where $k \in \{1, 2, \dots, K\}$, $i \in \{1, 2, \dots, I\}$, $m \in \{1, 2, \dots, M\}$ and $a_{k,i,m}$ means whether subchannel m is assigned to user i of BS k . Assume the

channel fading is the same within a subchannel and let $h_{u,m}$ be the channel gains on subchannel m for the satellite user. Similarly, let $h_{k,m}$ and $g_{k,i,m}$ be the channel gains from BS k to the satellite and to BS user i on subchannel m . Then the received mixed signal on subchannel m at the satellite can be expressed as

$$y_m = a_{u,m}h_{u,m}u_m + \sum_{k=1}^K \sum_{i=1}^I a_{k,i,m}h_{k,m}z_{k,i,m} + n_1, \quad (6.15)$$

where n_1 is the additive white Gaussian noise (AWGN).

Meanwhile, the mixed signal is transmitted to the terrestrial gateway and transmitted to the cloud via wired transmission. Let $h_{e,m}$ be the channel gains from the satellite to the gateway on subchannel m , and the mixed signal at the cloud is

$$y_{ie,m} = a_{u,m}h_{ue,m}u_m + \sum_{k=1}^K \sum_{i=1}^I a_{k,i,m}h_{ke,m}z_{k,i,m} + n_{e,m}, \quad (6.16)$$

where $h_{ue,m} = h_{u,m}h_{e,m}$, $h_{ke,m} = h_{k,m}h_{e,m}$, $n_{e,m} = h_{e,m}n_1 + n_2$, and n_2 is the AWGN at the gateway.

Note that the cloud has the signal information of all BSs since the processing procedure is executed at the cloud. Let $\hat{h}_{k,m}$ and $\hat{h}_{e,m}$ be the CSI obtained from BSs and the gateway, we can then subtract the interference from the mixed signal.

$$\begin{aligned} \bar{u}_m &= y_{ie,m} - \sum_{k=1}^K \sum_{i=1}^I a_{k,i,m}\hat{h}_{ke,m}z_{k,i,m} \\ &= a_{u,m}h_{ue,m}u_m + \sum_{k=1}^K \sum_{i=1}^I a_{k,i,m}\Delta h_{ke,m}z_{k,i,m} + n_{e,m}, \end{aligned} \quad (6.17)$$

where $\Delta h_{ke,m} = \hat{h}_{ke,m} - h_{ke,m}$.

Define $p_{k,i,m}$ as the transmit power from BS k to user i on subchannel m . Then the received SNR at user i from BS k on subchannel m is

$$SNR_{k,i,m} = \frac{|g_{k,i,m}|^2 p_{k,i,m}}{\sigma_{n_B}}, \quad (6.18)$$

where σ_{n_B} is the AWGN power. Since we mainly investigate the interference between the terrestrial network and the satellite network in this chapter, we do not discuss the inter-interference between BSs, which is view as part of the AWGN. According to the Shannon's theorem, the capacity can be calculated by

$$C_{k,i,m} = \log_2(1 + SNR_{k,i,m}) = \log_2 \left(1 + \frac{|g_{k,i,m}|^2 p_{k,i,m}}{\sigma_{n_B}} \right). \quad (6.19)$$

6.2.3 Problem Formulation

In the CTSN, the satellite user and terrestrial BSs share the same frequency band and the interference caused by BSs can be mitigated by utilizing the CSI at the cloud. However, the performance of the interference mitigation is critically determined by the precision of CSI. In real cases, it is difficult to obtain perfect CSI because of the complex channel state. In the case of imperfect CSI, the interference caused by BSs cannot be fully canceled and the SINR at the satellite will deteriorate due to the interference from BSs.

Let ρ_k and ρ_e be the CSI errors of $h_{k,m}$ and $h_{e,m}$, where $\rho_k \sim N(0, \varepsilon_k)$, $\rho_e \sim N(0, \varepsilon_e)$ follow normal distribution. The obtained CSI can be expressed as $\widehat{h}_{k,m} = (1 - \rho_k)h_{k,m}$ and $\widehat{h}_{e,m} = (1 - \rho_e)h_{e,m}$. Then we can obtain $E(|\Delta h_{ke,m}|^2) = (\varepsilon_k + \varepsilon_e)|h_{ke,m}|^2$ and the interference power on subchannel m is $\sum_{k=1}^K \sum_{i=1}^I a_{k,i,m}(\varepsilon_k + \varepsilon_e)|h_{ke,m}|^2 p_{k,i,m}$. In order to guarantee the QoS of the satellite user, the interference power should be constrained within the maximum tolerable interference level P_m^{th} on each subchannel m .

$$\sum_{k=1}^K \sum_{i=1}^I a_{k,i,m}(\varepsilon_k + \varepsilon_e)|h_{ke,m}|^2 p_{k,i,m} \leq P_m^{th}, \forall m. \quad (6.20)$$

We can see that the transmit power of BSs on each subchannel is constrained according to different channel gains and channel error. It is important to allocate resource reasonably to maximize the total capacity of the terrestrial system. In addition to the interference level constraint, the other constraints in the resource allocation problem are listed as follows.

- **Total power constraint.**

$$\sum_{i=1}^I \sum_{m=1}^M a_{k,i,m} p_{k,i,m} \leq P_k^{\max}, \forall k, \quad (6.21)$$

where P_k^{\max} is the maximal transmit power of each BS.

- **User scheduling constraint.** For each BS, a subchannel is allocated to no more than one user at a time. We have:

$$\sum_{i=1}^I a_{k,i,m} \leq 1, \forall k, m. \quad (6.22)$$

Under the above constraints, our target is to maximize the total capacity of the terrestrial system. The optimization problem can be formulated as:

$$\begin{aligned}
& \max_{a_{k,i,m}, p_{k,i,m}} \sum_{k=1}^K \sum_{i=1}^I \sum_{m=1}^M a_{k,i,m} C_{k,i,m} \\
& \text{s.t. } C1 : \sum_{i=1}^I \sum_{m=1}^M a_{k,i,m} p_{k,i,m} \leq P_k^{\max}, \forall k, \\
& C2 : p_{k,i,m} \geq 0, \forall k, i, m, \\
& C3 : \sum_{k=1}^K \sum_{i=1}^I a_{k,i,m} (\varepsilon_k + \varepsilon_e) |h_{k,i,m}|^2 p_{k,i,m} \leq P_m^{\text{th}}, \forall m, \\
& C4 : \sum_{i=1}^I a_{k,i,m} \leq 1, \forall k, m, \\
& C5 : a_{k,i,m} \in \{0, 1\}.
\end{aligned} \tag{6.23}$$

6.2.4 Subchannel and Power Allocation Algorithm

In the previous section, we formulate the optimization problem as (6.23). However, it is a non-convex problem due to the integer constraints in C5, which adds to the complexity. In this section, we relax the subchannel allocation indicators from integers to continuous variables to transform this non-convex problem into a convex problem. Then we solve the transformed optimization problem by means of the Lagrangian dual decomposition method.

6.2.4.1 Transformation of Optimization Problem

The original optimization problem in (6.23) is a mixed integer non-convex problem. One may use the brute-force method to obtain the optimal solution, but it is has NP complexity. The non-convex property is caused by the integer subchannel allocation indicators $a_{k,i,m}$. To solve this, we can relax $a_{k,i,m}$ to a continuous variable that $a_{k,i,m} \in [0, 1]$ to transform the problem into a convex problem [23]. The integer value of $a_{k,i,m}$ means whether subchannel m is assigned to user i of BS k . Relatively, the continuous value of $a_{k,i,m}$ within $[0, 1]$ can be interpreted as the fraction of time that subchannel m is assigned to user i of BS k during one transmission frame. In the continuous case, the meanings of constraints C1 and C3 are the same as the integer case, which are the constraints of total transmit power of BSs and the interference power on subchannel m . Also, the user scheduling constraint C4 does not change when $a_{k,i,m}$ is relaxed to a continuous variable. In the continuous case, it means that the fraction of time of a subchannel assigned to all users cannot exceed one transmission frame during one transmission frame. Then, the optimization problem in (6.23) can be transformed into:

$$\begin{aligned}
& \min_{a_{k,i,m}, p_{k,i,m}} - \sum_{k=1}^K \sum_{i=1}^I \sum_{m=1}^M a_{k,i,m} C_{k,i,m} \\
& \text{s.t. } C1 : P_k^{\max} - \sum_{i=1}^I \sum_{m=1}^M a_{k,i,m} p_{k,i,m} \geq 0, \forall k, \\
& C2 : p_{k,i,m} \geq 0, \forall k, i, m, \\
& C3 : P_m^{\text{th}} - \sum_{k=1}^K \sum_{i=1}^I (\varepsilon_k + \varepsilon_e) |h_{ke,m}|^2 a_{k,i,m} p_{k,i,m} \geq 0, \\
& C4 : 1 - \sum_{i=1}^I a_{k,i,m} \geq 0, \forall k, m, \\
& C5 : a_{k,i,m} \in [0, 1], \forall k, i, m.
\end{aligned} \tag{6.24}$$

Note that we have transformed the optimization problem into the standard form. It can be proved that the Hessian matrix of $-\sum_{k=1}^K \sum_{i=1}^I \sum_{m=1}^M a_{k,i,m} C_{k,i,m}$ is positive semidefinite, and thus the optimization function is convex. Also, it is easy to prove that all the constraint functions in (6.24) are concave. In this case, the optimization problem (6.24) is a convex optimization problem and has only one unique optimal solution.

6.2.4.2 Dual Decomposition Method

We have transformed the optimization problem into a standard convex optimization problem by relaxing the subchannel allocation indicator. We now solve this problem by means of the Lagrangian dual decomposition method. The Lagrangian function is

$$\begin{aligned}
L(\{a_{k,i,m}\}, \{p_{k,i,m}\}, \boldsymbol{\lambda}, \boldsymbol{\mu}, \boldsymbol{\eta}) = & - \sum_{k=1}^K \sum_{i=1}^I \sum_{m=1}^M a_{k,i,m} C_{k,i,m} \\
& - \sum_{k=1}^K \lambda_k (P_k^{\max} - \sum_{i=1}^I \sum_{m=1}^M a_{k,i,m} p_{k,i,m}) \\
& - \sum_{m=1}^M \mu_m (P_m^{\text{th}} - \sum_{k=1}^K \sum_{i=1}^I (\varepsilon_k + \varepsilon_e) |h_{ke,m}|^2 a_{k,i,m} p_{k,i,m}) \\
& - \sum_{k=1}^K \sum_{m=1}^M \eta_{k,m} (1 - \sum_{i=1}^I a_{k,i,m}),
\end{aligned} \tag{6.25}$$

where $\boldsymbol{\lambda}, \boldsymbol{\mu}, \boldsymbol{\eta}$ are the Lagrange multipliers vectors for the constraints C1, C3 and C4 in (6.24). Thus, the Lagrangian dual function is given by:

$$\theta(\boldsymbol{\lambda}, \boldsymbol{\mu}, \boldsymbol{\eta}) = \inf \left\{ L(\{a_{k,i,m}\}, \{p_{k,i,m}\}, \boldsymbol{\lambda}, \boldsymbol{\mu}, \boldsymbol{\eta}) \mid \begin{array}{l} p_{k,i,m} \geq 0, a_{k,i,m} \in [0, 1], \forall k, i, m \end{array} \right\}. \tag{6.26}$$

Then the dual problem is:

$$\begin{aligned} & \max_{\lambda, \mu, \eta} \theta(\lambda, \mu, \eta) \\ & \text{s.t. } \lambda, \mu, \eta \geq 0. \end{aligned} \quad (6.27)$$

The Lagrangian dual function in (6.26) can be decomposed into a master problem and $K \times M$ subproblems as:

$$\begin{aligned} \theta(\lambda, \mu, \eta) = & \sum_{k=1}^K \sum_{m=1}^M \inf \left\{ L_{k,m}(\{a_{k,i,m}\}, \{p_{k,i,m}\}, \lambda, \mu, \eta) \mid \right. \\ & \left. p_{k,i,m} \geq 0, a_{k,i,m} \in [0, 1], \forall k, i, m \right\} \\ & - \sum_{k=1}^K \lambda_k P_k^{\max} - \sum_{m=1}^M \mu_m P_m^{\max} - \sum_{k=1}^K \sum_{m=1}^M \eta_{k,m}. \end{aligned} \quad (6.28)$$

where

$$\begin{aligned} L_{k,m}(\{a_{k,i,m}\}, \{p_{k,i,m}\}, \lambda, \mu, \eta) = & - \sum_{i=1}^I a_{k,i,m} C_{k,i,m} + \sum_{i=1}^I \lambda_k a_{k,i,m} p_{k,i,m} \\ & + \sum_{i=1}^I \mu_m (\varepsilon_k + \varepsilon_e) |h_{ke,m}|^2 a_{k,i,m} p_{k,i,m} + \sum_{i=1}^I \eta_{k,m} a_{k,i,m}. \end{aligned} \quad (6.29)$$

Since we have decomposed the Lagrangian dual function in (6.26) into a master problem and $K \times M$ subproblems, we can then solve the dual problem iteratively by solving each subproblem. For each subproblem, the optimal solutions $\bar{p}_{k,i,m}$ and $\bar{a}_{k,i,m}$ satisfy the conditions

$$\frac{\partial L_{k,m}}{\partial \bar{p}_{k,i,m}} = -\frac{1}{\ln 2} \left(\frac{|g_{k,i,m}|^2}{|g_{k,i,m}|^2 \bar{p}_{k,i,m} + \sigma_{n_B}} \right) + \lambda_k + \mu_m (\varepsilon_k + \varepsilon_e) |h_{ke,m}|^2 \begin{cases} = 0, \bar{p}_{k,i,m} > 0, \\ \geq 0, \bar{p}_{k,i,m} = 0. \end{cases} \quad (6.30)$$

$$\frac{\partial L_{k,m}}{\partial \bar{a}_{k,i,m}} = -\log_2 \left(1 + \frac{|g_{k,i,m}|^2 \bar{p}_{k,i,m}}{\sigma_{n_B}} \right) + \lambda_k \bar{p}_{k,i,m} \quad (6.31)$$

$$+ \mu_m (\varepsilon_k + \varepsilon_e) |h_{ke,m}|^2 \bar{p}_{k,i,m} + \eta_{k,m} \begin{cases} \geq 0, \bar{a}_{k,i,m} = 0, \\ = 0, 0 < \bar{a}_{k,i,m} < 1, \\ \leq 0, \bar{a}_{k,i,m} = 1. \end{cases}$$

From (6.30), we can obtain the optimal power allocated from BS k to user i on subchannel m is:

$$\bar{p}_{k,i,m} = \left(\frac{1}{\ln 2} \left(\frac{1}{\lambda_k + \mu_m (\varepsilon_k + \varepsilon_e) |h_{ke,m}|^2} \right) - \frac{\sigma_{n_B}}{|g_{k,i,m}|^2} \right)^+, \quad (6.32)$$

where $(x)^+ = \max(0, x)$.

The optimal power allocation $\bar{p}_{k,i,m}$ is given as (6.32), which follows a multi-level water filling form. The water level is influenced by $(\varepsilon_k + \varepsilon_e)|h_{ke,m}|^2$ for different BS k . The BS k with larger CSI error ε_k and larger channel gain to the satellite $h_{k,m}$ will have a lower water level, which can reduce the interference caused at the satellite. Also, the BS user i with larger $|g_{k,i,m}|^2/\sigma_{n_B}$ will be allocated larger transmit power to improve the capacity performance.

Next, we come to the subchannel allocation of $\bar{a}_{k,i,m}$. The partial derivative in (6.31) can be rewritten as

$$\frac{\partial L_{k,m}}{\partial \bar{a}_{k,i,m}} = H_{k,i,m} + \eta_{k,m} \begin{cases} \geq 0, \bar{a}_{k,i,m} = 0, \\ = 0, 0 < \bar{a}_{k,i,m} < 1, \\ \leq 0, \bar{a}_{k,i,m} = 1. \end{cases} \quad (6.33)$$

where

$$\begin{aligned} H_{k,i,m} = & -\log_2\left(1 + \frac{|g_{k,i,m}|^2 \bar{p}_{k,i,m}}{\sigma_{n_B}}\right) + \lambda_k \bar{p}_{k,i,m} \\ & + \mu_m (\varepsilon_k + \varepsilon_e) |h_{ke,m}|^2 \bar{p}_{k,i,m}. \end{aligned} \quad (6.34)$$

From (6.33), we can find that the optimal subchannel allocation tends to allocate subchannel m to user i with the smallest $H_{k,i,m}$ for each BS k . Thus we have

$$\bar{a}_{k,i^*,m} = 1|_{i^* = \min_i H_{k,i,m}, \forall k, m}. \quad (6.35)$$

The optimal solution of $\bar{p}_{k,i,m}$ and $\bar{a}_{k,i,m}$ are in the form of λ and μ . Since $\theta(\lambda, \mu, \eta)$ of (6.26) is not differentiable, we use the subgradient method to obtain λ and μ iteratively, i.e.,

$$\begin{aligned} \lambda_k^{(j+1)} &= \left[\lambda_k^j - \beta_1^{(j)} (P_k^{\max} - \sum_{i=1}^I \sum_{m=1}^M s_{k,i,m}) \right]^+, \\ \mu_m^{(j+1)} &= \left[\mu_m^j - \beta_2^{(j)} (P_m^{\max} - \sum_{k=1}^K \sum_{i=1}^I t_{k,m} s_{k,i,m}) \right]^+, \\ s_{k,i,m} &= a_{k,i,m} p_{k,i,m}, t_{k,m} = (\varepsilon_k + \varepsilon_e) |h_{ke,m}|^2, \end{aligned} \quad (6.36)$$

where $j \in \{1, 2, \dots, J_{\max}\}$ is the iteration step, which is no more than J_{\max} , and $\beta_1^{(j)}, \beta_2^{(j)}$ are the step sizes of iteration j .

We can find that the optimal solution $\bar{p}_{k,i,m}$ and $\bar{a}_{k,i,m}$ are only in the form of λ and μ . Thus η is not necessary to be calculated. Since all signal processing procedures are executed at the cloud, the cloud has access to all the information needed for the iteration process. Upon each iteration, we update the Lagrange multipliers λ and μ according to (6.36), and then update $\bar{p}_{k,i,m}$ and $\bar{a}_{k,i,m}$ according to (6.32) and (6.35). We summarize the algorithm as Algorithm 5.

Algorithm 5 Centralized iterative resource allocation algorithm

```

1: Initialize  $J_{max}$  and Lagrangian variables vectors  $\lambda, \mu$ , set  $j = 0$ 
2: Initialize  $p_{k,i,m}$  with a uniform power distribution among all subchannels for each BS
3: Initialize  $a_{k,i,m}$  with subchannel allocation method in [24]
4: repeat
5:   for  $k = 1$  to  $K$  do
6:     Update  $\lambda_k$  according to (6.36)
7:   end for
8:   for  $m = 1$  to  $M$  do
9:     Update  $\mu_m$  according to (6.36)
10:   end for
11:   for  $k = 1$  to  $K$  do
12:     for  $m = 1$  to  $M$  do
13:       for  $i = 1$  to  $I$  do
14:         Update  $\bar{p}_{k,i,m}$  according to (6.32)
15:         Calculate  $H_{k,i,m}$  according to (6.34)
16:       end for
17:       Update  $\bar{a}_{k,i,m}$  according to (6.35)
18:     end for
19:   end for
20: until Convergence or  $j = J_{max}$ 

```

6.2.5 Performance Evaluation

In this section, we give the numerical simulation results of the proposed allocation algorithm to evaluate the performance in the scenario of the CTSN. The carrier frequency is 2 GHz in the S frequency band. The bandwidth B is set as 10 MHz and is divided into $M = 20$ subchannels. Then the noise power on each subchannel is $\sigma_{n_B} = \frac{B}{M} N_0$, where $N_0 = -174$ dBm/Hz is the AWGN power spectral density. The coverage radius of BS is 50 m and the maximum transmit powers of BSs are uniformly set as $P_k^{max} = P_B^{max}$. I users are randomly distributed within the coverage radius for each BS. The satellite is assume to be MEO on the orbit of 10,000 km. The channel gains from BSs to BS users are modeled according to [25], while the channel gains from BSs to the satellite are modeled according to [11]. Since BSs are generally established at open areas, we consider there is no shadowing from BSs to the satellite and $h_{k,m}$ follow Rician distribution. The CSI errors are set according to [26]. Also, we add the interference level limit to the subchannel allocation algorithm in [24] for comparing in the simulation, which is named as “Existing Algorithm”.

Figure 6.6 gives the convergence process of Algorithm 5, where we set the number of BSs $K = 50$, and the maximal transmit power $P_B^{max} = 30$ dBm. Since the interference is caused at the satellite, we consider the equivalent interference level at the satellite, which is set as $P_m^{th} = -200$ dBm for all m . We can observe that for both $I = 20$ and $I = 10$, the average capacity of BSs converges within less than ten iteration steps. The relatively fast convergence speed of the iterative algorithm proves the feasibility of the scheme in real networks.

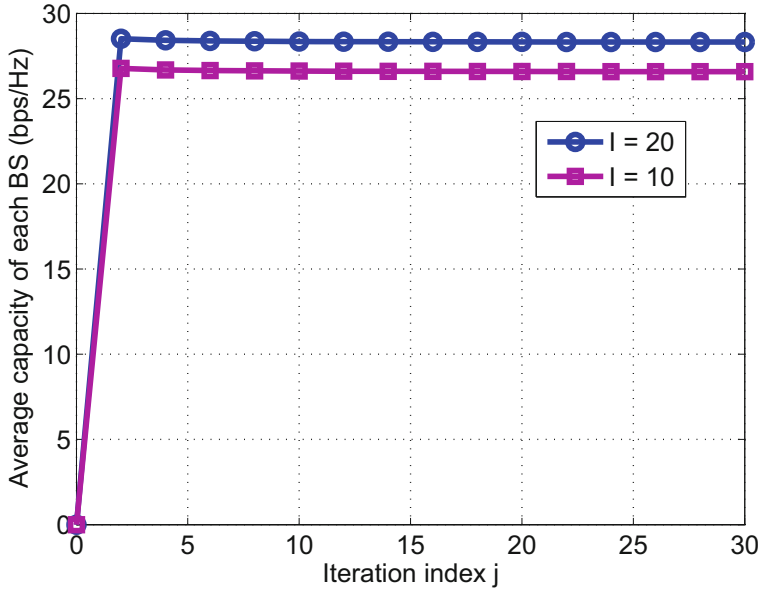


Fig. 6.6 The convergence process over the number of iterations

In Fig. 6.7, we study the total capacity of all BSs with different BS numbers K and different BS user numbers I with the same variables setting as Fig. 6.6. We can observe that when the BS number increases from 10 to 50, the total capacity almost increases linearly for 270–1270 bps/Hz when user number $I = 15$. There is about 6% capacity loss for $K = 50$ compared with $K = 10$, which is caused by the interference level limit. The capacity loss will be larger when the BS number increases and the capacity loss will reach about 10% when $K = 100$. Also, we can observe that when the number of users of each BS increases from $I = 15$ to $I = 20$, there is about 2.5% gaining in the capacity. The increasing of users will bring more possible selections for each subchannel when doing allocation, and thus the mean capacity of each subchannel will increase. Besides, for users number $I = 15$, the proposed algorithm outperforms the “Existing Algorithm” by about 10% for different numbers of BSs, which proves the optimality of the proposed algorithm.

Figure 6.8 shows the total capacity of all BSs for interference level between -200 and -180 dBm. The number of BSs and the number of users are set as $K = 10$ and $I = 15$. As the interference level increases, the total capacity will first increase because larger interference level means larger possible transmit power. The increasing speed is nearly logarithm linear since the relation between the interference and transmit power is linear and the relation between capacity and transmit power is logarithmic. When the interference level continues to increase, all BSs will reach the maximum transmit power and the total capacity will no longer increase. We can also observe that when the maximum transmit power

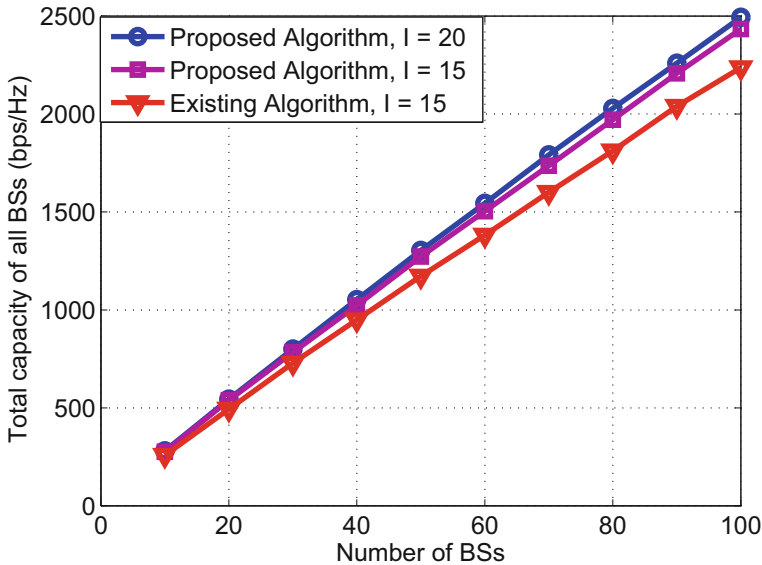


Fig. 6.7 Total capacity of all BSs of different K and I

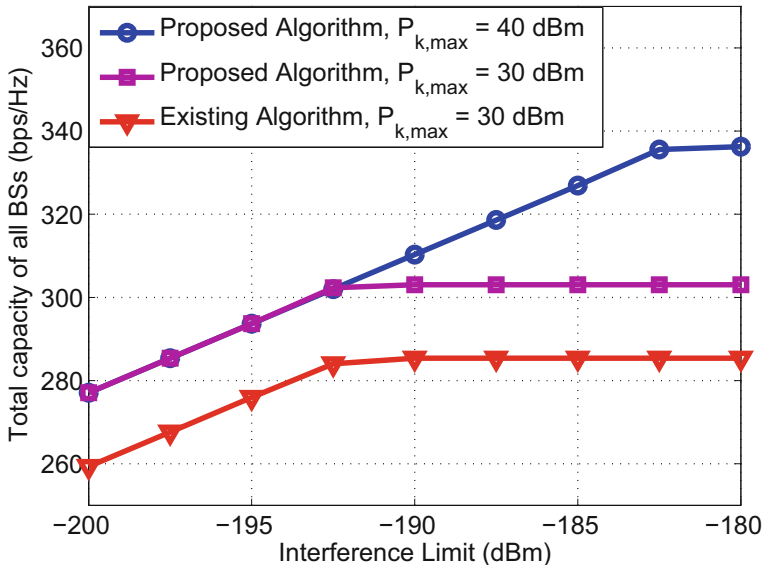


Fig. 6.8 Total capacity of all BSs of different interference level and BS power

of BSs increases, the increasing process will be longer when the interference level increases. This is because BSs can afford larger transmit power when larger interference is allowed. When the interference level is small, we can find that increasing the maximum transmit power does not increase the capacity obviously

since the main limit is from the interference level limit and no BS can reach the maximum transmit power. Besides, we can observe that the capacity gaining between the proposed algorithm and “existing algorithm” is nearly a constant when the interference level changes. Thus, the proposed algorithm will have relatively larger gaining in percentage when the interference level is small.

6.3 Summary

In the chapter, we propose two resource allocation schemes for two multiple access integrated system. First, we investigate the problem of interference controlling and power allocation in a terrestrial-satellite spectrum sharing network. Second, we propose the concept of the Cloud Based Integrated Terrestrial-Satellite Network (CTSN), where both base stations of the cellular networks and the satellite are connected to a cloud central unit and the signal processing procedures are executed centrally at the cloud, and a resource allocation scheme is proposed to maximize the total capacity of the terrestrial system.

References

1. S. Maleki, S. Chatzinotas, B. Evans, K. Liolis, J. Grotz, A.V. Coralli, N. Chuberre, Cognitive spectrum utilization in Ka band multibeam satellite communications. *IEEE Commun. Mag.*, **53**(3), 24–29 (2015)
2. 3rd Generation Partnership Project (3GPP), Feasibility study on new services and markets technology enablers – enhanced mobile broadband (2016)
3. C. Jiang, L. Kuang, Z. Han, Y. Ren, L. Hanzo, Information credibility modeling in cooperative networks: equilibrium and mechanism design. *IEEE J. Sel. Areas Commun.* **35**(2), 432–448 (2017)
4. C. Jiang, H. Zhang, Z. Han, Y. Ren, V. Leung, L. Hanzo, Information-sharing outage-probability analysis of vehicular networks. *IEEE Trans. Veh. Technol.* **65**(12), 9479–9492 (2016)
5. E. Lagunas, S.K. Sharma, S. Maleki, S. Chatzinotas, B. Ottersten, Resource allocation for cognitive satellite communications with incumbent terrestrial networks. *IEEE Trans. Cogn. Commun. Netw.* **1**(3), 305–317 (2015)
6. A.H. Khan, M.A. Imran, B.G. Evans, Semi-adaptive beamforming for OFDM based hybrid terrestrial-satellite mobile system. *IEEE Trans. Wirel. Commun.*, **11**(10), 3424–3433 (2012)
7. K. Kang, J.M. Park, H.W. Kim, T.C. Hong, B.J. Ku, D. Chang, Analysis of interference and availability between satellite and ground components in an integrated mobile-satellite service system. *Int. J. Satell. Comm. Netw.* **33**(4), 351–366 (2015)
8. B.R. Marks, G.P. Wright, A general inner approximation algorithm for nonconvex mathematical programs. *Oper. Res.* **26**(4), 681–683 (1978)
9. J. Papandriopoulos, J.S. Evans, SCALE: a low-complexity distributed protocol for spectrum balancing in multiuser DSL networks. *IEEE Trans. Inf. Theory* **55**(8), 3711–3724 (2009)
10. S. Boyd, L. Vandenberghe, *Convex Optimization* (Cambridge University Press, Cambridge, 2004)

11. E. Lutz, D. Cygan, M. Dippold, F. Dolainsky, W. Papke, The land mobile satellite communication channel-recording, statistics, and channel model. *IEEE Trans. Veh. Technol.* **40**(2), 375–386 (1991)
12. A. Ghosh, T.A. Thomas, M.C. Cudak, et al., Millimeter-wave enhanced local area systems: a high-data-rate approach for future wireless networks. *IEEE J. Sel. Areas Commun.* **32**(6), 1152–1163 (2014)
13. S.H. Park, O. Simeone, O. Sahin, S. Shamai, Joint precoding and multivariate backhaul compression for the downlink of cloud radio access networks. *IEEE Trans. Signal Process.* **61**(22), 5646–5658 (2013)
14. J. Wang, C. Jiang, Z. Han, Y. Ren, L. Hanzo, Network association strategies for an energy harvesting aided super-WiFi network relying on measured solar activity. *IEEE J. Sel. Areas Commun.* **34**(12), 3785–3797 (2016)
15. Y. Meng, C. Jiang, L. Xu, Y. Ren, Z. Han, User association in heterogeneous networks: a social interaction approach. *IEEE Trans. Veh. Technol.* **65**(12), 9982–9993 (2016)
16. H. Zhang, C. Jiang, X. Chu, X. Wang, T. Quek, Resource allocation for cognitive small cell networks: a cooperative bargaining game theoretic approach. *IEEE Trans. Wirel. Commun.*, **14**(6), 3481–3493 (2015)
17. H. Zhang, C. Jiang, N. Beaulieu, X. Chu, X. Wen, M. Tao, Resource allocation in spectrum-sharing OFDMA femtocells with heterogeneous services. *IEEE Trans. Wirel. Commun.* **62**(7), 2366–2377 (2014)
18. J. Du, C. Jiang, Y. Qian, Z. Han, Y. Ren, Resource allocation with video traffic prediction in cloud-based space systems. *IEEE Trans. Multimedia* **18**(5), 820–830 (2016)
19. C. Jiang, Y. Chen, Y. Ren, K.J.R. Liu, Maximizing network capacity with optimal source selection: a network science perspective. *IEEE Trans. Signal Process. Lett.* **22**(7), 938–942 (2015)
20. V. Deslandes, J. Tronc, A.L. Beylot, Analysis of interference issues in integrated satellite and terrestrial mobile systems, in *Proceedings of the IEEE ASMS/SPSC*, 2010, pp. 256–261
21. K. An, M. Lin, J. Ouyang, Y. Huang, G. Zheng, Symbol error analysis of hybrid satellite-terrestrial cooperative networks with cochannel interference. *IEEE Commun. Lett.* **18**(11), 1947–1950 (2014)
22. K. An, M. Lin, T. Liang, J. Wang, J. Wang, Y. Huang, A.L. Swindlehurst, Performance analysis of multi-antenna hybrid satellite-terrestrial relay networks in the presence of interference. *IEEE Trans. Commun.* **63**(11), 4390–4404 (2015)
23. C.Y. Wong, R.S. Cheng, K.B. Lataief, R.D. Murch, Multiuser OFDM with adaptive subcarrier, bit, and power allocation. *IEEE J. Sel. Areas Commun.* **17**(10), 1747–1758 (1999)
24. Z. Shen, J.G. Andrews, B.L. Evans, Adaptive resource allocation in multiuser OFDM systems with proportional rate constraints. *IEEE Trans. Wirel. Commun.* **4**(6), 2726–2737 (2005)
25. Further Advancements for E-UTRA, Physical Layer Aspects, 3GPP Std. TR 36.814 v9.0.0 (2010)
26. A. Mukherjee, A.L. Swindlehurst, Robust beamforming for security in MIMO wiretap channels with imperfect CSI. *IEEE Trans. Signal Process.* **59**(1), 351–361 (2011)

Chapter 7

Conclusions and Future Challenges

7.1 Conclusions

This book mainly discusses the architectures of terrestrial-satellite networks as well as the possible techniques and challenges.

We first introduced the technique of beamforming in satellite systems, and discussed the main challenges as well as prospective applications. Based on beamforming, we proposed a multimedia multicast integrated terrestrial-satellite network. By serving users that require the same contents as a group using multicasting, higher efficiency can be achieved. As a practical application of beamforming in satellite networks, the work of SCS was presented briefly.

Then, we discussed the possible methods for interference cancelation reception in terrestrial-satellite communication networks when reusing the frequency band between the two networks. Based on channel estimation and centralized processing, we proposed several interference coordination schemes for different scenarios in the integrated satellite and terrestrial network.

Due to the limitation of spectrum resources, we discussed the problems of spectrum coexistence between GEO and Terrestrial Systems, and between GEO and NEGO systems. Then, we investigated the technique of CR to improve the utilization rate of the spectrum. It was first advanced a strategy for SU to search available spectrums with asynchronous MAC-layer sensing. Then, we discussed the asynchronous cooperative sensing situation and derive the optimal sensing parameters. Furthermore, we proposed a density control mechanism for managing number of secondary transmitters around one primary receiver.

Finally, taking both the two systems into consideration, we proposed two resource allocation schemes for two multiple access integrated system. First, by introducing the concept of interference temperature limit, the optimal power allocation scheme was proposed in a terrestrial-satellite spectrum sharing network.

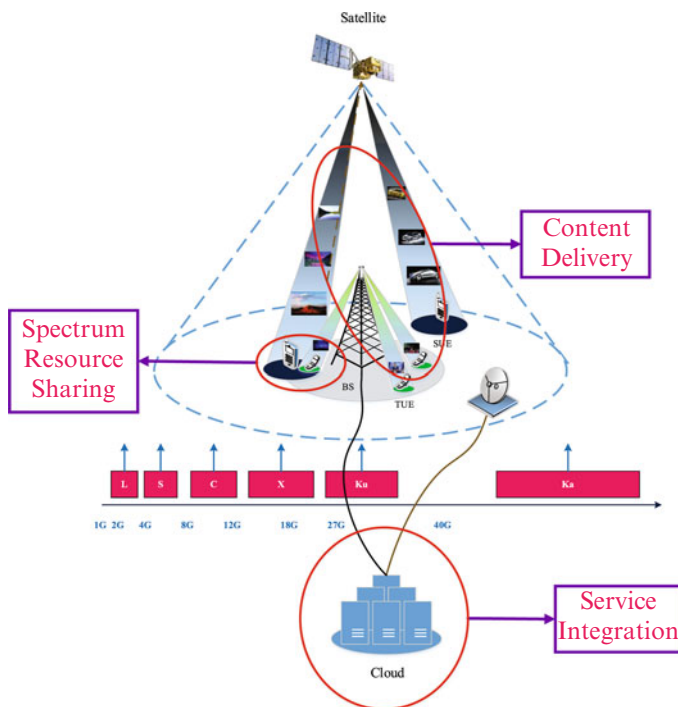


Fig. 7.1 Key technologies

Second, we proposed the concept of the CTSN for centralized resource management, and a resource allocation scheme in respect to subchannel and power was proposed to maximize the total capacity of the terrestrial system.

7.2 Future Challenges

While the integrated satellite and terrestrial network may bring lots of benefits in the development of communication, it also leads to many new technical challenges. As shown in Fig. 7.1, there might be three areas where innovative technological solutions are expected. Firstly, the satellite-based and the terrestrial networks have to be able to share the available spectrum resources to simultaneously maximize the joint benefits. Secondly, the network services have to be centrally coordinated and integrated to ensure transparent delivery and efficient management. Thirdly, new content delivery mechanisms are required to leverage the high multicast capabilities of satellite-based systems.

Figure 7.2 gives the scenario of spectrum resource sharing. Spectrum sharing will enable the two systems to use the available spectrum resources jointly

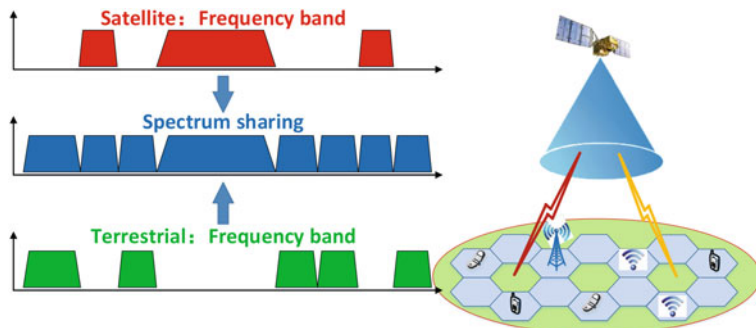


Fig. 7.2 Spectrum resource sharing

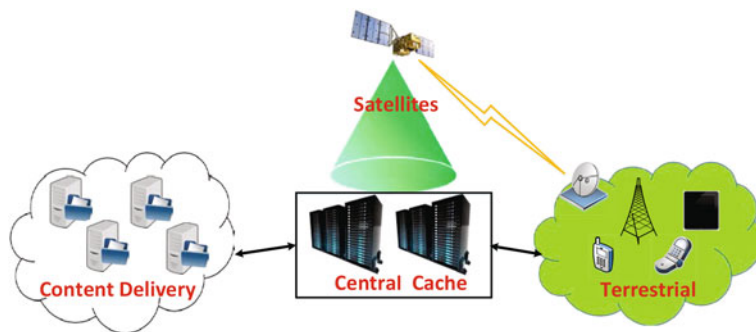


Fig. 7.3 Content delivery

once interferences can be coordinated. This will ensure efficient spectrum usage. To achieve this, challenges include the antenna and RF, the interference cancelation, as well as the spectrum management.

Likewise, service integration will make ubiquitous mobile Internet possible once the IP protocol is adapted to operate in the satellite networks. Under such a circumstance, special conditions in space do matter; for example, long delays, asymmetric links, and limited on-board processing resources. Meanwhile, functional modules have to be closely studied and separated into delay-sensitive modules which should be placed on-board, and computationally-complex modules which should be deployed on the ground.

In addition, a good content delivery architecture may efficiently multi-cast/broadcast high volumes of multimedia over large areas if intelligent traffic routing is established, as shown in Fig. 7.3. The challenge lies in that it may be difficult to design a good source/channel code for large-scale broadcasts with little feedback. The code has to be able to recover from errors and disruptions caused by interferences and weather conditions. The service impacts of routing through satellite also require thorough studies to ensure reliability and efficiency.